

**AD-A239 968**



WRDC-TR-90-2121  
Volume II

Thermal Energy Storage and Heat Transfer Support Program

Task 4 - Thermionic Energy Conversion Studies

Mysore L. Ramalingam  
UES, Inc.  
4401 Dayton-Xenia Road  
Dayton, Ohio 45432-1894

1 March 1991

Final Report for the Period June 1987 - September 1990

Approved for Public Release; Distribution Unlimited

Aero Propulsion and Power Laboratory  
Wright Laboratory  
Air Force Systems Command  
Wright-Patterson Air Force Base, Ohio 45433



91 8 29 018

**91-09280**

## NOTICE

WHEN GOVERNMENT DRAWINGS, SPECIFICATIONS, OR OTHER DATA ARE USED FOR ANY PURPOSE OTHER THAN IN CONNECTION WITH A DEFINITELY GOVERNMENT-RELATED PROCUREMENT, THE UNITED STATES GOVERNMENT INCURS NO RESPONSIBILITY OR ANY OBLIGATION WHATSOEVER. THE FACT THAT THE GOVERNMENT MAY HAVE FORMULATED OR IN ANY WAY SUPPLIED THE SAID DRAWINGS, SPECIFICATIONS, OR OTHER DATA, IS NOT TO BE REGARDED BY IMPLICATION, OR OTHERWISE IN ANY MANNER CONSTRUED, AS LICENSING THE HOLDER, OR ANY OTHER PERSON OR CORPORATION; OR AS CONVEYING ANY RIGHTS OR PERMISSION TO MANUFACTURE, USE, OR SELL ANY PATENTED INVENTION THAT MAY IN ANY WAY BE RELATED THERETO.

THIS REPORT HAS BEEN REVIEWED BY THE OFFICE OF PUBLIC AFFAIRS (ASD/PA) AND IS RELEASABLE TO THE NATIONAL TECHNICAL INFORMATION SERVICE (NTIS). AT NTIS IT WILL BE AVAILABLE TO THE GENERAL PUBLIC INCLUDING FOREIGN NATIONS.

THIS TECHNICAL REPORT HAS BEEN REVIEWED AND IS APPROVED FOR PUBLICATION.



ANGEL S. REYES  
Power Technology Branch  
Aerospace Power Division  
Aero Propulsion and Power Directorate



JERRY E. BEAM  
Power Technology Branch  
Aerospace Power Division  
Aero Propulsion and Power Directorate

FOR THE COMMANDER



William U. Borger  
Chief, Aerospace Power Division  
Aero Propulsion and Power Directorate

IF YOUR ADDRESS HAS CHANGED, IF YOU WISH TO BE REMOVED FROM OUR MAILING LIST, OR IF THE ADDRESSEE IS NO LONGER EMPLOYED BY YOUR ORGANIZATION PLEASE NOTIFY HL/POOS-3, WRIGHT-PATTERSON AFB, OH 45433-6563 TO HELP MAINTAIN A CURRENT MAILING LIST.

COPIES OF THIS REPORT SHOULD NOT BE RETURNED UNLESS RETURN IS REQUIRED BY SECURITY CONSIDERATIONS, CONTRACTUAL OBLIGATIONS, OR NOTICE ON A SPECIFIC DOCUMENT.

# REPORT DOCUMENTATION PAGE

Form Approved  
OMB No. 0704-0188

| <b>1a. REPORT SECURITY CLASSIFICATION</b><br>UNCLASSIFIED   |   | <b>1b. ABSTRACTIVE MARKINGS</b><br>N/A  |                                      |                    |             |         |                        |        |      |    |   |  |
|---|---|---|--------------------------------------|--------------------|-------------|---------|------------------------|--------|------|----|---|--|
| <b>2a. SECURITY CLASSIFICATION AUTHORITY</b><br>N/A   |   | <b>3. DISTRIBUTION/AVAILABILITY OF REPORT</b><br>Approved for public release,<br>distribution unlimited   |                                      |                    |             |         |                        |        |      |    |   |  |
| <b>2b. SECURITY CLASSIFICATION/DOWNGRADING SCHEDULE</b><br>N/A  |   |   |                                      |                    |             |         |                        |        |      |    |   |  |
| <b>4. PERFORMING ORGANIZATION REPORT NUMBER(S)</b><br>CES-799-TR-90-004 ✓   |   | <b>5. MONITORING ORGANIZATION REPORT NUMBER(S)</b><br>WRDC-TR-90-2121, Volume II  |                                      |                    |             |         |                        |        |      |    |   |  |
| <b>6a. NAME OF PERFORMING ORGANIZATION</b><br>CES, Inc.   | <b>6b. OFFICE SYMBOL (if applicable)</b><br>SESD    | <b>7a. NAME OF MONITORING ORGANIZATION</b><br>Aero Propulsion & Power Lab (WL/POOS)<br>Wright Laboratory  |                                      |                    |             |         |                        |        |      |    |   |  |
| <b>6c. ADDRESS (City, State, and ZIP Code)</b><br>4401 Dayton-Xenia Road<br>Dayton, OH 45432  |   | <b>7b. ADDRESS (City, State, and ZIP Code)</b><br>Wright Patterson AFB, OH 45433-6563   |                                      |                    |             |         |                        |        |      |    |   |  |
| <b>8a. NAME OF FUNDING/SPONSORING ORGANIZATION</b><br>WRDC/POOS-3   | <b>8b. OFFICE SYMBOL (if applicable)</b><br>WL/POOS | <b>9. PROCUREMENT INSTRUMENT IDENTIFICATION NUMBER</b><br>F33615-87-C-2738  |                                      |                    |             |         |                        |        |      |    |   |  |
| <b>10. ADDRESS (City, State, and ZIP Code)</b><br>Aero Propulsion and Power Laboratory<br>WL/POOS<br>Wright Patterson AFB, OH 45433-6563  |   | <b>10. SOURCE OF FUNDING NUMBERS</b> <table border="1" style="width: 100%; border-collapse: collapse; margin-top: 5px;"> <thead> <tr> <th style="width: 25%;">PROGRAM ELEMENT NO</th> <th style="width: 25%;">PROJECT NO.</th> <th style="width: 25%;">TASK NO</th> <th style="width: 25%;">WORK UNIT ACCESSION NO</th> </tr> </thead> <tbody> <tr> <td style="text-align: center;">62203F</td> <td style="text-align: center;">3145</td> <td style="text-align: center;">20</td> <td style="text-align: center;">51</td> </tr> </tbody> </table> |                                      | PROGRAM ELEMENT NO | PROJECT NO. | TASK NO | WORK UNIT ACCESSION NO | 62203F | 3145 | 20 | 51  |  |
| PROGRAM ELEMENT NO  | PROJECT NO.   | TASK NO   | WORK UNIT ACCESSION NO               |                    |             |         |                        |        |      |    |   |  |
| 62203F  | 3145  | 20  | 51                                   |                    |             |         |                        |        |      |    |   |  |
| <b>11. TITLE (Include Security Classification)</b><br>Thermal Energy Storage and Heat Transfer Support Program<br>Vol. II Task 4 - Thermionic Energy Conversion Studies   |   |   |                                      |                    |             |         |                        |        |      |    |   |  |
| <b>12. PERSONAL AUTHOR(S)</b><br>Ramalingam, Mysore L.  |   |   |                                      |                    |             |         |                        |        |      |    |   |  |
| <b>13a. TYPE OF REPORT</b><br>Final   | <b>13b. TIME COVERED</b><br>FROM 7-1-87 TO 9/30/90  | <b>14. DATE OF REPORT (Year, Month, Day)</b><br>1991 March 1  | <b>15. PAGE COUNT</b><br>147         |                    |             |         |                        |        |      |    |   |  |
| <b>16. SUPPLEMENTARY NOTATION</b><br>N/A  |   |   |                                      |                    |             |         |                        |        |      |    |   |  |
| <table border="1" style="width: 100%; border-collapse: collapse;"> <thead> <tr> <th colspan="3">COSATI CODES</th> </tr> <tr> <th style="width: 33%;">F.T.D.</th> <th style="width: 33%;">GROUP</th> <th style="width: 33%;">SUB-GROUP</th> </tr> </thead> <tbody> <tr> <td> </td> <td> </td> <td> </td> </tr> </tbody> </table>   |   | COSATI CODES  |                                      |                    | F.T.D.      | GROUP   | SUB-GROUP              |        |      |    | <b>18. SUBJECT TERMS (Continue on reverse if necessary and identify by block number)</b><br>Thermionics, Energy Conversion, High Temperature,<br>Refractory Alloys, Current Output, Cesium Processing |  |
| COSATI CODES  |   |   |                                      |                    |             |         |                        |        |      |    |   |  |
| F.T.D.  | GROUP   | SUB-GROUP   |                                      |                    |             |         |                        |        |      |    |   |  |
|   |   |   |                                      |                    |             |         |                        |        |      |    |   |  |
| <b>19. ABSTRACT (Continue on reverse if necessary and identify by block number)</b><br><p>This report provides the technical details on the research activities for Task - 4 of Contract# F33615-87-C-2738 during the period of July 87 to August 89. Details on the fabrication and utility installation for the three thermionic diode test stations and the diode processing station are discussed along with the instrumentation for actually testing the diodes. Experimental results as well as analytical characterization results have been provided in the form of J-V characteristics and discrepancies between the two have been explained. Emitter temperature calibration results have also been provided.</p> |   |   |                                      |                    |             |         |                        |        |      |    |   |  |
| <b>20. DISTRIBUTION/AVAILABILITY OF ABSTRACT</b><br><input checked="" type="checkbox"/> UNCLASSIFIED/UNLIMITED <input type="checkbox"/> SAME AS RPT <input type="checkbox"/> DTIC USERS   |   | <b>21. ABSTRACT SECURITY CLASSIFICATION</b><br>UNCLASSIFIED   |                                      |                    |             |         |                        |        |      |    |   |  |
| <b>22a. NAME OF RESPONSIBLE INDIVIDUAL</b><br>Dr. JEFF E. BEAM  |   | <b>22b. TELEPHONE (Include Area Code)</b><br>(513) 255-2922   | <b>22c. OFFICE SYMBOL</b><br>WL/POOS |                    |             |         |                        |        |      |    |   |  |

## FOREWORD

This final report was prepared as part of the contract deliverables under the "Thermal Energy Storage and Heat Transfer Support Program," Contract No. F33615-87-C-2738. This contract was administered by the Aero Propulsion and Power Laboratory (APPL) of Wright Research and Development Center (WRDC) (now Wright Laboratory (WL)) and co-sponsored by the Strategic Defense Initiative Organization (SDIO). Dr. J.E. Beam, Ms. J.E. Johnson, Mr. M. Morgan and Mr. A.S. Reyes were the Air Force Technical Monitors at various stages of this program.

The present report outlines the research effort performed under Task-4, Thermionic Energy Conversion Studies concerning the specific work done on establishing diode test stations and performance mapping of the Lanthanum Hexaboride diode. The other tasks of this program, namely; Task-1, Heat Transport System Studies; Task-2 Thermal Energy Storage Study; Task-3 Innovative Radiator Study and Task-5, Heat Pipe Life Test Study are covered under separate documents.

The entire work described here was performed on-site at the Thermal Laboratory (WL/POOS) by UES, Inc., Dayton, OH with Dr. M.L. Ramalingam as the Principal Investigator for the task and Dr. R. Ponnappan as the Program Manager. Messrs. D. Brigner (UES) and D. Reinmuller (WRDC) provided the technical support. UES Scientific Services Division and Drafting Group provided the documentation services.

The thermionics related activities on this contract were terminated on August 6, 1989 after the completion of the rejuvenation of the NASA, LeRC facilities and successful testing, characterization and verification of the output results on the Lanthanum Hexaboride and Rhenium-Niobium diodes.



|                    |                                     |
|--------------------|-------------------------------------|
| Accession For      |                                     |
| NTIS GRA&I         | <input checked="" type="checkbox"/> |
| DTIC TAB           | <input type="checkbox"/>            |
| Unannounced        | <input type="checkbox"/>            |
| Justification      |                                     |
| By _____           |                                     |
| Distribution/      |                                     |
| Availability Codes |                                     |
| Dist               | Avail and/or Special                |
| A-1                |                                     |

## TABLE OF CONTENTS

| <b>SECTION</b> | <b>TITLE</b>   | <b>PAGE</b> |
|----------------|--|-------------|
| I              | INTRODUCTION .....   | 1           |
|                | 1.1 The Diminiode Test Stations .....  | 2           |
|                | 1.2 The TECO Diode Test Station .....  | 4           |
|                | 1.3 The Diode Processing Station .....   | 6           |
| II             | INSTRUMENT CALIBRATION AND ANALYSIS .....  | 9           |
|                | 2.1 Emitter Temperature to Output Voltage<br>Calibration (LaB <sub>6</sub> ) ..... | 9           |
|                | 2.2 Emitter Temperature to Output Voltage<br>Calibration (ASTAR-811C) .....        | 11          |
| III            | EXPERIMENTAL SETUP .....   | 22          |
|                | 3.1 Diminiode Test Stations .....  | 22          |
|                | 3.1.1 Vacuum System .....  | 22          |
|                | 3.1.2 Emitter Heating and Temperature<br>Measurement System .....                  | 22          |
|                | 3.1.3 Output Load System .....   | 24          |
|                | 3.1.4 Data Acquisition/Processing System .....                                     | 31          |
|                | 3.1.5 Electrode Cooling System .....   | 33          |
|                | 3.1.6 General Electrical Schematics and<br>Associated Components Design .....      | 35          |
|                | 3.2 TECO Diode Test Station .....  | 35          |
|                | 3.3 Diode Processing Station .....   | 42          |
|                | 3.3.1 Vacuum Processing the Diode .....  | 42          |
|                | 3.3.2 Cesium Reservoir Sealing Technique .....                                     | 43          |
| IV             | DIODE TESTING PROCEDURE .....  | 45          |
|                | 4.1 Performance Verification Testing .....   | 45          |
|                | 4.2 Primary Variables Optimization .....   | 45          |

## TABLE OF CONTENTS (Cont'd)

| <u>SECTION</u> | <u>TITLE</u>  | <u>PAGE</u> |
|----------------|---|-------------|
| V              | <b>RESULTS AND DISCUSSIONS</b> .....                    | 47          |
|                | 5.1 <b>Thermionic Emission Characteristics from</b>     |             |
|                | <b>Lanthanum Hexaboride</b> .....                       | 47          |
|                | 5.1.1 <b>Verification of Performance</b> .....          | 48          |
|                | 5.1.2 <b>Multi-Stage Cesium Reservoir Temperature</b>   |             |
|                | <b>Optimization</b> .....                               | 51          |
|                | 5.1.3 <b>Multi-Stage Collector Temperature</b>          |             |
|                | <b>Optimization</b> .....                               | 61          |
|                | 5.1.4 <b>Emitter Temperature</b>                        |             |
|                | <b>Optimization</b> .....                               | 70          |
|                | 5.1.5 <b>Ignition and De-ignition Studies</b> .....     | 75          |
|                | 5.2 <b>ASTAR-811C Diode Performance</b> .....           | 86          |
|                | 5.2.1 <b>Current and Power Density</b>                  |             |
|                | <b>Characteristics</b> .....                            | 87          |
|                | 5.3 <b>Performance of the Etched Rhenium-Niobium</b>    |             |
|                | <b>Diode</b> .....                                      | 89          |
|                | 5.3.1 <b>General Performance</b> .....                  | 89          |
|                | 5.3.2 <b>Peak Power Density as a Function of</b>        |             |
|                | <b>Emitter Temperature</b> .....                        | 89          |
|                | 5.4 <b>Characterization of the Lanthanum Hexaboride</b> |             |
|                | <b>Diode with a 1-D Code</b> .....                      | 89          |
|                | 5.4.1 <b>Code Description and Simulation</b>            |             |
|                | <b>Procedure</b> .....                                  | 92          |
|                | 5.4.2 <b>Performance of the Code</b> .....              | 96          |
|                | 5.4.3 <b>Application of the Code</b> .....              | 104         |
| VI             | <b>CONCLUSIONS AND FUTURE ACTIVITIES</b> .....          | 108         |

## LIST OF TABLES

| <b>TABLE</b> | <b>TITLE</b>   | <b>PAGE</b> |
|--------------|--|-------------|
| 2.1          | Error Limits for Analytical Plots (LaB <sub>6</sub> ) .....  | 15          |
| 2.2          | Error Limits for Analytical Plots (ASTAR-811C) .....   | 21          |
| 3.1          | Diode Performance with Shunt on the Collector<br>Side and No Resistance on the Guard Side .....      | 27          |
| 3.2          | Diode Performance with Various Resistances on<br>the Guard Side .....                                | 28          |
| 3.3          | Diode Performance with Shunt on the Emitter Side<br>and No Resistance on the Guard Side .....        | 29          |
| 3.4          | Diode Performance with Shunt on the Emitter Side<br>and 2.5 k-ohm Resistance on the Guard Side ..... | 30          |
| 5.1          | Summary of Important Parameters for the Performance<br>Tests on the Lanthanum Hexaboride Diode ..... | 52          |
| 5.2          | Ignition Point Current Densities and Output Voltages<br>for Various Emitter Temperatures .....       | 79          |
| 5.3          | Cesium Reservoir Temperature Optimization Ignition<br>Test Results .....                             | 82          |
| 5.4          | Collector Temperature Optimization Ignition<br>Test Results .....                                    | 83          |

## LIST OF FIGURES

| <b>FIGURE</b> | <b>TITLE</b>   | <b>PAGE</b> |
|---------------|--|-------------|
| 1.1           | A Cross-Sectional View of the Lanthanum<br>Hexaboride Diminiode .....                        | 3           |
| 1.2           | A Cross-Sectional View of the TECO Fixed<br>Gap Diode .....                                  | 5           |
| 1.3           | Cutaway View of the Multipurpose Diode<br>Processing Chamber .....                           | 7           |
| 2.1           | Final Correlation between Emitter Temperature<br>and Pyrometer Output Voltage .....          | 10          |
| 2.2           | Optical Pyrometer Temperature as a Function<br>of the Pyrometer Output Voltage .....         | 12          |
| 2.3           | Diode Target Temperature as a Function of the<br>Pyrometer Temperature .....                 | 13          |
| 2.4           | Emitter Temperature as a Function of the Diode<br>Target Temperature .....                   | 14          |
| 2.5           | Experimental Calibration Data and Polynomial<br>Fit for ASTAR-811C Diode .....               | 18          |
| 2.6           | Actual Emitter Temperature Versus Pyrometer Output<br>Voltage for the ASTAR-811C Diode ..... | 19          |
| 3.1           | Schematic Representing Experimental Setup and<br>Associated Subsystems .....                 | 23          |
| 3.2           | Simplified Electrical Schematic for the Output<br>Load Circuit .....                         | 25          |
| 3.3           | Computer System Design for Data Acquisition<br>and Processing .....                          | 32          |
| 3.4           | Water Cooling System Schematic for the Test<br>Station .....                                 | 34          |

## LIST OF FIGURES (Cont'd)

| <u>FIGURE</u> | <u>TITLE</u>  | <u>PAGE</u> |
|---------------|---|-------------|
| 3.5           | Electrical Schematic for Filament and High Voltage<br>Control Panel .....                                       | 36          |
| 3.6           | Electrical Schematic for the High Voltage<br>Power Supply .....   | 37          |
| 3.7           | Electrical Schematic for Cesium and Collector<br>Heaters Control Panel .....                                    | 38          |
| 3.8           | Electrical Schematic for the Signal Cycles Board .....  | 39          |
| 3.9           | Safety Interlock Circuit Schematic for the TECO<br>Diode Station .....  | 40          |
| 3.10          | Air Cooling System Schematic for the TECO<br>Diode Station .....  | 41          |
| 5.1           | Output Current Density and Output Power Density -<br>NASA Characteristics .....                                 | 49          |
| 5.2           | Comparison of Output Characteristics with the<br>Emitter at 1700 K .....  | 50          |
| 5.3           | Output Current Density Characteristics for<br>Various Cesium Reservoir Temperatures .....                       | 54          |
| 5.4           | Output Power Density Characteristics for Various<br>Cesium Reservoir Temperatures .....                         | 55          |
| 5.5           | Optimized Electrode Output Current Density<br>Characteristic Envelope for Cesium Pressure .....                 | 57          |
| 5.6           | Optimized Electrode Output Power Density<br>Characteristic Envelope for Cesium Pressure .....                   | 58          |
| 5.7           | Effects of Cesium Reservoir Temperature on the<br>Short Circuit Current Density and Peak<br>Power Density ..... | 59          |

**LIST OF FIGURES (Cont'd)**

| <b><u>FIGURE</u></b> | <b><u>TITLE</u></b>  | <b><u>PAGE</u></b> |
|----------------------|--|--------------------|
| 5.8                  | Final Stage Cesium Reservoir Temperature Optimized<br>Output Current Density Characteristics .....       | 62                 |
| 5.9                  | Final Stage Cesium Reservoir Temperature Optimized<br>Output Power Density Characteristics .....         | 63                 |
| 5.10                 | Output Current Density Characteristics for Various<br>Collector Temperatures .....                       | 64                 |
| 5.11                 | Output Power Density Characteristics for Various<br>Collector Temperatures .....                         | 65                 |
| 5.12                 | Optimized Electrode Output Current Density<br>Characteristic Envelope for Collector<br>Temperature ..... | 67                 |
| 5.13                 | Optimized Electrode Output Power Density Envelope for<br>Collector Temperature .....                     | 68                 |
| 5.14                 | Effects of Collector Temperature on the Short Circuit<br>Current Density and Peak Power Density .....    | 69                 |
| 5.15                 | Final Stage Collector Temperature Optimized Output<br>Current Density Characteristics .....              | 71                 |
| 5.16                 | Final Stage Collector Temperature Optimized Output<br>Power Density Characteristics .....                | 72                 |
| 5.17                 | Output Current Density Characteristics for Various<br>Emitter Temperatures .....                         | 73                 |
| 5.18                 | Optimized Electrode Output Current Density<br>Characteristic Envelope for Emitter<br>Temperature .....   | 74                 |
| 5.19                 | Output Power Density Characteristics for Various<br>Emitter Temperatures .....                           | 76                 |

## LIST OF FIGURES (Cont'd)

| <b>FIGURE</b> | <b>TITLE</b>  | <b>PAGE</b> |
|---------------|---|-------------|
| 5.20          | Optimized Electrode Output Power Density Characteristic<br>Envelope for Emitter Temperature .....                 | 77          |
| 5.21          | Effects of Emitter Temperature on the Short Circuit<br>Current Density and Peak Power Density .....               | 78          |
| 5.22          | Experimental Data and Linear Approximation for<br>Variation of Ignition Voltage with Emitter<br>Temperature ..... | 80          |
| 5.23          | Ignition Characteristics for Cesium Reservoir<br>Temperature Optimization .....                                   | 84          |
| 5.24          | Ignition Characteristics for Collector<br>Temperature Optimization .....  | 85          |
| 5.25          | Output Characteristics of ASTAR-811C Diode for a<br>Cesium Reservoir Temperature of 651 K .....                   | 88          |
| 5.26          | Output Characteristics of Re-Nb Diode for a Cesium<br>Reservoir Temperature of 473 K .....                        | 90          |
| 5.27          | Variation of Peak Power Density as a Function of<br>Emitter Temperature .....                                     | 91          |
| 5.28          | Flow Chart for Repeated Runs of the TEC Program .....   | 93          |
| 5.29          | Flow Chart for the One-Dimensional TEC Program .....  | 94          |
| 5.30          | Simulated Characteristics for Various Iterations and<br>a Cesium Pressure of 1.0 Torr .....                       | 97          |
| 5.31          | Simulated Characteristics for Various Iterations and<br>a Cesium Pressure of 0.5 Torr .....                       | 98          |
| 5.32          | Simulated Characteristics for Various Iterations<br>and a Cesium Pressure of 0.1 Torr .....                       | 99          |

## LIST OF FIGURES (Cont'd)

| <b>FIGURE</b> | <b>TITLE</b>  | <b>PAGE</b> |
|---------------|---|-------------|
| 5.33          | Operation Under Various Emitter Temperatures for<br>High Cesium Vapor Pressures .....                         | 101         |
| 5.34          | Operation Under Varied Collector Temperatures for High<br>Cesium Vapor Pressures .....                        | 102         |
| 5.35          | Operation Under Varied Emitter Temperatures and Lower<br>Cesium Pressures .....                               | 103         |
| 5.36          | Operation Under Varied Collector Temperatures for<br>Lower Cesium Pressures .....                             | 105         |
| 5.37          | Simulated Characteristics Corresponding to<br>Experimental Cesium Reservoir Temperature<br>Optimization ..... | 106         |

## NOMENCLATURE

|       |   |
|-------|---|
| AC    | Alternating Current                           |
| A/D   | Analog to Digital                             |
| AFWAL | Air Force Wright Aeronautical Laboratories    |
| APL   | Aero Propulsion Laboratory                    |
| ART   | Applied Research and Technology               |
| ASU   | Arizona State University                      |
| ATI   | Advanced Thermionic Initiative                |
| DC    | Direct Current                                |
| EB    | Electron Bombardment                          |
| HIPP  | Hot Isostatic Pressing Process                |
| HP    | Hewlett Packard                               |
| IST   | Innovative Science and Technology             |
| JPL   | Jet Propulsion Laboratory                     |
| J-V   | Output Current Density-Voltage                |
| LaB6  | Lanthanum Hexaboride                          |
| LeRC  | Lewis Research Center                         |
| NASA  | National Aeronautics and Space Administration |
| P     | Peak Power Density                            |
| PC    | Personal Computer                             |
| $T_E$ | Emitter Temperature                           |
| $T_P$ | Pyrometer Temperature                         |
| $T_T$ | Target Temperature                            |
| TEC   | Thermionic Energy Conversion                  |
| WPAFB | Wright-Patterson Air Force Base               |
| WRDC  | Wright Research and Development Center        |
| Z-248 | Zenith 248                                    |

## SECTION I

### INTRODUCTION

Thermionic Energy Conversion (TEC) was part of the space nuclear research activities being investigated at NASA Lewis Research Center (LeRC) in the early seventies [1,2]. Before the termination of these activities in 1973, Lanthanum Hexaboride ( $\text{LaB}_6$ ) was one of the important materials being studied as a part of the diode-screening project [3]. The TEC activities were then continued at LeRC by NASA's applied research technology (ART) program [4]. The TEC-ART activities were terminated due to programmatic retrenchment and transferred to the Jet Propulsion Lab (JPL) where the research on metal hexaboride has since received less prominence [5,6].

A twin diminiode station, a TECO diode station and diode processing station were acquired by the Aero Propulsion Laboratory of WRDC/WPAFB, in 1987. These stations are now currently being rejuvenated and upgraded with improved instrumentation and testing facilities. The planar diminiode tested in the twin station has an emitter made from sintered  $\text{LaB}_6$  and a collector made from arc melted  $\text{LaB}_6$ . The constructional details and configuration are explained in detail in earlier documents [7,8,9,10,11]. However the details of the instrumentation and the data acquisition and processing system used were different, and this report provides some of the details on these aspects. Before actually conducting the optimization tests, an initial sequence of tests was conducted to verify the performance of the diminiode. In this sequence of tests, the cesium reservoir temperature was maintained at 460 K, and the collector temperature was maintained at 900 K while the emitter temperature was varied from 1500 K to 1700 K in intervals of 50°C. Both current density and power density characteristics were generated at various emitter temperatures and compared with similar results obtained at NASA LeRC. These results and some of the calibration requirements for measuring the emitter temperature accurately are discussed in this report along with certain important features in the characteristics such as ignition point and de-ignition point, open circuit voltage and short circuit current. After confirming the normal operation of the diminiode as well as the testing facility, a test plan was generated and executed for the first and second stage optimization tests.

## 1.1 The Diminiode Test Stations

This constitutes a pair of diminiode test stations that were combined to form one unit with several common facilities that were either activated or de-activated depending on which test station was in operation. These two stations were well equipped to test variable gap, small electrode, planar diodes which could be mounted along with their cooling consoles, directly to a 6-inch-diameter flange. The vacuum chambers were water cooled but the diode components themselves were equipped to provide either water or gas cooling.

Figure 1.1 shows the cross-section of the NASA diminiode as reproduced from Ref. 1. The base of the diminiode consists of three concentric conductors (niobium, 1% zirconium) bonded together with intervening annuli of aluminum oxide insulation. The bonding of the conductors to the insulators was done by the Hot Isostatic Pressing Process (HIPP). By using this construction method, low resistance electrical paths were provided for the collector and guard. The center and second steps at the bottom of the diminiode base served as the electrical taps for the collector and guard.

The cap of the diminiode consists of a tantalum electron bombardment target. This top piece was located on the machined shoulders of a standard tantalum tube. The tube was attached to the diminiode base and served as the cesium reservoir. Cesium was sealed in the tube after internal degassing and initial pyrometry calibrations were completed. The sealing of the reservoir was conducted in a specially designed station and was completed by brazing the tantalum ball in place.

The collector and guard were cut from the same material and were attached to the diminiode base by diffusion bonding or high temperature brazing. The outside diameter for the guard corresponds to the diameter of the emitter, which was fusion bonded to the diminiode cap and electron bombardment target.

Thermocouples measured the cesium reservoir, collector and guard temperatures. Optical pyrometry was used to measure the electron bombardment target temperature which was then

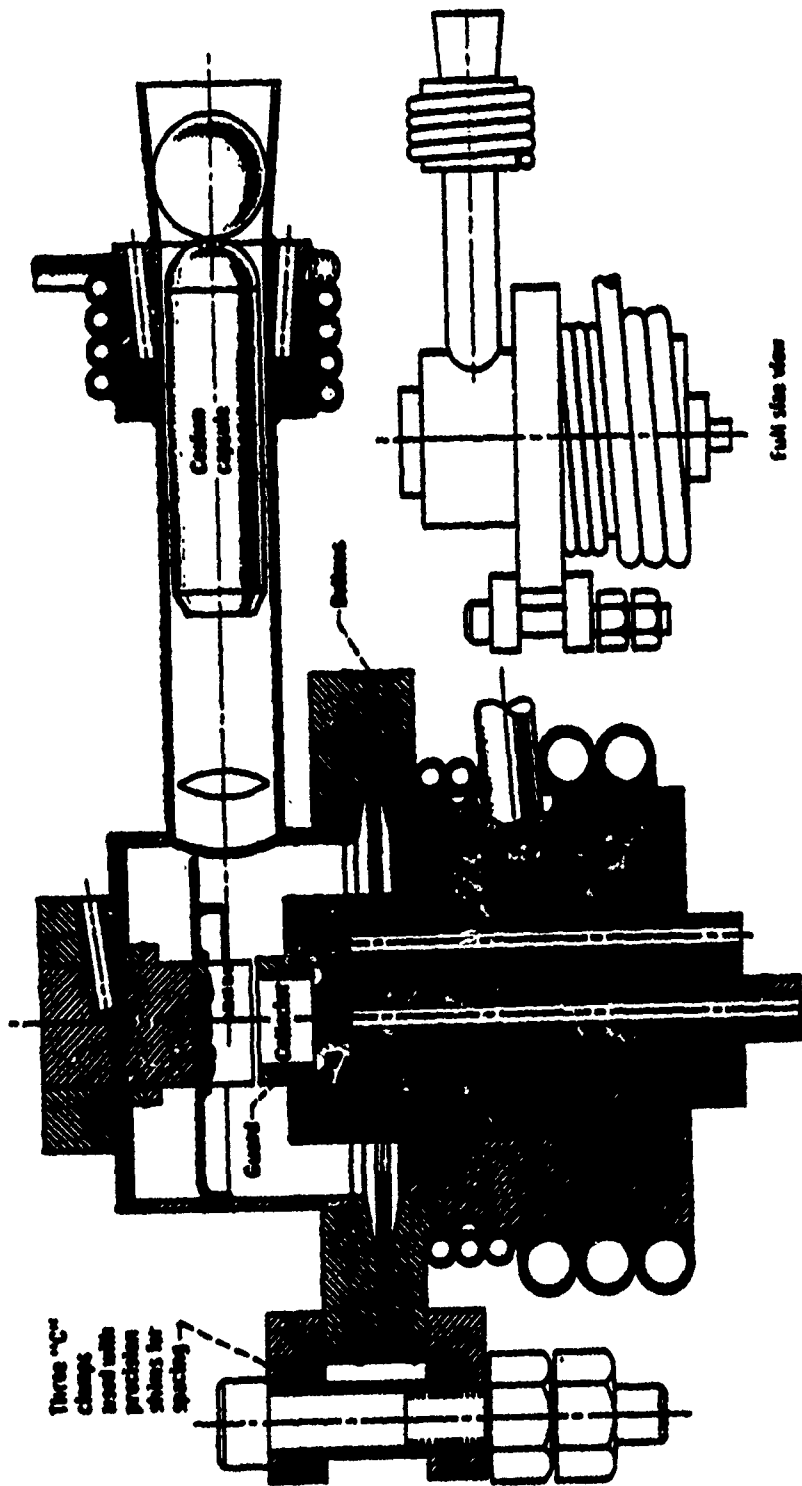


Figure 1.1 A Cross-Sectional View of the Lanthanum Hexaboride Diminide.

converted to the emitter temperature through a series of calibration curves. The emitter was heated by electron bombardment and thermal control coils were used to adjust the temperature of the guarded collector and cesium reservoir. Though a provision for adjusting the interelectrode gap, by placing precision shims between a simple diaphragm bellows, was provided, the gap was not changed during the course of the tests conducted after rejuvenation of the facility. It was maintained constant at the last tested value of 0.25 mm.

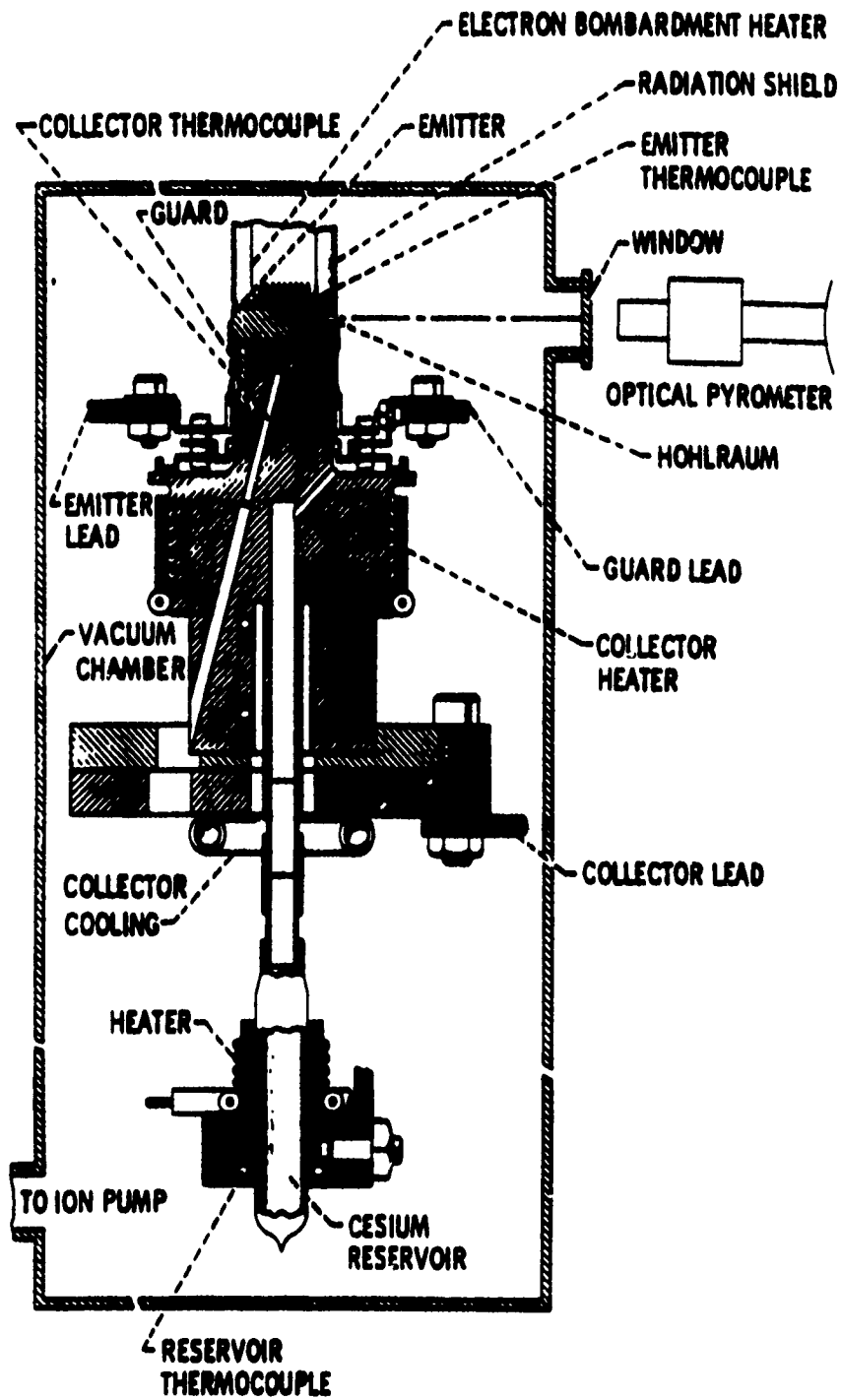
## 1.2 The TECO Diode Test Station

This is a diode test station that was originally developed to test planar diodes with cesium reservoirs located away from the interelectrode gap. These diodes were developed by Thermo-Electron Corp. and tested at NASA, LeRC. As most of the equipment on this station were either destroyed or missing, except for the vacuum system and chamber, the entire station had to be rebuilt with new equipment. Unlike the diode test stations, the diode was mounted to a framework within the vacuum chamber.

Figure 1.2 shows the cross-sectional drawing of the guard ring diode. The collector body and leadthrough flanges are fabricated from niobium. The tubulation and cesium reservoir are fabricated from copper and joined to the niobium collector by an intermediate nickel joint. The lower portion of the collector accommodates both the collector heaters and a calorimeter section for measuring heat through the collector. This calorimeter can be calibrated by the collector heaters.

The guard ring is fabricated by casting the sapphire between two niobium tubes and then shrink-fitting this composite tube over the collector body. The assembled shrink fit is then diffusion-bonded by a four-hour exposure to 1600°C in vacuum. After diffusion bonding, the collector and guard ring are machined for final assembly.

The emitter, which has been fabricated from rhenium, is supported by a rhenium sleeve which is in turn supported by a niobium leadthrough flange. The emitter-to-sleeve and sleeve-to-flange joints are made by electron beam welds. The emitter lead, the guard ring lead and the



CONVERTER CONFIGURATION

Figure 1.2 Cross-Sectional View of the TECO Fixed Gap Diode.

diode sealing flange are insulated from one another by copper-nickel braided alumina insulators. The guard ring lead is electrically connected to the guard ring by a threaded connection. Final assembly of the diode is made by screwing this emitter assembly into the collector body with the guard ring leadthrough engaging mating threads on the guard ring. The emitter assembly is then welded to the collector body. The diode structure is then provided with necessary heating and cooling coils to complete the immediate instrumentation needs. As in the diminiode test stations, thermocouples were used to measure the cesium reservoir, collector and guard ring temperatures, and optical pyrometry was used to measure the electron bombardment target temperature initially but then it was replaced with a W-Re thermocouple when the emitter temperature controller was acquired.

### 1.3 The Diode Processing Station

Figure 1.3 is a cutaway view of the multipurpose vacuum chamber that is used for diminiode processing which includes bake out, filling and sealing of cesium [7]. In this chamber following only one pump-down the diminiode mode of baked-out components undergoes a final high temperature degassing, internal and external pyrometry, and fusion sealing after the cesium capsule insertion. The cesium itself was an off-the-shelf component like the other interchangeable parts of the diminiode. A cesium ampule, a degassed tantalum ball and a diminiode go into the station before its closure. Then, after the pump down and degassing at 450°C to below  $10^{-6}$  torr, the diminiode enters the final stages of processing.

As electron bombardment heats the emitter assembly, continual thermal sensing and coolant adjustments bring the diminiode to predetermined bake-out conditions. That state depends on the electrodes, the brazes and the insulator limit. During temperature rise, the pyrometric cavity in the emitter allows calibrations of the tungsten lined external black body hole and the high temperature thermocouple. The outer black body hole then permits emitter-temperature calibrations subsequent to closing the diminiode. This capability enables checking output shifts of the high temperature thermocouples, using high temperature pyrometry. While the diminiode is at maximum degassing temperatures, electron bombardment of the open end of the reservoir to just below the melting point of the copper-foil insert prepares it for the brazed

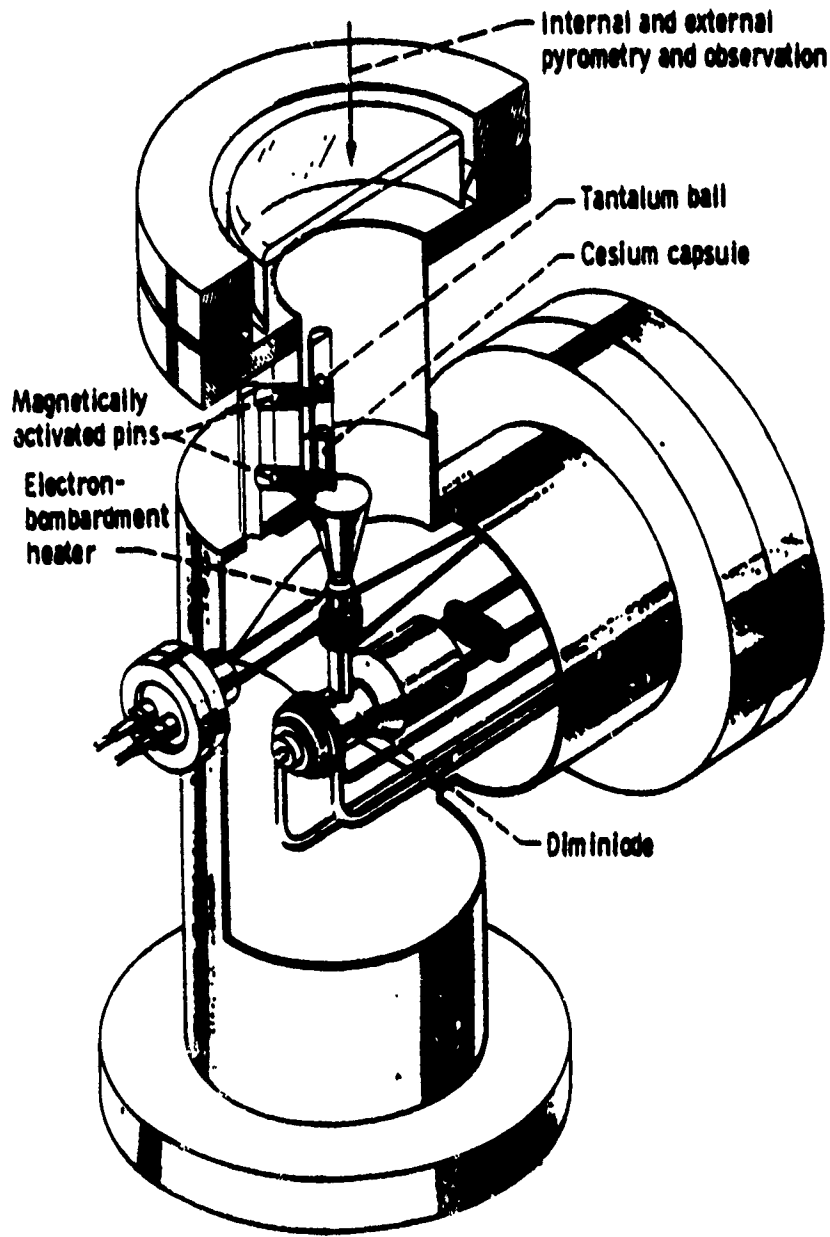


**Figure 1.3** Cutaway View of the Multipurpose Diode Processing Chamber.

closure. Following this part of the bake-out, cooling gives a downward calibration to check the upward one. Next, magnetically pulling the lower pin in the guide tube drops the cesium caprile into the diminiode reservoir. If the pressure rises, another brief bake-out removes contaminants.

The same process follows the release of the previously degassed tantalum sphere, which lodges in the funnel opening of the side tube. Then electron bombardment brazes this ball in the end of the reservoir with copper. This completes the processing phase of a new diminiode.

The diode/diminiode processing station is currently being equipped with new emitter, collector and cesium reservoir temperature controllers. A design for a mock-up device has been completed in order to establish optimum operating parameters for an efficient cesium reservoir seal.

## SECTION II

### INSTRUMENT CALIBRATION AND ANALYSIS

The construction of the diimide is such that it is a vacuum sealed device, so it is not possible to measure the temperature of the emitter directly. However, when these devices were originally fabricated, NASA Lewis engineers calibrated the target temperature as a function of the emitter temperature. Thus progressive corrections had to be applied in several stages to arrive at the accurate emitter temperature. This section provides details on the calibration procedures and the corrections applied to the pyrometer output in order to obtain the actual emitter temperature.

A manually balanced disappearing filament pyrometer was used to measure emitter temperature. Measuring the emitter temperature was accomplished by focusing the pyrometer on the black-body cavity located in the electron bombardment target. A voltage signal corresponding to the temperature of the electron bombardment target was sent to the data acquisition system from the pyrometer. The data acquisition system was programmed to sense this voltage signal, convert it to a digital form and send it to the computer. A computer program corrects the voltage signal for several factors causing attenuation, such as the energy scatter created by the sapphire viewport, the temperature gradient between emitter and target, etc. The correction was accomplished with several equations generated by analytical curve fitting techniques. This allowed the emitter temperature to be read directly from the computer screen.

#### 2.1 Emitter Temperature to Output Voltage Calibration (L&B)

Figure 2.1 represents the final correlation between emitter temperature and pyrometer output voltage for the three scales representing the entire temperature range over which the emitter could possibly be heated. The temperature corresponding to the three scales were

Scale - 1: 700°C to 1350°C

Scale - 2: 1350°C to 1850°C

Scale - 3: 1850°C to 2500°C

# EMITTER TEMPERATURE Vs. OUTPUT VOLTAGE

(Plots of calculated values after conversion)

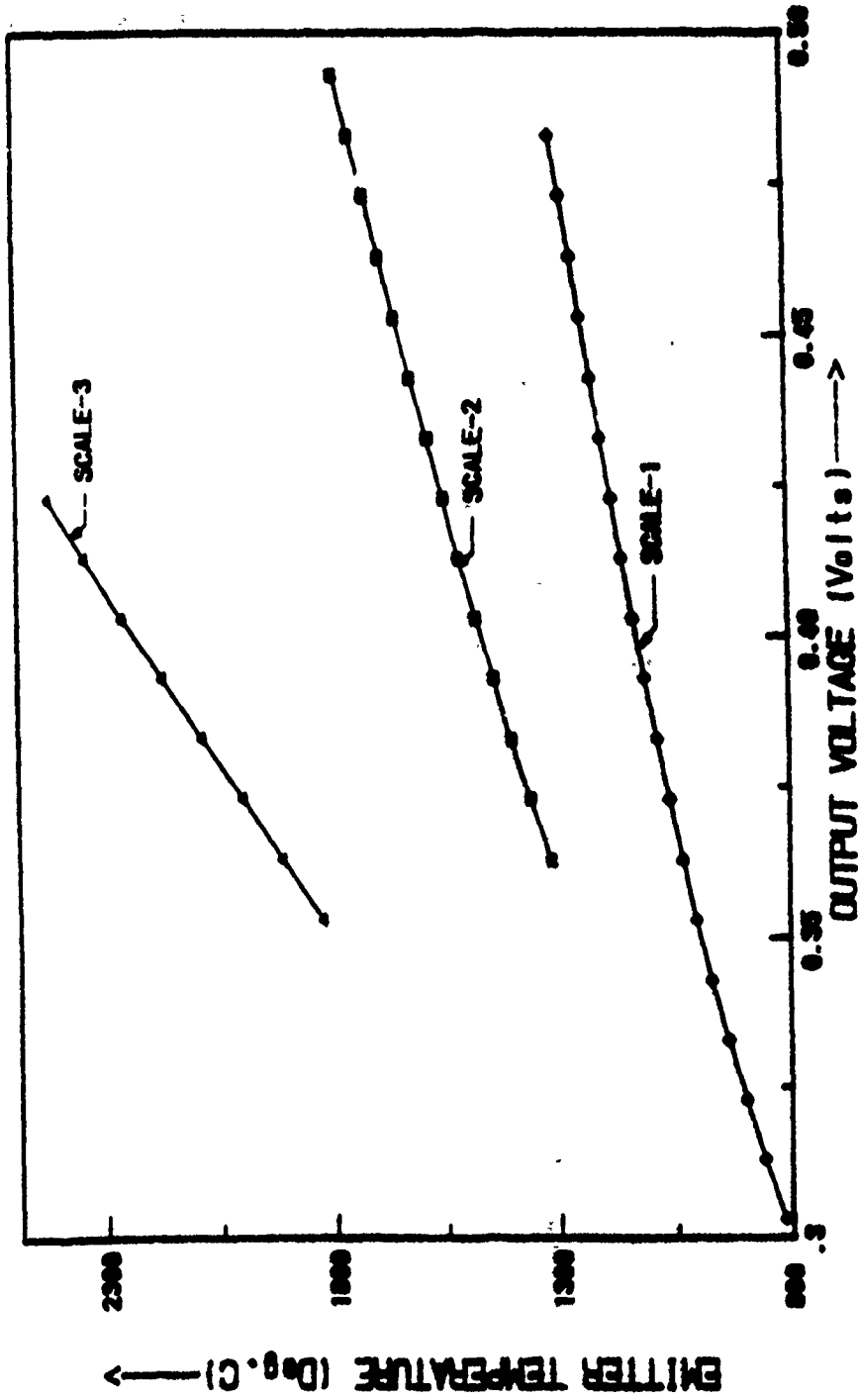


Figure 2.1 Final Correlation between Emitter Temperature and Pyrometer Output Voltage.

Though the calibration data were not available over the range of each scale, it was suitably extrapolated without introducing any large systematic errors. Figure 2.1 is the outcome of three stages of conversions viz., a) conversion of output voltage to pyrometer temperature, (Figure 2.2) b) conversion of optical pyrometer temperature to target temperature (Figure 2.3) and c) conversion of target temperature to emitter temperature (Figure 2.4). Only the final calculated values after conversion are indicated in the figure, for each of the three scales. The corresponding analytical equations were represented by the following relations;

$$T_e = 39137.204 (V_o)^3 - 52699.16 (V_o)^2 + 25665.662 (V_o) - 3211.25 \quad (2.1)$$

(for  $700 \leq T \leq 1350^\circ\text{C}$ )

$$T_e = 25633.516 (V_o)^3 - 37154.638 (V_o)^2 + 21232.537 (V_o) - 2723.734 \quad (2.2)$$

(for  $1350 \leq T \leq 1850^\circ\text{C}$ )

$$T_e = 8444.806 (V_o)^3 - 12127.68 (V_o)^2 + 14152.041 (V_o) - 2028.642 \quad (2.3)$$

(for  $1850 \leq T \leq 2500^\circ\text{C}$ )

However, the error limits for all the conversions are presented in Table 2.1. From the table it was observed that the highest value for maximum error was 1.96% and the lowest value for minimum error was 0.0007%. Equations (2.1), (2.2), and (2.3) were incorporated in the software for performance and optimization testing and accessed with function switches whenever needed.

## 2.2 Emitter Temperature to Output Voltage Calibration (ASTAR-811C)

The ASTAR-811C diode had a Tantalum alloy as the emitter and Niobium/Zirconium as the collector. Details of the various calibration curves and the corresponding curve fits are as follows:

The temperature range for the emitter was divided into four scales:

Scale - 1:  $850^\circ\text{C}$  to  $1250^\circ\text{C}$

Scale - 2:  $1250^\circ\text{C}$  to  $1600^\circ\text{C}$

Scale - 3:  $1600^\circ\text{C}$  to  $1900^\circ\text{C}$

Scale - 4:  $1900^\circ\text{C}$  to  $2500^\circ\text{C}$

# PYROMETER TEMPERATURE Vs. OUTPUT VOLTAGE

(SC-1=700-1350C; SC-2=1350-1850C; SC-3=1850-2500C)

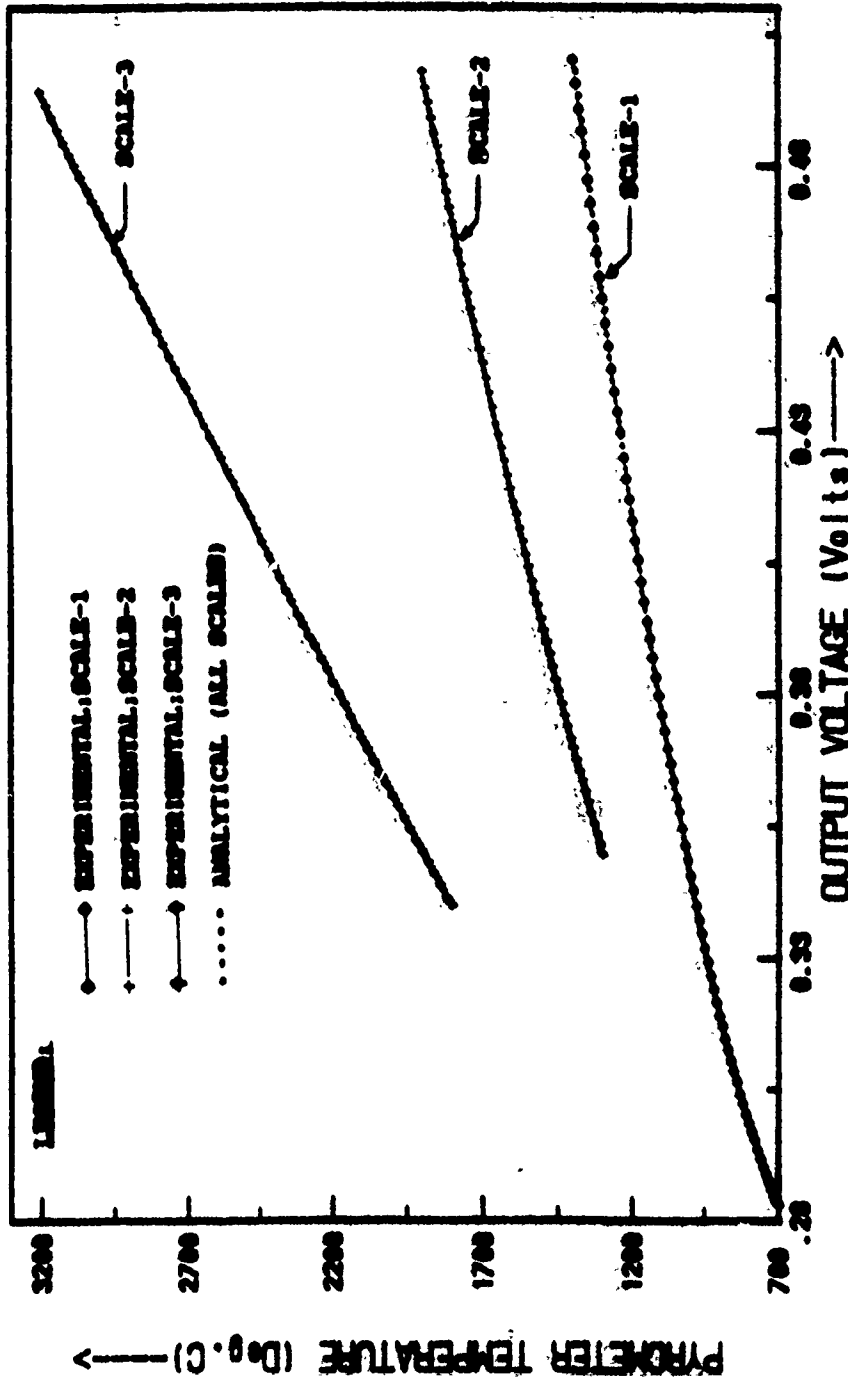


Figure 2.2 Optical Pyrometer Temperature as a Function of the Pyrometer Output Voltage.

TARGET Vs. OPT. PYROMETER TEMPERATURE  
 (SC-1=700-1350C; SC-2=1350-1850C; SC-3=1850-2500C)

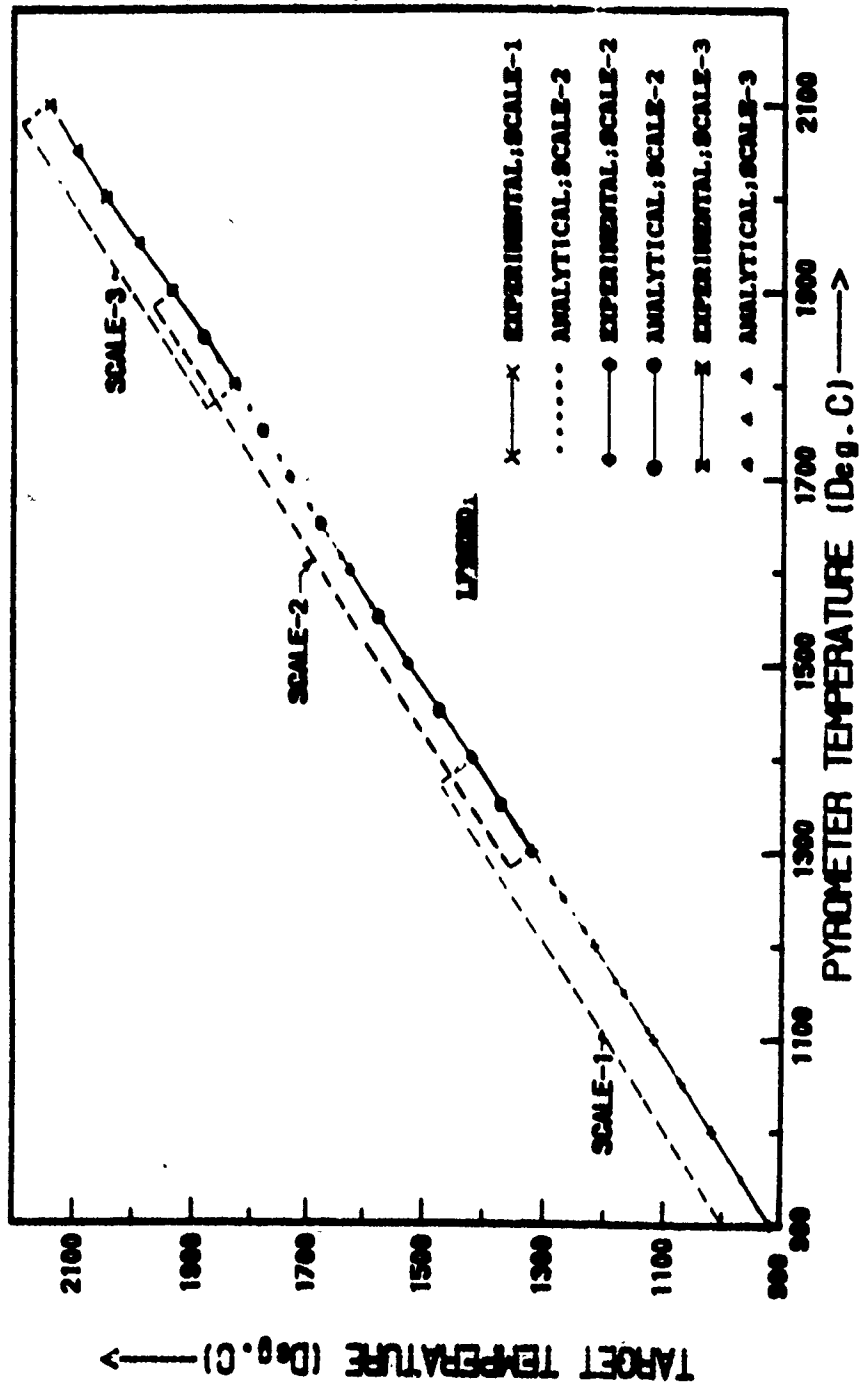


Figure 2.3 Diode Target Temperature as a Function of the Pyrometer Temperature.

# EMITTER Vs. TARGET TEMPERATURE

(Experimental & Analytical Plots for Le86 Diminide)

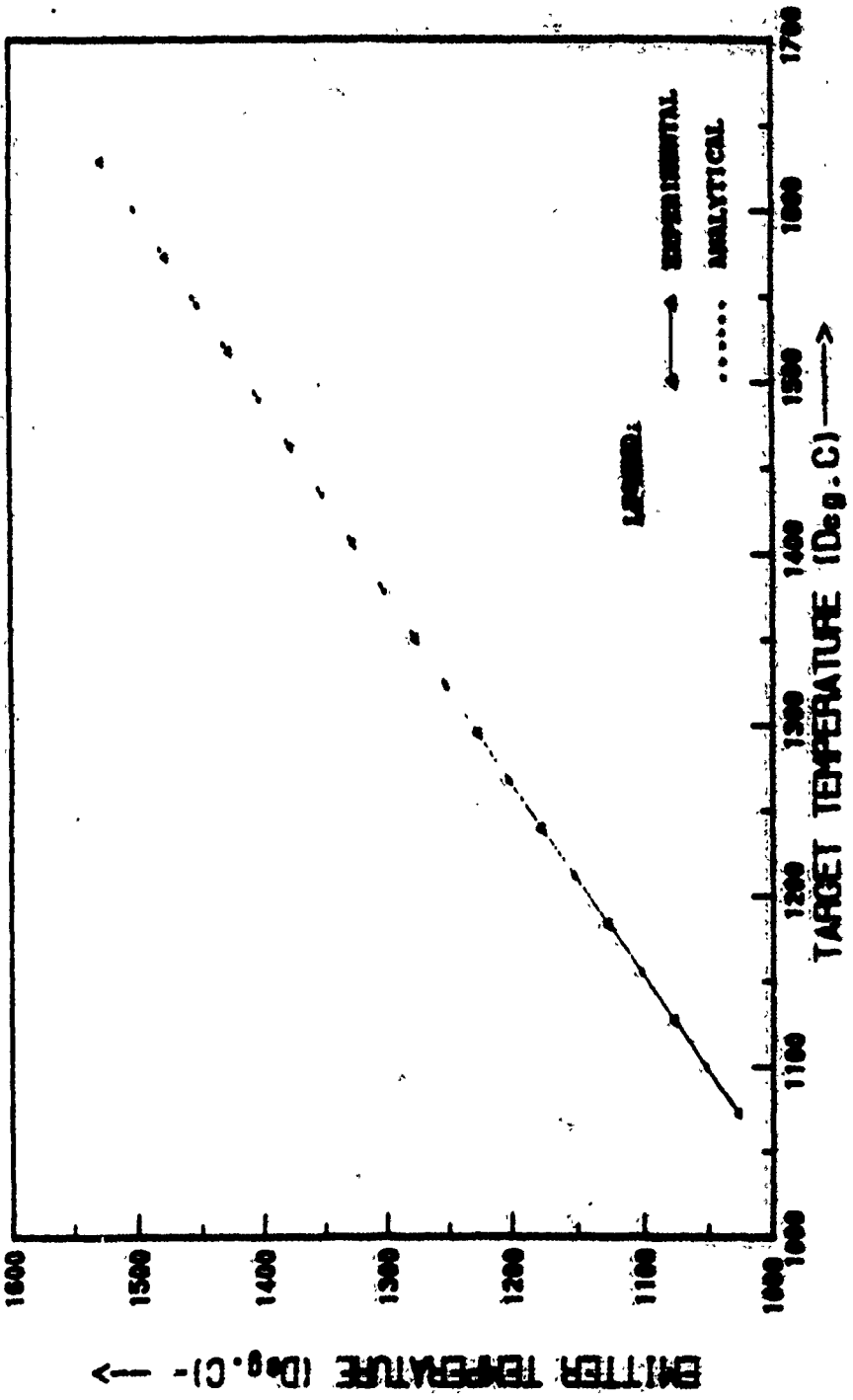


Figure 2.4 Emitter Temperature as a Function of the Diode Target Temperature.

Table 2.1 Error Limits for Analytical Plots (LaB<sub>6</sub>).

| Sl. No. | Conversion                        | Scale $\beta$ | Maximum Error(%)        | Minimum Error(%)        | Average Error(%)        | RMS Error(%)            |
|---------|-----------------------------------|---------------|-------------------------|-------------------------|-------------------------|-------------------------|
| 1       | Emitter Temp. to Target Temp.     | -             | -3.478x10 <sup>-2</sup> | -2.713x10 <sup>-3</sup> | +3.779x10 <sup>-6</sup> | +6.326x10 <sup>-3</sup> |
| 2       | Target Temp. to Pyrometer Temp.   | 1             | -0.1338                 | +7.819x10 <sup>-4</sup> | +6.359x10 <sup>-4</sup> | +0.0293                 |
| 3       | Target Temp. to Pyrometer Temp.   | 2             | +0.2364                 | +7.024x10 <sup>-2</sup> | -1.028x10 <sup>-4</sup> | +0.0614                 |
| 4       | Target Temp. to Pyrometer Temp.   | 3             | -0.2591                 | -0.0103                 | +6.367x10 <sup>-4</sup> | +8.749x10 <sup>-2</sup> |
| 5       | Pyrometer Temp. to Output Voltage | 1             | +1.9664                 | +0.0176                 | +5.002x10 <sup>-2</sup> | +5.556x10 <sup>-2</sup> |
| 6       | Pyrometer Temp. to Output Voltage | 2             | +0.2703                 | -6.426x10 <sup>-3</sup> | +9.133x10 <sup>-3</sup> | +1.271x10 <sup>-2</sup> |
| 7       | Pyrometer Temp. to Output Voltage | 3             | -0.2200                 | +9.328x10 <sup>-4</sup> | -6.811x10 <sup>-3</sup> | +1.052x10 <sup>-2</sup> |

a) Conversion of Output Voltage to Pyrometer Temperature

Since this is a function of the pyrometer itself, it is not expected to change from one diode to another. Polynomial curve fits were generated for each scale according to the following equations:

$$T_p = 43330.322 (V_o)^3 - 58345.293 (V_o)^2 + 28415.454 (V_o) - 3637.663 (\pm 1.97\%) \quad (2.4)$$

(for  $850^\circ\text{C} \leq T \leq 1250^\circ\text{C}$ )

$$T_p = 27906.683 (V_o)^3 - 40449.992 (V_o)^2 + 23115.427 (V_o) - 3026.804 (\pm 0.27\%) \quad (2.5)$$

(for  $1250^\circ\text{C} \leq T \leq 1600^\circ\text{C}$ )

$$T_p = 27906.683 (V_o)^3 - 40449.992 (V_o)^2 + 23115.427 (V_o) - 3026.804 (\pm 0.27\%) \quad (2.6)$$

(for  $1600^\circ\text{C} \leq T \leq 1900^\circ\text{C}$ )

$$T_p = 9060.329 (V_o)^3 - 13022.368 (V_o)^2 + 15183.551 (V_o) - 2211.006 (\pm 0.227\%) \quad (2.7)$$

(for  $1900^\circ\text{C} \leq T \leq 2500^\circ\text{C}$ )

Here,  $V_o$  represents the pyrometer output voltage and  $T_p$  represents the optical pyrometer temperature.

b) Conversion of Optical Pyrometer Temperature to the Target Temperature

This is a function of the attenuation that the viewport offers to the radiation being emitted from the source. The variations for these parameters were found to be linear and could be represented by the following equation:

$$T_T = 1.007 (T_p) + 9.871 (\pm 0.13\%) \quad (2.8)$$

(for  $850^\circ\text{C} \leq T \leq 1250^\circ\text{C}$ )

$$T_T = 1.024 (T_p) + 10.143 (\pm 0.24\%) \quad (2.9)$$

(for  $1250^\circ\text{C} \leq T \leq 1600^\circ\text{C}$ )

$$T_T = 1.024 (T_p) + 10.143 (\pm 0.24\%) \quad (2.10)$$

(for  $1600^\circ\text{C} \leq T \leq 1900^\circ\text{C}$ )

$$T_T = 1.039 (T_p) + 37.300 (\pm 0.26\%) \quad (2.11)$$

(for  $1900^\circ\text{C} \leq T \leq 2500^\circ\text{C}$ )

In these set of equations,  $T_T$  represents the target temperature.

c) Conversion of Target Temperature to Emitter Temperature

Figure 2.5 represents the plots of emitter temperature as a function of the target temperature for the ASTAR - 811C, Nb - 1 at.% Zr diminiode. The experimental data for the two temperature ranges was obtained from NASA, LeRC files. The most accurate curve fits for this data exhibited linear variations that agreed with the following first order approximations.

$$T_E = 0.887 (T_T) + 82.640 (\pm 0.895\%) \quad (2.12)$$

(for  $1250^\circ\text{C} \leq T \leq 1600^\circ\text{C}$ )

$$T_E = 0.794 (T_T) + 229.891 (\pm 0.989\%) \quad (2.13)$$

(for  $1600^\circ\text{C} \leq T \leq 1900^\circ\text{C}$ )

Here  $T_E$  represents the emitter temperature which is at all times, less than the target temperature. From the figure, it seems that the experimental calibration data is identified in groups or clusters over the entire temperature range but these clusters all lie on the same linear approximation.

d) Conversion of Output Voltage to Emitter Temperature

Figure 2.6 represents the analytical plots of emitter temperature as a function of pyrometer output voltage. These plots were generated with the following polynomials that were

# EMITTER TEMPERATURE VERSUS TARGET TEMP.

(ASTAR 811C - Niobium Zirconium Diimplode)

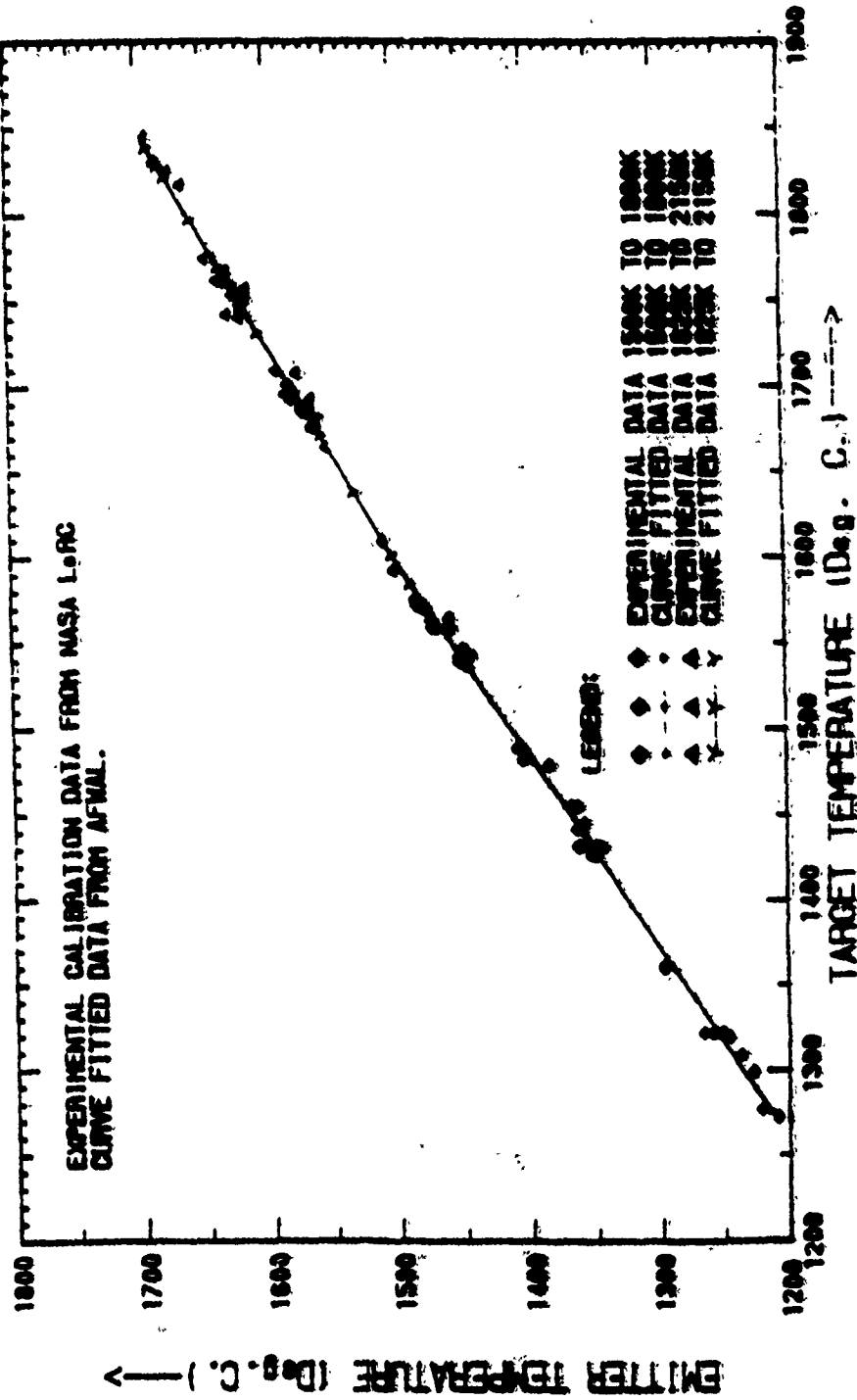


Figure 2.5 Experimental Calibration Data and Polynomial Fit for ASTAR-811C Diode.

# EMITTER TEMPERATURE VERSUS OUTPUT VOLTAGE

(ASTAR 811C - Niobium Zirconium Diminiode)

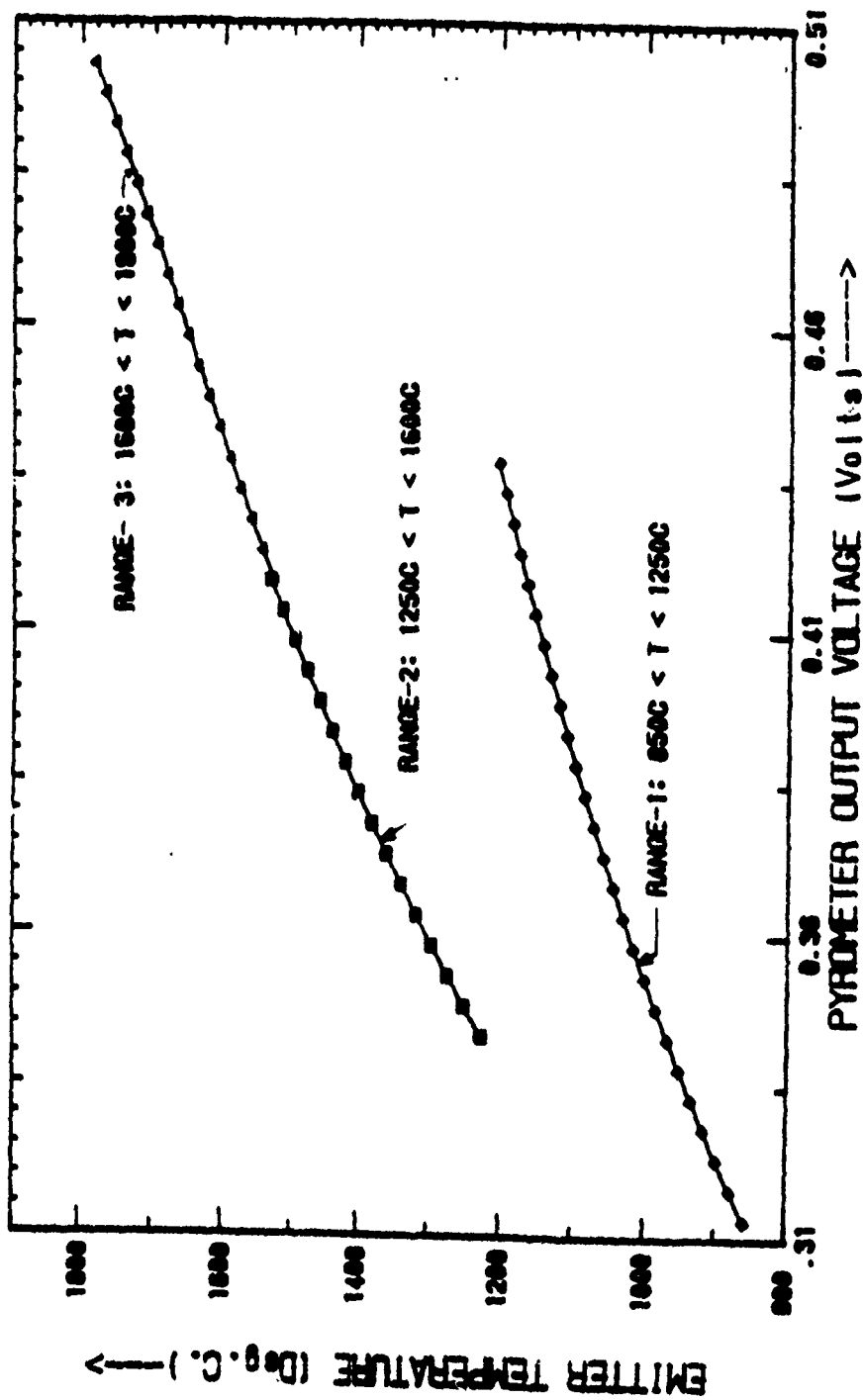


Figure 2.6 Actual Emitter Temperature Versus Pyrometer Output Voltage for the ASTAR-811C Diode.

obtained by substituting for  $T_p$  as a function of  $V_p$  in equations 2.8 - 2.11 and subsequently substituting for  $T_r$  as a function of  $V_p$  in equations 2.12 and 2.13.

$$T_E = 38710.92 (V_p)^3 - 52125.159 (V_p)^2 + 25386.111 (V_p) - 3167.215 \quad (2.14)$$

(for  $850^\circ\text{C} \leq T \leq 1250^\circ\text{C}$ )

$$T_E = 25354.31 (V_p)^3 - 36749.941 (V_p)^2 + 21001.267 (V_p) - 2676.330 \quad (2.15)$$

(for  $1250^\circ\text{C} \leq T \leq 1600^\circ\text{C}$ )

$$T_E = 22701.752 (V_p)^3 - 32905.177 (V_p)^2 + 18804.122 (V_p) - 2240.436 \quad (2.16)$$

(for  $1600^\circ\text{C} \leq T \leq 1900^\circ\text{C}$ )

$$T_E = 7481.711 (V_p)^3 - 10753.428 (V_p)^2 + 12538.060 (V_p) - 1855.419 \quad (2.17)$$

(for  $1900^\circ\text{C} \leq T \leq 2500^\circ\text{C}$ )

The various limits for each of the curve fits are indicated in Table 2.2.

Table 2.2 Error Limits for Analytical Plots (ASTAR-811C).

| Sl. No. | Conversion                        | Temperature Range(°C) | Maximum Error(%) | Minimum Error(%)        | Average Error(%)        | RMS Error(%)            |
|---------|-----------------------------------|-----------------------|------------------|-------------------------|-------------------------|-------------------------|
| 1       | Emitter Temp. to Target Temp.     | 1250 to 1600          | -0.8951          | $1.2904 \times 10^{-2}$ | $2.1828 \times 10^{-3}$ | $7.5875 \times 10^{-2}$ |
| 2       | Emitter Temp. to Target Temp.     | 1600 to 1900          | -0.9896          | $1.1079 \times 10^{-2}$ | $1.7099 \times 10^{-3}$ | 0.0611                  |
| 3       | Target Temp. to Pyrometer Temp.   | 850 to 1250           | -0.1338          | $7.819 \times 10^{-4}$  | $6.359 \times 10^{-4}$  | 0.0293                  |
| 4       | Target Temp. to Pyrometer Temp.   | 1250 to 1600          | 0.2364           | $7.024 \times 10^{-2}$  | $-1.028 \times 10^{-4}$ | 0.0614                  |
| 5       | Target Temp. to Pyrometer Temp.   | 1600 to 1900          | 0.2364           | $7.024 \times 10^{-2}$  | $-1.028 \times 10^{-4}$ | 0.0614                  |
| 6       | Target Temp. to Pyrometer Temp.   | 1900 to 2500          | -0.2591          | -0.0103                 | $6.367 \times 10^{-4}$  | $8.149 \times 10^{-2}$  |
| 7       | Pyrometer Temp. to Output Voltage | 850 to 1250           | 1.9664           | 0.0176                  | $5.002 \times 10^{-2}$  | $5.556 \times 10^{-2}$  |
| 8       | Pyrometer Temp. to Output Voltage | 1250 to 1600          | 0.2703           | $-6.426 \times 10^{-3}$ | $9.133 \times 10^{-3}$  | $1.271 \times 10^{-2}$  |
| 9       | Pyrometer Temp. to Output Voltage | 1600 to 1900          | 0.2703           | $-6.426 \times 10^{-3}$ | $9.133 \times 10^{-3}$  | $1.271 \times 10^{-2}$  |
| 10      | Pyrometer Temp. to Output Voltage | 1900 to 2500          | -0.2200          | $9.328 \times 10^{-4}$  | $-6.811 \times 10^{-3}$ | $1.052 \times 10^{-2}$  |

## SECTION III

### EXPERIMENTAL SETUP

#### 3.1 Diminiode Test Stations

The experimental setup for the NASA Diminiode station consists of four subsystems. These are the vacuum system, emitter heating and temperature measurement system, data acquisition system and the output load and control system. A general discussion of these subsystems will be presented in this section. A more detailed discussion of the data acquisition system and the temperature measurement and control system will be included in the next section. A schematic representing the entire experimental setup and associated subsystems is shown in Figure 3.1.

##### 3.1.1 The Vacuum System

Since the whole purpose of the energy conversion process is to extract electrons from the emitter surface and transmit them to the collector surface, it is imperative that a clean low pressure environment be provided to avoid electron deviation. As a result the diminiodes are tested in a vacuum chamber under a pressure of  $10^{-7}$  torr or lower. This provides the dual purpose of providing a clean environment as well as minimizing electron deviation.

A turbomolecular pump was provided to rough the system to approximately  $10^{-4}$  torr. An ion pump was then activated to take the pressure down to at least  $10^{-6}$  torr. A vacuum of  $10^{-6}$  torr or better is required to minimize electron deviation and also to improve efficiency of heating by electron bombardment. The vacuum level was monitored with an ion gauge whose output was directly transmitted to the computer in the data processing system through the data acquisition system. Thus the vacuum level was directly displayed on the monitor and stored along with other test data.

##### 3.1.2 Emitter Heating and Temperature Measurement System

The emitter was indirectly heated by electron bombardment (EB) heating. This was accomplished using a tungsten filament which was resistance heated by an AC power supply.

# Experimental Setup Schematic

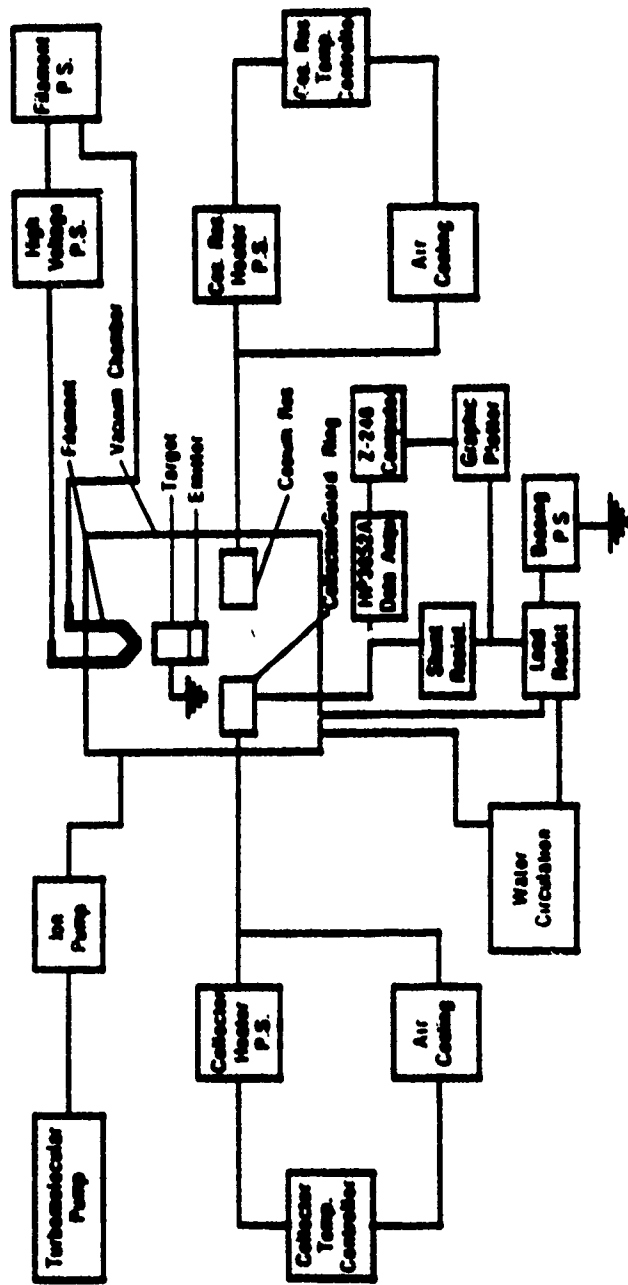


Figure 3.1 Schematic Representing Experimental Setup and Associated Subsystems.

To heat the filament, the power was gradually increased up to approximately 100 watts, at which level the temperature would be greater than 2600 K and the filament would be hot enough to emit electrons with high kinetic energies. A floating DC bombardment power supply provided the necessary energy to direct the electrons from the filament to the electron bombardment target. The energy imparted by the impinging electrons heated up the EB target, which in turn provided the necessary heat input to the emitter by conduction.

The cesium reservoir and collector temperatures were controlled using compressed air for cooling and resistance heaters for heating. Microprocessor type controllers were used to control the power output to the resistance heaters. These controllers were supplied with the appropriate temperature signals by thermocouples placed in the diode to measure collector, guard and cesium reservoir temperatures. The emitter temperature was indirectly measured using an optical pyrometer. The optical pyrometer output was then converted to emitter temperature and transmitted to the computer. The pyrometer was held in position by an attachment to the diode station body. This attachment was designed, fabricated and assembled using accessories from old microscopic equipment. An assembly drawing and detailed drawings of the parts are provided in Appendix A.

### 3.1.3 Output Load System

The experimental setup described earlier, provided the overall view of all the components associated with the test instrumentation. By far, the most important elements are the output load circuit that was used to load the diode and draw the output and the data acquisition/processing system which allowed the output data to be accepted, converted to a digital format and then processed in the computer.

Figure 3.2 is a simplified schematic of the converter output load circuit. The converter output voltage was measured across the emitter and collector and fed directly to the HP-3852A acquisition system along with the converter output current, which was measured across a shunt (0.0033 ohms) resistance.

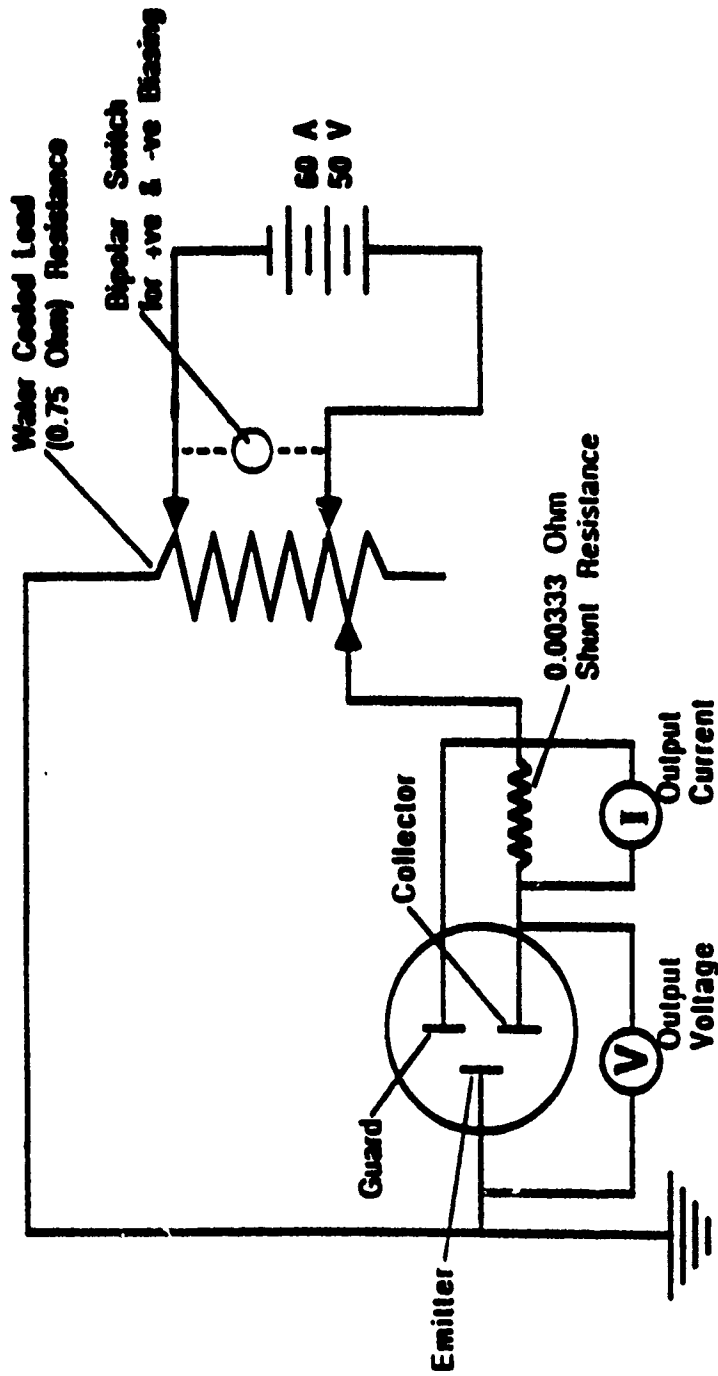


Figure 3.2 Simplified Electrical Schematic for the Output Load Circuit.

Biasing of the diode was accomplished after several trials as the collector-guard circuit gave spurious current outputs. Several different combinations of the circuits were attempted in order to eliminate the possibility of getting exaggerated current output.

Tables 3.1, 3.2, 3.3 and 3.4 provide the summaries for the four different configurations that were tested to obtain the optimum output load circuit. The operating conditions for the diode were maintained identical for each of the four configurations in order to extract a meaningful comparison.

The first configuration tested was with the shunt resistance on the collector side and with no resistance on the Guard side. The appropriate circuit to measure the actual magnitude of the output current would be cct. #2 where the Guard was left open. The current output was found to be 0.73 A. In each of the other three circuits, the collector shunt registered much lower currents indicating that Guard was interfering with the path of least resistance for the electrons. These results are presented in Table 3.1.

The second configuration tested was one with no change on the collector side but with several resistances on the Guard side. The output current measured across the collector shunt resistance was normal in all the cases except where small resistances were connected in the Guard circuit seemed to interfere with that in the collector circuit. By introducing a large resistance (2500 ohms) in the Guard circuit, more than 99% of the diode current output was forced through the collector shunt resistance. The results of these tests are indicated in Table 3.2.

Tables 3.3 and 3.4 represent similar results for the other two configurations where the shunt resistance was hooked up to the electrical load output circuit on the emitter side of the load. The behavior was similar to that observed in the first two configurations, but the cable movement of the shunt from the collector side to the emitter side did not make any difference. As a consequence of these tests, future diode testing will be done with a large (at least 500 ohms) resistance in the Guard circuit so that the electrons take the path of least resistance through the collector shunt.

**Table 3.1 Diode Performance with Shunt on the Collector Side and No Resistance on the Guard Side.**

**TEST PARAMETERS:** 1) Target Temperature =  $1730 \pm 15^\circ\text{C}$ .  
 2) Emitter Temperature =  $1635 \pm 15^\circ\text{C}$ .  
 3) Collector Temperature =  $578 \pm 3^\circ\text{C}$ .  
 4) Cesium Reservoir Temperature =  $168 \pm 3^\circ\text{C}$

**NOMENCLATURE :**  $V_{gsh}$  - Voltage across guard shunt, Volts.  
 $I_{gsh}$  - Current across guard shunt, Amps.  
 $V_{csh}$  - Voltage across collector shunt, Volts.  
 $I_{csh}$  - Current across collector shunt, Amps.  
 $V_l$  - Voltage across the load resistance, Volts.  
 $I_l$  - Current across the load resistance, Amps.  
 $V_o$  - Output voltage of the diode, Volts.

| Sl. # | Circuit | $V_{gsh}$ | $I_{gsh}$ | $V_{csh}$ | $I_{csh}$ | $V_l$ | $I_l$ | $V_o$ |
|-------|---------|-----------|-----------|-----------|-----------|-------|-------|-------|
| 1     |         | -         | -         | .0013     | .239      | .367  | 1.29  | .977  |
| 2     |         | -         | -         | .0037     | .730      | .538  | .717  | .542  |
| 3     |         | -         | -         | .0018     | .343      | .262  | .349  | .255  |
| 4     |         | -         | -         | .0066     | 1.31      | .961  | 1.28  | .973  |

**Table 3.2 Diode Performance with Various Resistances on the Guard Side.**

- TEST PARAMETERS:**
- 1) Target Temperature =  $1730 \pm 15^\circ\text{C}$ .
  - 2) Emitter Temperature =  $1635 \pm 15^\circ\text{C}$ .
  - 3) Collector Temperature =  $578 \pm 3^\circ\text{C}$ .
  - 4) Cesium Reservoir Temperature =  $168 \pm 3^\circ\text{C}$ .

- NOMENCLATURE**
- $V_{gsh}$  - Voltage across guard shunt, Volts.
  - $I_{gsh}$  - Current across guard shunt, Amps.
  - $V_{csh}$  - Voltage across collector shunt, Volts.
  - $I_{csh}$  - Current across collector shunt, Amps.
  - $V_L$  - Voltage across the load resistance, Volts.
  - $I_L$  - Current across the load resistance, Amps.
  - $V_{ce}$  - Output voltage of the diode, Volts.

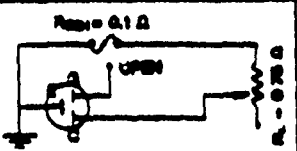
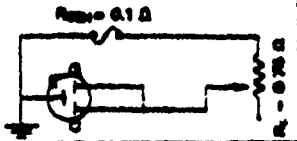
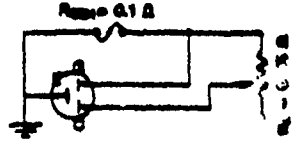
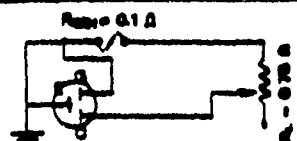
| Sl. # | Circuit | $V_{gsh}$ | $I_{gsh}$ | $V_{csh}$ | $I_{csh}$ | $V_L$ | $I_L$ | $V_{ce}$ |
|-------|---------|-----------|-----------|-----------|-----------|-------|-------|----------|
| 1     |         | .096      | .960      | .325      | .263      | .895  | 1.19  | .926     |
| 2     |         | -         | -         | .072      | .727      | .531  | .708  | .609     |
| 3     |         | 1.35      | .001      | .071      | .713      | .526  | .701  | .597     |
| 4     |         | 1.35      | .003      | .072      | .723      | .529  | .705  | .604     |
| 5     |         | 1.90      | .004      | .071      | .717      | .525  | .700  | .597     |
| 6     |         | 1.29      | .003      | .072      | .734      | .535  | .713  | .612     |
| 7     |         | .541      | .433      | .049      | .475      | .669  | .892  | .723     |

**Table 3.3 Diode Performance with Shunt on the Emitter Side and No Resistance on the Guard Side.**

**TEST PARAMETERS:** 1) Target Temperature =  $1730 \pm 15^\circ\text{C}$ .  
 2) Emitter Temperature =  $1635 \pm 15^\circ\text{C}$ .  
 3) Collector Temperature =  $578 \pm 3^\circ\text{C}$ .  
 4) Cesium Reservoir Temperature =  $168 \pm 3^\circ\text{C}$

**NOMENCLATURE**

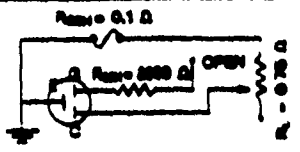
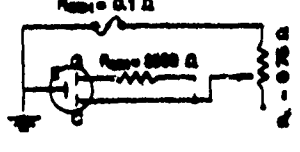
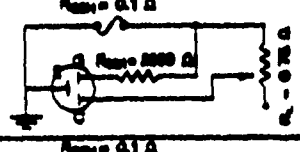
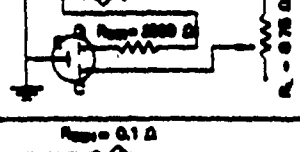
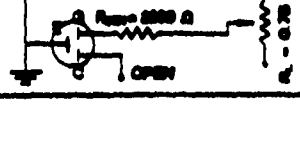
- $V_{gsh}$  - Voltage across guard shunt, Volts.
- $I_{gsh}$  - Current across guard shunt, Amps.
- $V_{csh}$  - Voltage across collector shunt, Volts.
- $I_{csh}$  - Current across collector shunt, Amps.
- $V_L$  - Voltage across the load resistance, Volts.
- $I_L$  - Current across the load resistance, Amps.
- $V_{ce}$  - Output voltage of the diode, Volts.

| Sl. # | Circuit   | $V_{gsh}$ | $I_{gsh}$ | $V_{csh}$ | $I_{csh}$ | $V_L$ | $I_L$ | $V_{ce}$ |
|-------|---|-----------|-----------|-----------|-----------|-------|-------|----------|
| 1     |    | -         | -         | .071      | .700      | .516  | .688  | .590     |
| 2     |   | -         | -         | .122      | 1.20      | .891  | 1.19  | 1.02     |
| 3     |  | -         | -         | .386      | 3.80      | .324  | .299  | .634     |
| 4     |  | -         | -         | .036      | .340      | .264  | .352  | .383     |

**Table 3.4 Diode Performance with Shunt on the Emitter Side and 2.5 k-ohm Resistance on the Guard Side.**

**TEST PARAMETERS:** 1) Target Temperature =  $1730 \pm 15^\circ\text{C}$ .  
 2) Emitter Temperature =  $1635 \pm 15^\circ\text{C}$ .  
 3) Collector Temperature =  $578 \pm 3^\circ\text{C}$ .  
 4) Cesium Reservoir Temperature =  $168 \pm 3^\circ\text{C}$

**NOMENCLATURE**  
 $V_{gsh}$  - Voltage across guard shunt, Volts.  
 $I_{gsh}$  - Current across guard shunt, Amps.  
 $V_{csh}$  - Voltage across collector shunt, Volts.  
 $I_{csh}$  - Current across collector shunt, Amps.  
 $V_l$  - Voltage across the load resistance, Volts.  
 $I_l$  - Current across the load resistance, Amps.  
 $V_{ce}$  - Output voltage of the diode, Volts.

| Sl. # | Circuit   | $V_{gsh}$ | $I_{gsh}$ | $V_{csh}$ | $I_{csh}$ | $V_l$ | $I_l$ | $V_{ce}$ |
|-------|---|-----------|-----------|-----------|-----------|-------|-------|----------|
| 1     |    | 0.0       | 0.0       | .071      | .710      | .525  | .700  | .600     |
| 2     |   | 1.31      | .001      | .072      | .730      | .535  | .713  | .615     |
| 3     |  | 1.85      | .001      | .073      | .740      | .541  | .721  | .622     |
| 4     |  | 1.91      | .001      | .069      | .680      | .504  | .672  | .577     |
| 5     |  | .120      | 1.10      | -         | -         | .874  | 1.17  | 1.02     |

Biassing the diode was accomplished initially by using a variable resistance box, but as this method does not allow negative output voltages, it was changed to a 50V, 60A DC power supply, which was connected across a water-cooled load resistance through a bipolar switch. The load resistances had to be water-cooled as they would get heated up at current levels of 5 amps or more. The water cooling was very effective in restricting the temperature rise above ambient to less than 10°C. The bipolar switch was introduced to bias the diode with both positive and negative voltages.

The disadvantages of using a setup such as this for biasing the diode is that it does not take advantage of the thermal inertia properties of the electrode materials. Manual biasing resulted in a sudden change in electrode temperatures which had to be brought back to its original level by manipulating the heaters and the cooling mechanism before further biasing. The outcome of this was that it took about 75 minutes to complete a sweep, and at this speed it would be impossible to complete performance mapping for a pair of electrodes in a reasonable period of time. Efforts are currently being made to develop a pulsing mechanism in the form of a low duty voltage pulse to reduce the sweeping period to less than 20 milliseconds. At this speed, the time taken is much lower than the time constant of the electrode material and so there is virtually no change in the temperature.

#### 3.1.4 Data Acquisition/Processing System

The data acquisition/processing system was made up primarily by an HP-3852A data acquisition system, a Zenith-248 computer and a Graphtec plotter. These were controlled using ASYST and in-house developed software to acquire and process the data. This subsystem will be covered in greater detail in the next section.

Because of the large amount of data involved in the study of electrical output characteristics of the diode, a computer system was required to control, collect and correlate converter output data. The computer system design for data acquisition and processing is shown in Figure 3.3. The entire system essentially consisted of

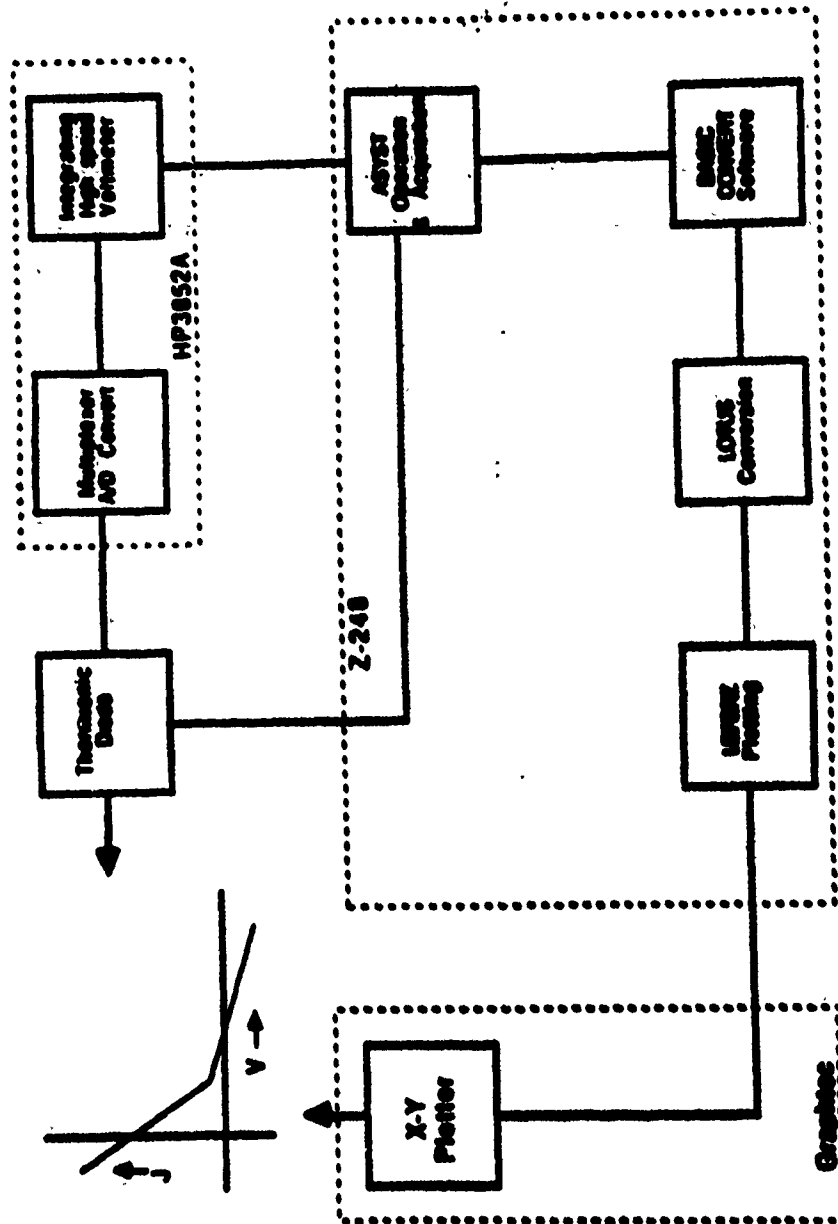


Figure 3.3 Computer System Design for Data Acquisition and Processing

- a) The test apparatus made up of the converter, DC power supply, load circuit, thermocouples, and optical pyrometer.
- b) The data acquisition system is an HP model HP-3852A. This system included a multiplexer, A/D converter and an integrating high speed voltmeter.
- c) The desk top PC, a Zenith-248 and the applicable software.
- d) The presentation equipment which was made up of a printer and Graphtec plotter.

During testing, signals from the diode thermocouples, the pyrometer and the load circuit were fed to the HP system. These signals were processed by the HP and accessed by the Z-248 using ASYST software. This data was then converted into the appropriate file format necessary for use with the Graphtec plotter. These files were then used to produce the required plots to analyze and characterize the diode.

### 3.1.5 Electrode Cooling System

The four major components of the thermionic diode system that required cooling were the vacuum chamber housing the diode, the load resistor, the collector, and the cesium reservoir. In spite of the presence of radiation shields, there was a lot of radiation heat input to the vacuum chamber walls surrounding the diode. This was sufficient to heat the chamber walls to temperatures on the order of 300°C which was quite high considering the thermal mass involved. For this purpose, the top half of the vacuum chamber was made with double wall construction to facilitate the circulation of water. The water conduit shown in Figure 3.4 essentially consists of a tapping from a high pressure line with inlet and outlet valves and instrumentation to measure inlet and outlet temperatures and flow rates. Compressed air lines with pressure gauges and regulators were used for cooling the collector and the cesium reservoir. An outlet for the water and air lines was provided on the framework supporting the thermionic

# WATER COOLING SYSTEM SCHEMATIC

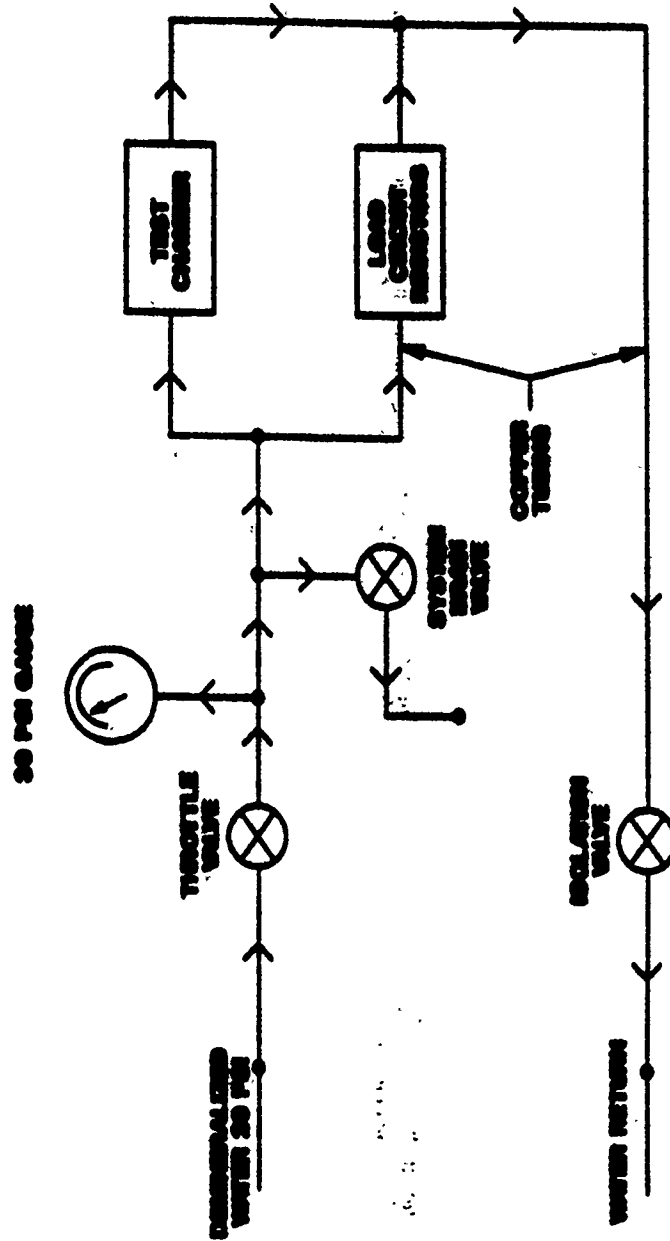


Figure 3.4 Water Cooling System Schematic for the Test Station.

test chamber. All the valves and gauges were mounted on the front panel board from which the various flows could be monitored and controlled.

### **3.1.6 General Electrical Schematics and Associated Components Design**

Figures 3.5 through 3.9 provide the detailed electrical schematics for the filament and high voltage control panel, the high voltage power supply, the cesium and collector heater control panel with a rear view of the Relay-Trans board, the signal cyler board and safety interlock circuit respectively. As many details as possible were provided on these schematics including color codes for the wiring so that they can be easily understood by anyone interested in setting up similar electrical circuits.

Every single system was initially dismantled and rewired to follow a strict color coding for all the wires. The wiring diagrams so generated also helped in understanding the functions of various sub-components that were key controlling elements in the entire structure. As the two diminiode stations are identical, only one system was stripped off all the wiring while retaining the other system operational. Several associated components that were either outdated or obsolete were redesigned and equipped with newer components.

### **3.2 The TECO Diode Station**

The TECO diode station, so called, because it was used to test the thermionic performance of a fixed gap diode manufactured by Thermo Electron Corporation had an etched Rhenium emitter and a Niobium collector. In this configuration, the cesium reservoir was located at the bottom of the collector region and was provided with a heater and a copper disk with copper water cooling conduits that provided the necessary cooling mechanism by heat conduction. Both air and water cooling conduits were provided for cooling the cesium reservoir as well as the collector. While the water cooling system was very similar to that of the diminiode test stations, the air cooling system shown in Figure 3.10, was designed for compressed air as well as Argon gas circulation.



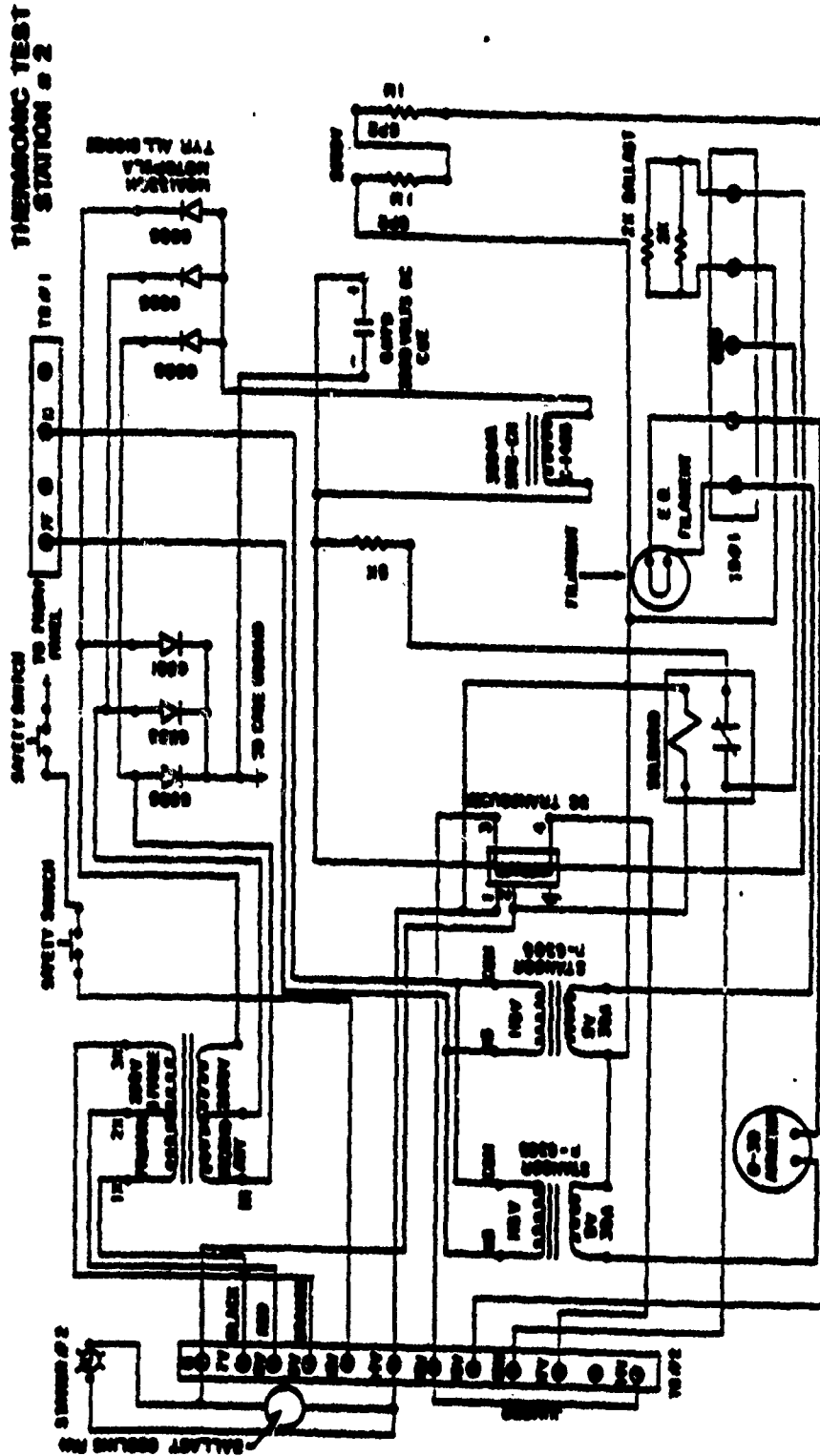


Figure 3.6 Electrical Schematic for the High Voltage Power Supply.



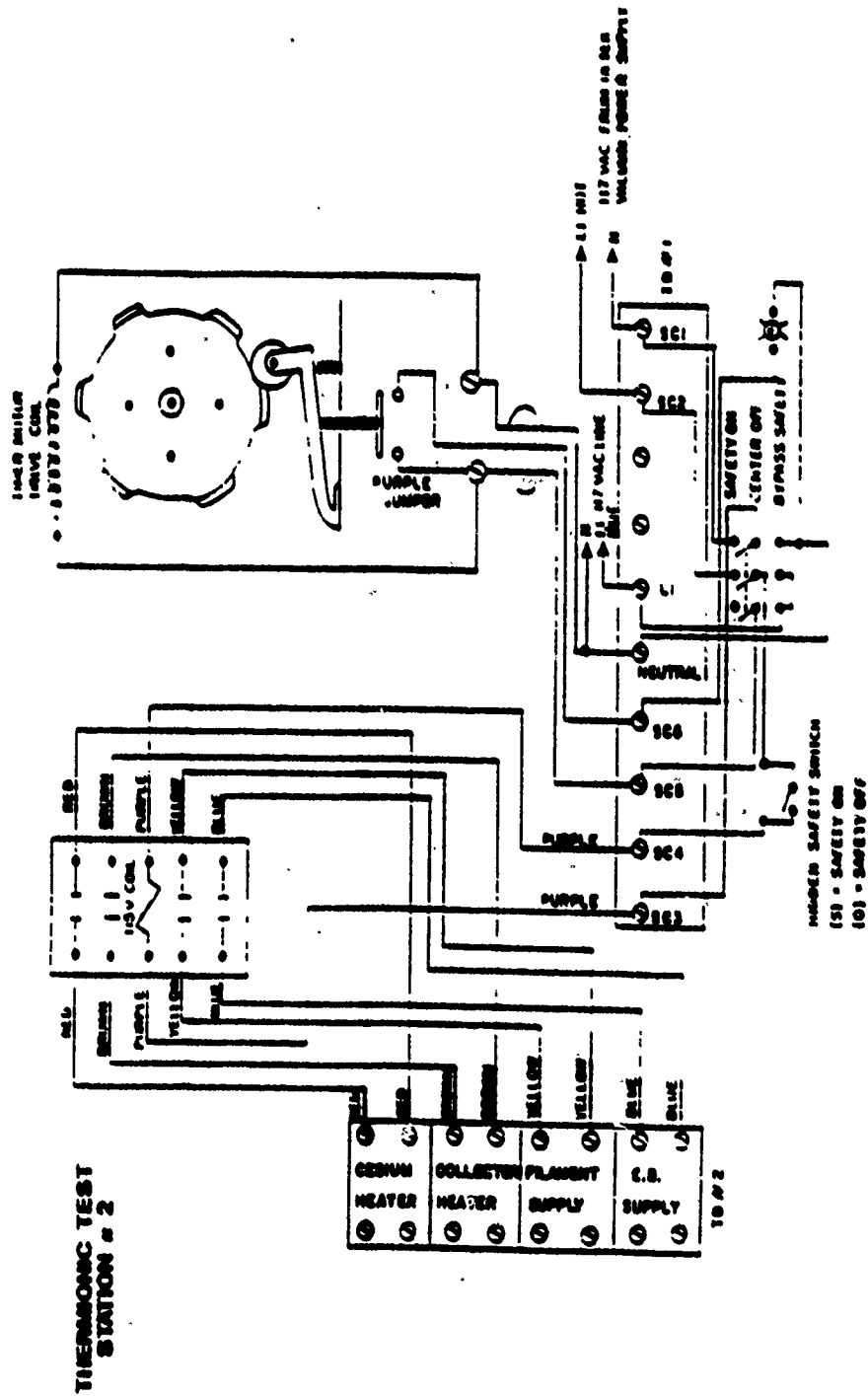
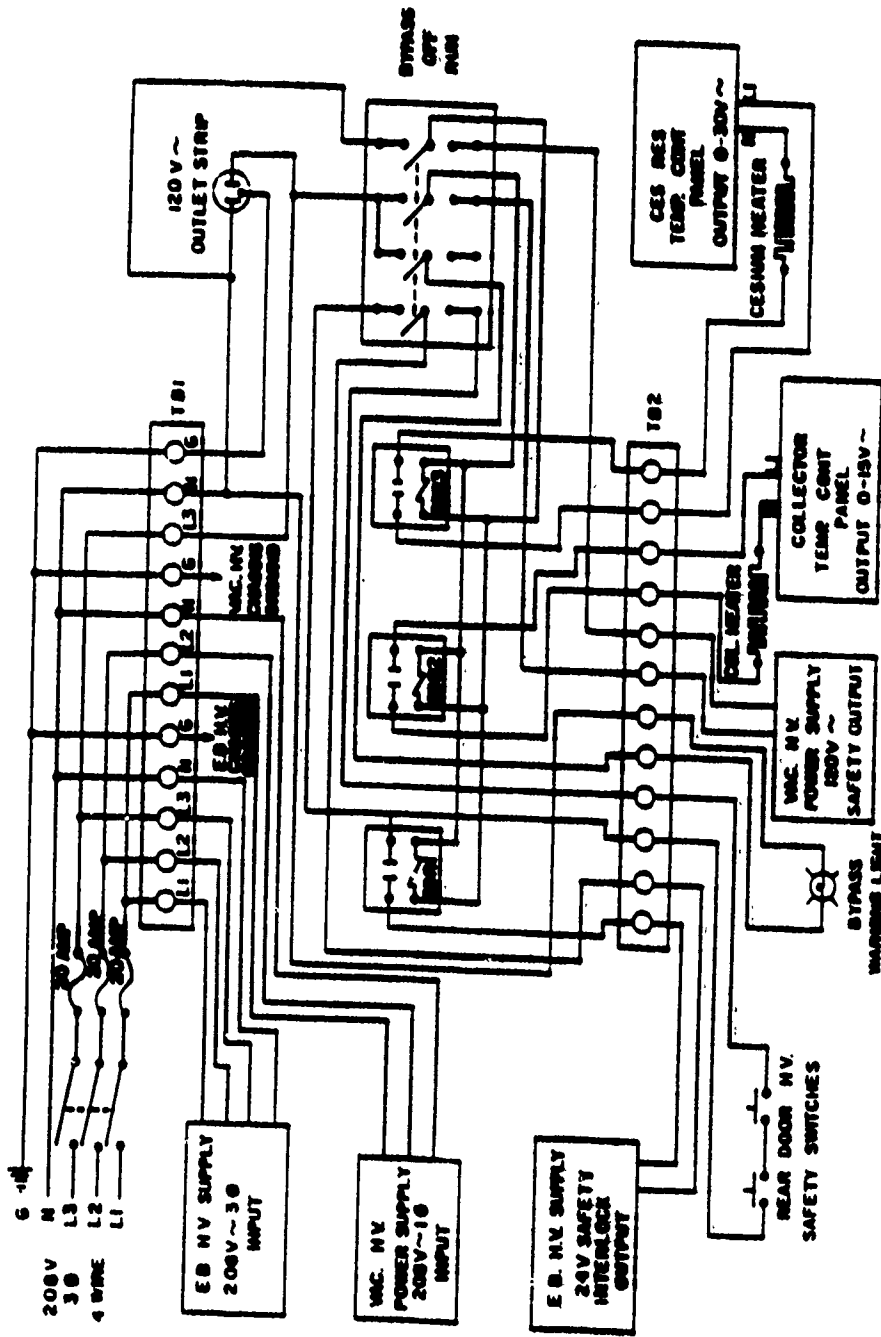


Figure 3.8 Electrical Schematic for the Signal Cycles Board.

**DIODE STATION NO. 3 SAFETY INTERLOCK CIRCUIT**



**Figure 3.9 Safety Interlock Circuit Schematic for the TECO Diode Station**

# AIR/GAS COOLING SYSTEM SCHEMATIC

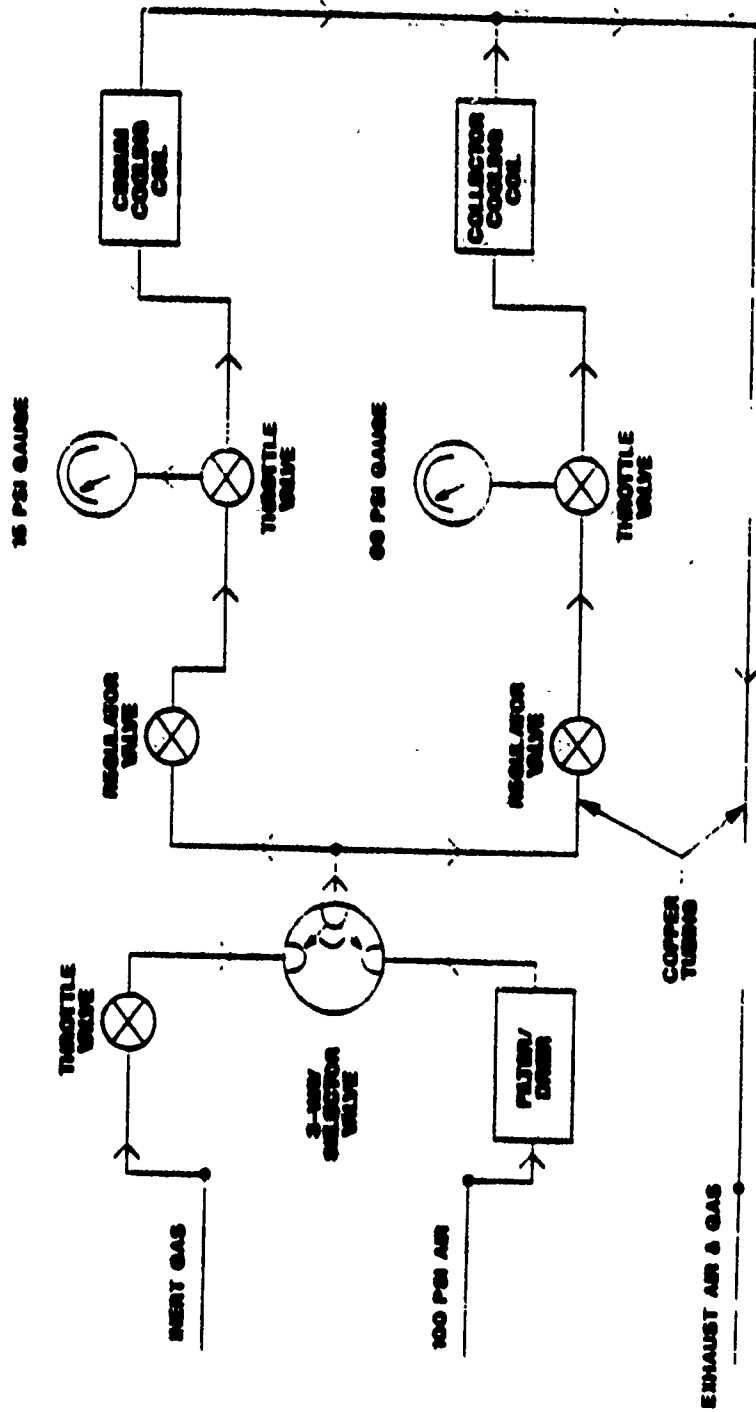


Figure 3.10 Air Cooling System Schematic for the TECO Diode Station.

An ion-pumped vacuum system provided a vacuum of less than  $10^{-7}$  torr for the chamber housing the diode. The emitter was heated by electron bombardment using a pancake type tungsten filament which was initially heated with an alternating current power supply. In this case an emitter temperature controller was used in conjunction with the electron bombardment power supply in order to control the temperature of the emitter. The W-Re thermocouple output was directly fed to the temperature controller which, in turn, controlled the power input to the filament as well as the bombardment power. This emitter temperature controller will eventually be run by the computer so that change in emitter temperatures between tests can be accomplished automatically. The collector and cesium reservoir were also provided with temperature controllers getting their input from Chromel-Alumel thermocouples. The output load circuit was similar to that used in the diminiode test stations except that in this case co-axial cable connections were provided so that an oscilloscope and a signal generator could be incorporated in the same circuit at a later date.

### 3.3 Diode Processing Station

This is a multipurpose vacuum chamber that can be used to fill cesium in a diode and seal it and then conduct a performance test on the same diode to determine the output current density and output voltage at various operating temperatures. The diode processing station is not fully equipped as yet but the equipment and components are being ordered and the entire system is currently being assembled. However, the functions of this system have been described in the following paragraphs.

#### 3.3.1 Vacuum Processing the Diminiode

To minimize costly time-consuming bake-out cycles, the multipurpose vacuum chamber facilitates all operations remaining to finish the diminiode. In this chamber following only one pump-down, the diminiode made of baked-out components undergoes a final high-temperature degassing, internal and external pyrometry, and fusion sealing after the cesium capsule insertion. The cesium itself is an off-the-shelf component like the other interchangeable parts of diminiodes. It comes in baked-out, brazed-shut, breakable molybdenum vials. One of these ampules, a degassed tantalum ball, and a diminiode go into the station before its closure.

Then, after the pump-down and degassing at 450°C to below  $10^{-6}$  torr, the diminiode enters the final stages of processing.

As electron bombardment heats the emitter assembly, continual thermal sensing and coolant adjustments bring the diminiode to predetermined bake-out conditions. That state depends on the electrodes, their brazes (if any), and the insulator limit (1400 K). During the temperature rise, the pyrometric cavity in the emitter allows calibrations of the tungsten-lined external black-body hole and the high-temperature thermocouple. The relation between these temperatures depends on the heat-flow rate, too. So the calibrations are comprehensive. Of course, the outer black-body hole then permits emitter-temperature calibrations subsequent to closing the diminiode. This capability enables checking output shifts of the high-temperature thermocouples, adapting a photo-multiplier for total-radiation measurements or using automatic pyrometry.

While the diminiode is at maximum degassing temperatures, electron bombardment of the open end of the reservoir to just below the melting point of the copper-foil insert prepares it for the brazed closure. Following this part of the bake-out, cooling gives a downward calibration to check the upward one.

Next, magnetically pulling the lower pin in the guide tube drops the cesium capsule into the diminiode reservoir. If the pressure rises, another brief bake-out removes contaminants. The same process follows the release of the previously degassed tantalum sphere, which lodges in the funnel opening of the side tube. Then electron bombardment brazes this ball in the end of the reservoir with copper. And the diminiode is complete.

### 3.3.2 Cesium Reservoir Sealing Technique

As mentioned earlier, the diode processing station was intended for filling cesium and sealing the cesium reservoir shut with a Tantalum ball and a braze alloy ring. As the laboratory was not equipped to fabricate diodes, a simulated structure was designed so that the operating parameters could be controlled and optimized for maximum weld penetration depth.

The assembled structure as well as the various parts that go into this design are indicated in Appendix B.

## SECTION IV

### DIODE TESTING PROCEDURE

The basic test procedure essentially involves completing one sweep of bias voltage to cause ignition and then de-ignition at constant electrode temperatures which are designated as the primary variables. Since the Lanthanum Hexaboride diminiode was tested for performance verification as well as primary variables optimization, the procedures for these two types of tests have been provided separately.

#### 4.1 Performance Verification Testing

The vacuum level was brought down to  $10^{-7}$  torr or better after initial assembly of the diminiode inside the vacuum chamber. The filament was then heated up to about 100 watts AC, before providing a bombardment power supply of 1000 watts DC. The bombardment power was adjusted till the required emitter temperature was obtained. The collector and cesium reservoir temperatures were then maintained at 900 K and 460 K respectively. The data acquisition and processing systems were then activated using the ASYST program. Once the temperatures had stabilized, the diode was biased with a positive bias voltage of +2 V. The bias voltage was then changed to a lower value and the temperatures adjusted once again and the output data such as current and voltage were recorded. This was repeated till a full cycle of biasing was completed and at least 30 data points were obtained. The data files were then converted to a format that could be used directly with the Graphtec plotter, to plot the output current density and the output power density characteristics. The emitter temperature was then changed with the same collector and cesium reservoir temperatures and the biasing process repeated till all the characteristics were obtained.

#### 4.2 Primary Variables Optimization

To determine the optimum characteristics of the NASA LaB<sub>6</sub> diminiode, the condensed procedure listed below was followed.

- 1) Using the test procedure outlined in the preceding section, hold emitter and collector temperatures constant.
- 2) Vary cesium reservoir temperature (350-550 K).
- 3) Obtain optimum cesium reservoir temperature.
- 4) Using the outlined procedure, hold emitter temperature constant and cesium reservoir temperature at optimized value.
- 5) Vary collector temperature (700-1000 K).
- 6) Obtain optimum collector temperature.
- 7) Using the outlined procedure, hold collector and cesium reservoir temperatures at optimum values.
- 8) Vary emitter temperature (1400-1700 K).
- 9) Obtain optimum emitter temperature.
- 10) Repeat 1) thru 9) iteratively to optimize all temperatures and obtain peak power density.

SECTION V  
RESULTS AND DISCUSSIONS

5.1 Thermionic Emission Characteristics from Lanthanum Hexaboride

The experimental thermionics program at the Aero Propulsion Laboratory of WPAFB was initiated with the acquisition of two diminiode test stations, a TECO diode test station and a diode processing station from NASA, LeRC through Arizona State University. The twin diminiode test stations have been refurbished with new cooling systems, a new data processing/acquisition system and an output load circuit with a biasing power supply. The HP-3852A data acquisition system is capable of handling 100,000 readings/sec, and has a built-in multiplexer - A/D converter. It interfaces with a Z-248 PC that controls the operations with the ASYST program. Steady state tests on diminiodes are currently being conducted manually by controlling the electrode and cesium reservoir temperatures using their respective cooling and heating systems, between data points. Efforts are currently directed towards developing an automated pulse generating circuit to sweep (voltage) the diminiode and generate an ignited mode J-V characteristic in less than 5 msec's thereby taking advantage of the converter's thermal inertia properties.

Performance verification tests were conducted on a planar diminode with sintered Lanthanum Hexaboride as the emitter material and arc melted Lanthanum Hexaboride as the collector material. The primary and secondary parametric variable conditions were obtained from a NASA report published earlier. It was found that the performance of the diode was well in agreement with similar characteristics generated earlier. Optimization tests by varying primary variables revealed that the operating point with maximum power density has a small shift with reference to the cesium reservoir temperature. After the completion of the performance optimization tests, the experimental characteristics were characterized by using a 1-D Thermionic Energy Conversion code, originally developed by Dr. Geoffrey Main from Georgia Tech. An attempt was made at simulating the optimized experimental characteristics using the computer code. It was found that there was good correspondence between experimental and analytical

results for moderate values of cesium pressure, but significant deviations were observed for large values of Cs pressure (>10 torr) and very small values of Cs pressure (<1.0 torr).

#### 5.1.1. Verification of Performance

##### a) Original Results Obtained at NASA LeRC

Figure 3.1 shows the output current density and output power density characteristics of the Lanthanum Hexaboride diminiode as obtained at NASA LeRC and published in Reference 1. These characteristics were generated at optimum cesium reservoir and optimum collector temperatures. These optimum temperatures were 850 K for the collector and 440 K for the cesium reservoir respectively. The emitter temperature was varied from 1500 K to 1700 K at intervals of 50°C. The maximum output power was 5.29 W/cm<sup>2</sup> at an output voltage of 0.45 V and an emitter temperature of 1700 K. Though the peak power occurred at an output voltage of 0.45 V, the most efficient operation of the Lanthanum Hexaboride diminiode occurred at 0.75 V and 5 A/cm<sup>2</sup> (3.8 W/cm<sup>2</sup>). There the work function of the 1700 K emitter was less than 2.64 eV, the Barrier Index was about 1.9 V and the calculated efficiency for optimum leads was 16 percent. However, back emission data were not available or this would have facilitated the determination of the collector work function. These were the results that were targeted in the effort to verify the performance of the Lanthanum Hexaboride diminiode after it was set up at AFWAL/WPAFB.

##### b) Performance Verification

As indicated earlier, after several attempts, the output load circuit was finalized so that the diminiode could be driven with a positive as well as a negative bias voltage. Figure 5.2 indicates a typical comparison of the NASA LeRC test results (NASA) as well as the AFWAL/WPAFB test results for the Lanthanum Hexaboride diminiode for an emitter temperature at 1700 K. The NASA results were obtained from the source indicated in Figure 5.1, and the AFWAL data points were the actual experimental data points acquired after setting up the diminiode station at the Aero Propulsion Laboratory (APL) of AFWAL/WPAFB. Tests were repeated for all the five emitter temperatures but only a representative characteristic corresponding to an emitter temperature of 1700 K has been indicated. The collector was figure

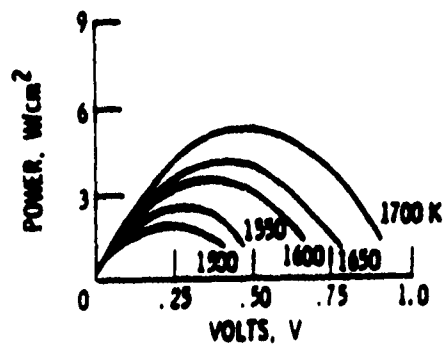
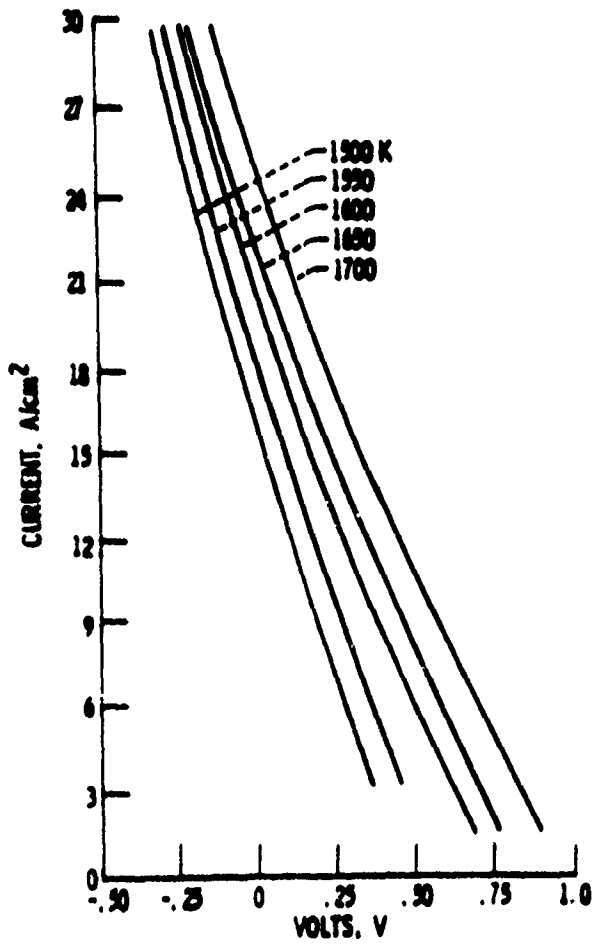


Figure 5.1 Output Current Density and Output Power Density - NASA Characteristics.

# CURRENT AND POWER DENSITY CHARACTERISTICS

(Lanthanum Hexaboride Diminished Output)

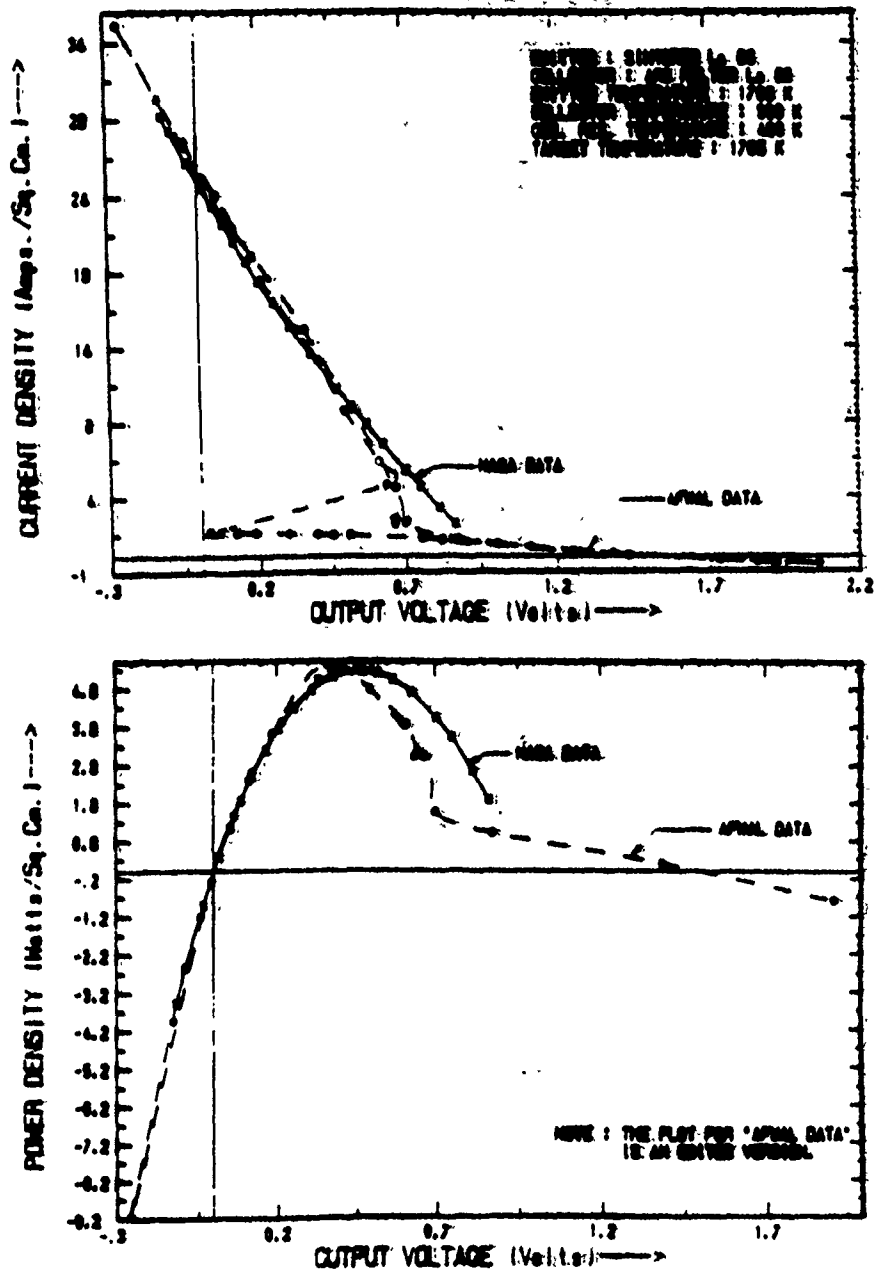


Figure 5.2

Comparison of Output Characteristics with the Emitter at 1700 K.

maintained at 900 K, and the cesium reservoir was maintained at 460 K for this test. The corresponding target temperature was 1765 K. As seen in Figure 5.2, there was excellent correspondence between the two sets of data points as exhibited by the respective changes in output current density with change in output voltage. Sufficient information was not available to compare the data at every point on the characteristic such as at ignition, after de-ignition, the open circuit voltage, etc. As a result only the AFWAL DATA characteristic display the key points such as ignition and de-ignition. Though de-ignition was not sharply defined, the fact that it did occur was clearly obvious by the evidence that the current densities followed the same magnitude before ignition and after de-ignition above an output voltage of 0.8 V. The open circuit voltage was found to be 1.55 V and the short circuit current density was 25.5 A/cm<sup>2</sup>.

There was close correspondence between the two sets of data points as far as the variation of power density with output voltage was concerned. However, it was found that there was a slight shift in the output voltages at which the power density characteristics peaked. This discrepancy is most likely a consequence of the fact that the biasing was manual for the tests conducted at AFWAL whereas it was automated for those conducted at NASA LeRC. This makes a lot of difference, specially in the assumption that the electrode temperatures remain constant during the sweep, which is not quite true for manual biasing. Thus there is a possibility that a small change in temperature between data points resulted in the power density peaks occurring at different output voltages. The verification tests were conducted at five different emitter temperatures in the range of 1500 K to 1700 K. A summary of the important parameters for the performance tests are shown in Table 5.1.

#### 5.1.2 Multi-Stage Cesium Reservoir Temperature Optimization

The performance from every pair of electrodes in a new diode has to be optimized with respect to the cesium reservoir temperature, the collector temperature and the emitter temperature in order to arrive at the optimum design point at which this diode will operate if it were to be used in a thermionic reactor. The optimization for each parametric temperature is done iteratively till the temperature corresponding to peak performance is obtained. This section

**Table 5.1 Summary of Important Parameters for the Performance Tests on the Lanthanum Hexaboride Diode.**

| Sl. # | $T_E$ | $J_{SC}$ | $V_{OC}$ | $V_{PP}$ | $P_P$ | $T_C$ | $T_R$ |
|-------|-------|----------|----------|----------|-------|-------|-------|
| 1     | 1700  | 25.5     | 1.52     | 0.47     | 3.2   | 900   | 460   |
| 2     | 1650  | 21.7     | 1.55     | 0.41     | 4.1   | 850   | 450   |
| 3     | 1600  | 18.5     | 1.50     | 0.35     | 2.8   | 850   | 440   |
| 4     | 1550  | 15.5     | 1.42     | 0.25     | 2.1   | 850   | 440   |
| 5     | 1500  | 13.8     | 1.20     | 0.17     | 1.1   | 850   | 440   |

$T_E$  . EMITTER TEMPERATURE. K

$T_C$  . COLLECTOR TEMPERATURE. K

$T_R$  . CESIUM RESERVOIR TEMPERATURE. K

$J_{SC}$  . SHORT CIRCUIT CURRENT DENSITY. Amps/Sq.Cm.

$V_{OC}$  . OPEN CIRCUIT VOLTAGE. Volts

$V_{PP}$  . OUTPUT VOLTAGE AT PEAK POWER. Volts.

$P_P$  . PEAK POWER DENSITY. Watts/Sq.Cm.

provides the details on the multi-stage cesium reservoir temperature optimization and recommends the optimum cesium reservoir temperature.

a) Preliminary Optimization

The data in Figures 5.3 and 5.4 have been presented to reflect the dependence of the output - current and output - power characteristics on the cesium reservoir temperature. Figure 5.3 includes a family of current - density characteristics where the cesium reservoir temperature was varied from 350 K to 550 K with the emitter temperature fixed at 1700 K and the collector temperature fixed at 900 K. As seen in the figure, the current densities increased with increase in cesium reservoir temperature initially but then decreased above a reservoir temperature of 485 K, in the positive quadrant. The slope of the Boltzmann line changed but the overall current and power densities decreased. This is also observable from Figure 5.4 which represents the power densities as a function of the diode output voltage.

The family of curves in Figure 5.4 defines an envelope curve, i.e., a curve that is tangent to all characteristics of the family. This envelope curve shown in Figure 5.5 which is technically termed the optimized output - current density characteristic with respect to the cesium reservoir temperature is called an optimum characteristic because for given fixed parameters and electrode output voltage, this characteristic yields the maximum output current density that can be achieved by varying the cesium reservoir temperature. In other words, all possible operating data points can only lie below this envelope no matter what the value of the cesium reservoir temperature. The cesium pressure at each point of the optimized characteristic equals that of the output - current density characteristic tangent to the envelope at the point in question. For relatively low output voltages, the points of tangency are on the ignited mode branches of the output -current density characteristics. This implies that at these voltages, the performance achieved by the unignited mode is better than that of the ignited mode.

Optimized output current density characteristics can also be presented as optimized electrode or terminal output - power density characteristics. This is done by plotting the product of current density and the voltage of points on the envelope versus the diode

# CESIUM OPTIMIZED OUTPUT CHARACTERISTICS

(Lanthanum Hexaboride Diminide Output)

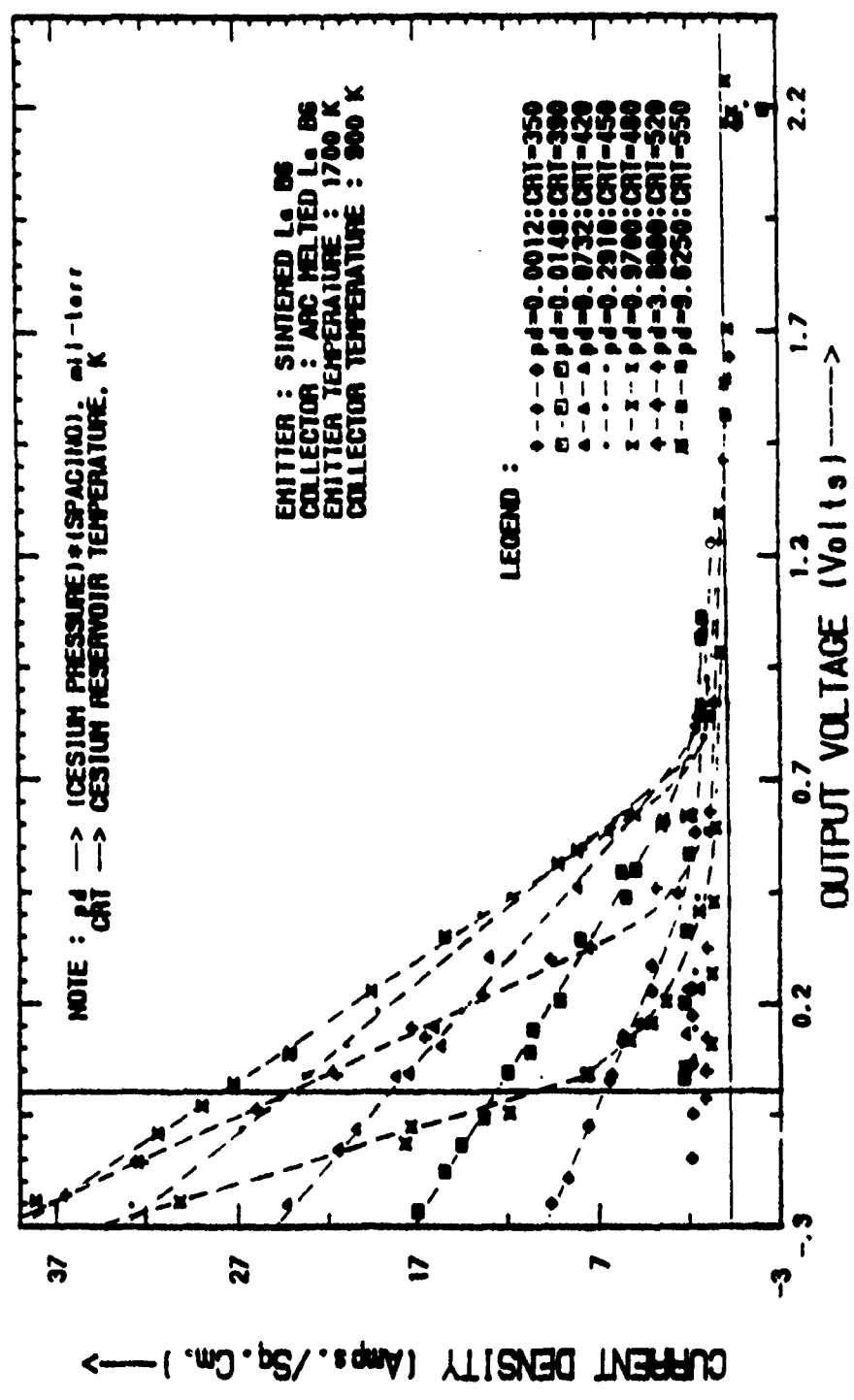


Figure 5.3 Output Current Density Characteristics for Various Cesium Reservoir Temperatures.

# CESIUM OPTIMIZED OUTPUT CHARACTERISTICS

## (Lanthanum Hexaboride Diminide Output)

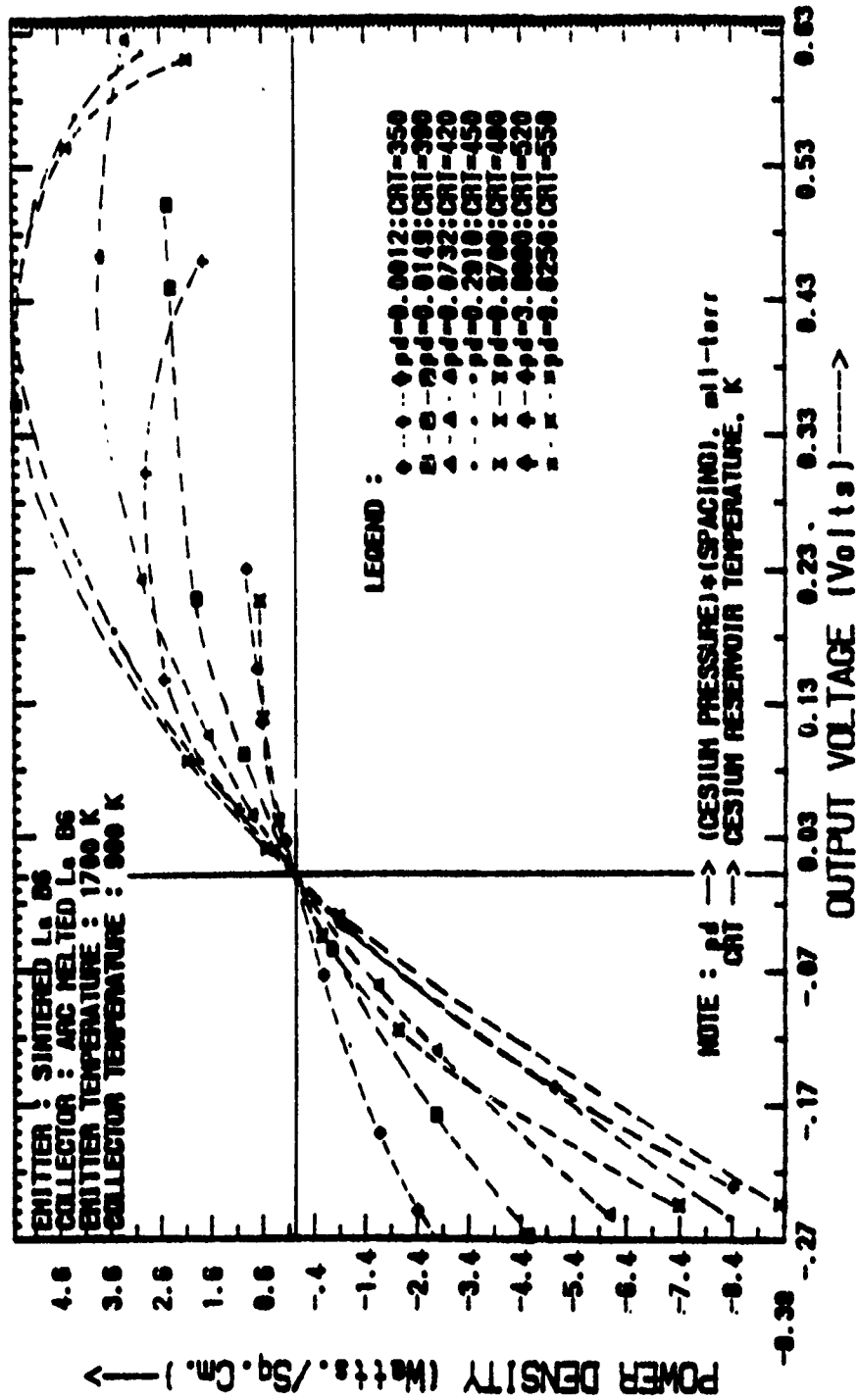


Figure 5.4 Output Power Density Characteristics for Various Cesium Reservoir Temperatures.

output voltage. The cesium-optimized power density characteristic corresponding to the cesium-optimized current density characteristic in Figure 5.5 is shown in Figure 5.6. The cesium optimized power density characteristic was found to peak at 0.395 volts. The significance of this peak is that from a design point of view, if this diode were to operate at an emitter temperature of 1700 K and a collector temperature of 900 K, the best output can only be obtained by operating the diode at the optimum cesium reservoir temperature and an output voltage of 0.395 volts.

b) Optimum Cesium Reservoir Temperature

The current density characteristics in Figure 5.3 only indicate that the optimum cesium reservoir temperature lies somewhere between 480 K and 520 K but does not narrow down the range any further to yield a better value. In order to narrow down this broad range from 40°C to 10°C or better, the short circuit current density and the peak power density for each cesium reservoir temperature were plotted as a function of a nondimensional temperature. These plots are indicated in Figure 5.7 where the nondimensional temperature was chosen as the ratio of emitter temperature to the cesium reservoir temperature. Ideally, the short circuit current density and the peak power density are expected to peak at the same nondimensional temperature but there may be a shift in the peaks as the cesium reservoir temperatures at which the tests were conducted were not very close together. As seen in Figure 5.7, the short circuit current density plot peaks at a nondimensional temperature of 6.8 whereas the peak power density plot peaks at 7.2. Thus, there is a small bandwidth in the cesium reservoir temperature variation, that translates to  $477 \pm 6$  K. If the criterion for maximum performance is peak power density, then the diode should be operated with the cesium reservoir temperature at the higher level.

c) Empirical Relationship Between Power Density and Output Voltage for Cesium Optimization

The peak power densities for the plot in Figure 5.7 were obtained by simulating curve fits for each one of the power density characteristics in Figure 5.4 over a

# ENVELOPE FOR THE CESIUM OPTIMIZED FAMILY (Lanthanum Hexaboride Diminide Output)

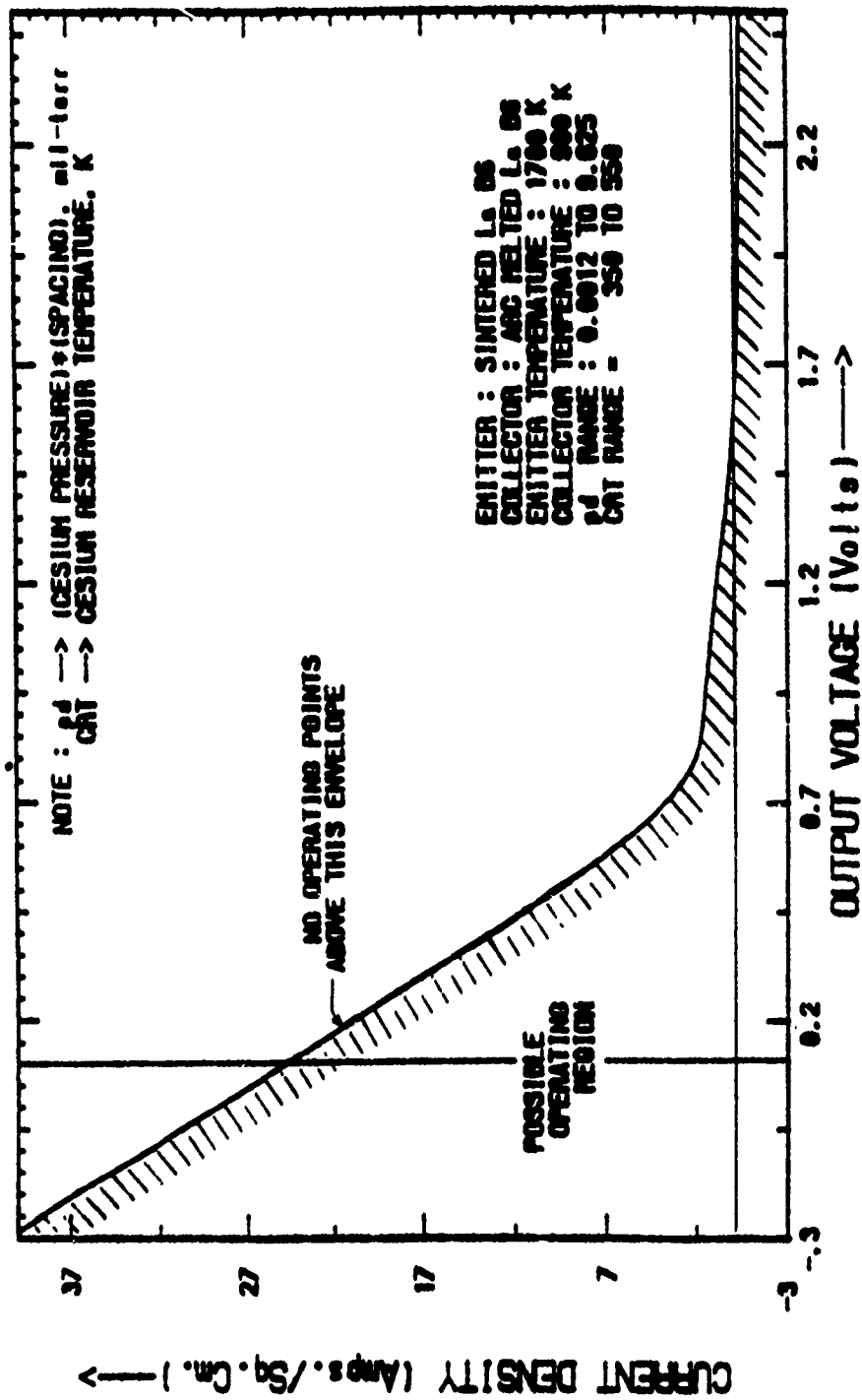


Figure 5.5 Optimized Electrode Output Current Density Characteristic Envelope for Cesium Pressure.

# ENVELOPE FOR THE CESIUM OPTIMIZED FAMILY

(Lanthanum Hexaboride Diimide Output)

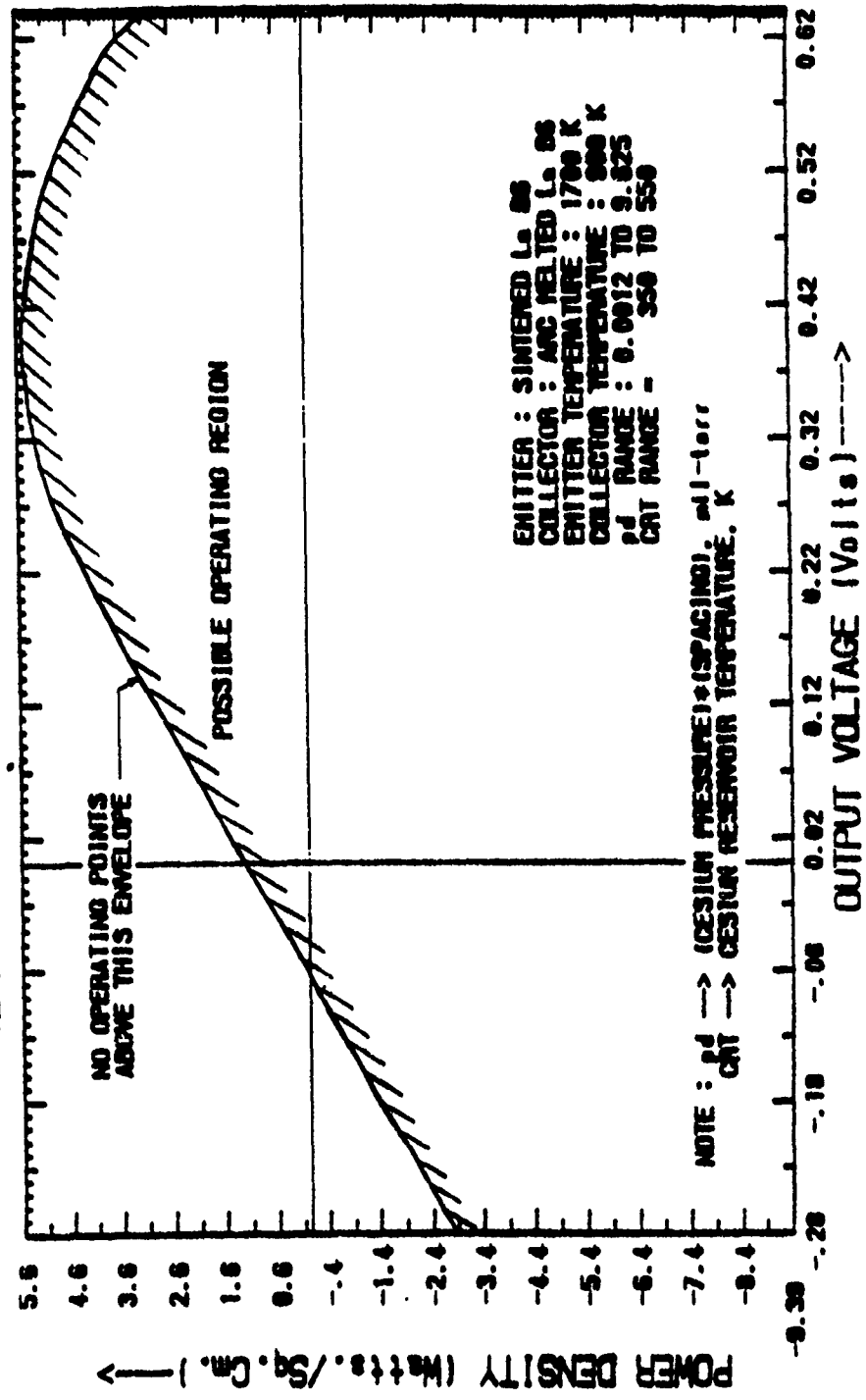


Figure 5.6 Optimized Electrode Output Power Density Characteristic Envelope for Cesium Pressure.

SHT. CCT. CURRENT & PEAK POWER DEN.  
(CESIUM RESERVOIR TEMPERATURE OPTIMIZATION)

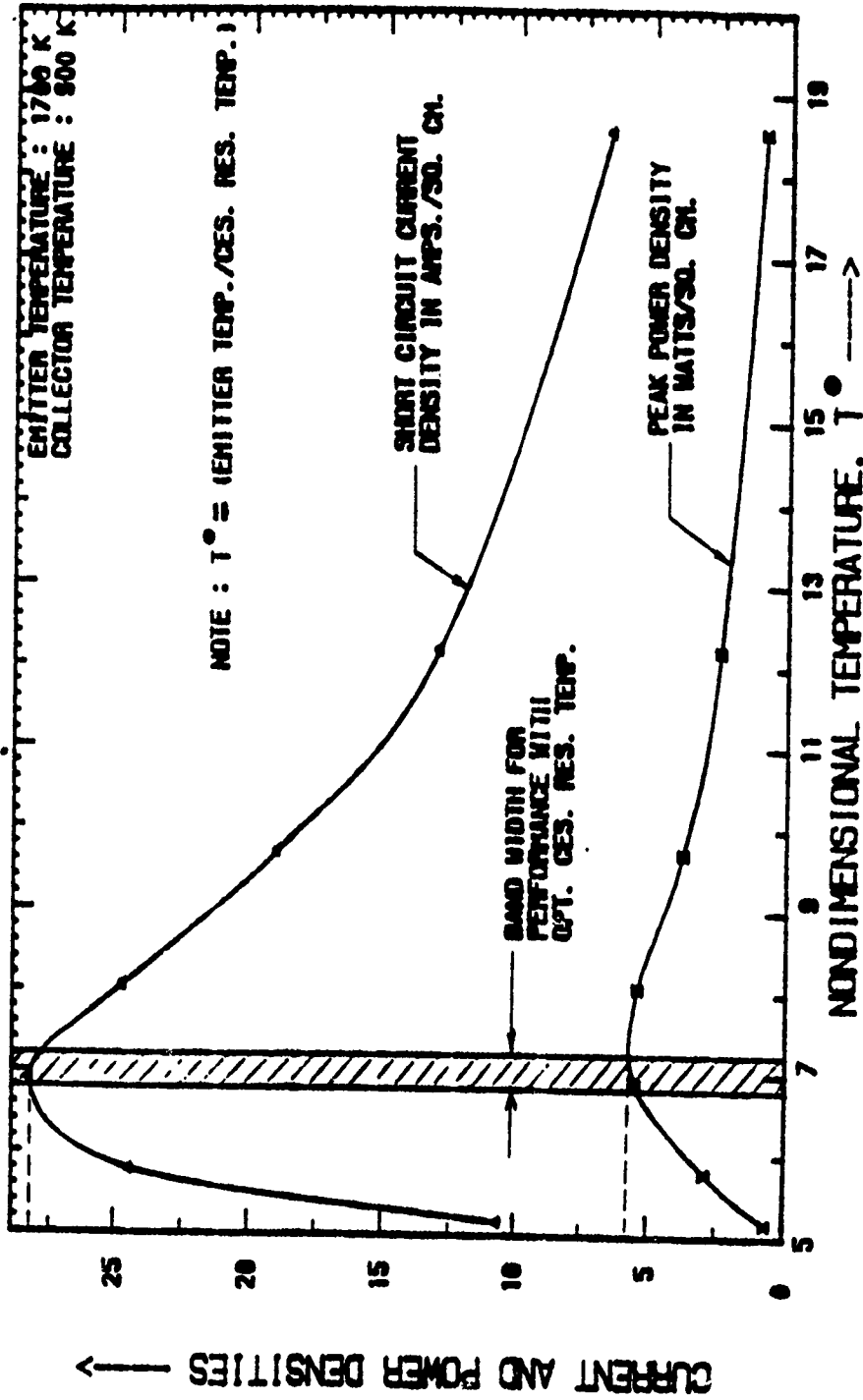


Figure 5.7 Effects of Cesium Reservoir Temperature on the Short Circuit Density and Peak Power Density.

voltage range of 0.00 to +0.75 volts. A summary of the equations (with minimum errors) that resulted from the curve fitting along with the error limits is provided below.

a)  $T_R = 350 \text{ K}$   

$$P = 5.488(V)^3 - 10.7199(V)^2 + 6.5094(V) - 0.0073 \quad (5.1)$$

Maximum error = 6.75%

b)  $T_R = 390 \text{ K}$   

$$P = 233.898(V)^6 - 116.1461(V)^5 - 22.2763(V)^4 + 13.6685(V)^3 \\ - 15.8978(V)^2 + 12.2152(V) - 0.0099 \quad (5.2)$$

Maximum error = 0.0093%

c)  $T_R = 420 \text{ K}$   

$$P = 4.5541(V)^3 - 23.5818(V)^2 + 18.1602(V) + 0.002 \quad (5.3)$$

Maximum error = -1.632%

d)  $T_R = 450 \text{ K}$   

$$P = -136.918(V)^6 + 65.484(V)^5 - 2.6845(V)^4 + 5.1515(V)^3 \\ - 29.611(V)^2 + 24.445(V) - 0.0063 \quad (5.4)$$

Maximum error = -0.013%

e)  $T_R = 480 \text{ K}$   

$$P = -159.057(V)^6 - 30.1783(V)^5 + 70.2534(V)^4 + 10.901(V)^3 \\ - 43.8937(V)^2 + 27.8117(V) - 0.0023 \quad (5.5)$$

Maximum error = -1.549%

f)  $T_R = 520 \text{ K}$   

$$P = 646.1684(V)^6 - 155.3342(V)^5 - 104.7557(V)^4 + 23.487(V)^3 \\ - 46.4499(V)^2 + 24.032(V) - 0.0055 \quad (5.6)$$

Maximum error = 0.0077%

g)  $T_R = 550 \text{ K}$   

$$P = 1047.7726(V)^5 - 73.8637(V)^4 + 173.1835(V)^3 - 53.5009(V)^2 \\ + 9.3878(V) + 0.0112 \quad (5.7)$$

Maximum error = 6.501%

In equations 5.1 through 5.7,  $P$  represents the power density in watts/cm<sup>2</sup>.  $T_r$  represents the cesium reservoir temperature and  $V$  represents the diode output voltage in volts. Each one of these equations was used in a BASIC program to compute the maximum power density for each cesium reservoir temperature.

d) Final Stage of Cesium Reservoir Temperature Optimization

The results of the second stage cesium reservoir temperature performance optimization tests are shown in Figures 5.8 and 5.9. Figure 5.8 indicates the output current density characteristics as a function of the output voltage for various cesium reservoir temperatures. During these cesium reservoir temperature optimization tests, the collector temperature was maintained at 885 K and the emitter temperature at 1700 K. It was found that the maximum short circuit current density occurred with a cesium reservoir temperature of 500 K but this was just about 1 A/cm<sup>2</sup> (or less) more than the corresponding value at 475 K. However, as seen in Figure 5.9 which are the corresponding plots for the power density as a function of output voltage, the plot for a cesium reservoir temperature of 485 K has a higher peak power density than the plot for 495 K. This observation together with the fact that the spread in the experimental data exceeds  $\pm 0.5$  A/cm<sup>2</sup> provides sufficient evidence that the optimum cesium reservoir temperature lies in the vicinity of 485 K.

5.1.3 Multi-Stage Collector Temperature Optimization

a) Collector Temperature Optimization

Figures 5.10 and 5.11 represent the collector optimized output current density and output power density characteristics respectively. As indicated in the figures, the emitter temperature was maintained at 1700 K, the cesium reservoir temperature was maintained at 485 K while the collector temperature was varied from 750 K to 1020 K. As in the cesium reservoir temperature optimization the current densities in the positive output quadrant increased with increase in the collector temperature to about 900 K and then started dropping for high collector temperatures. The slope of the Boltzmann line however did not indicate a significant change as in the cesium reservoir temperature optimization. Further, the variation in current densities over the entire collector temperature range is very small compared to the corresponding

# CES. RES. OPTIMIZED OUTPUT CHARACTERISTICS

(Second Stage Ces. Res. Temp. Optimization ; Load)

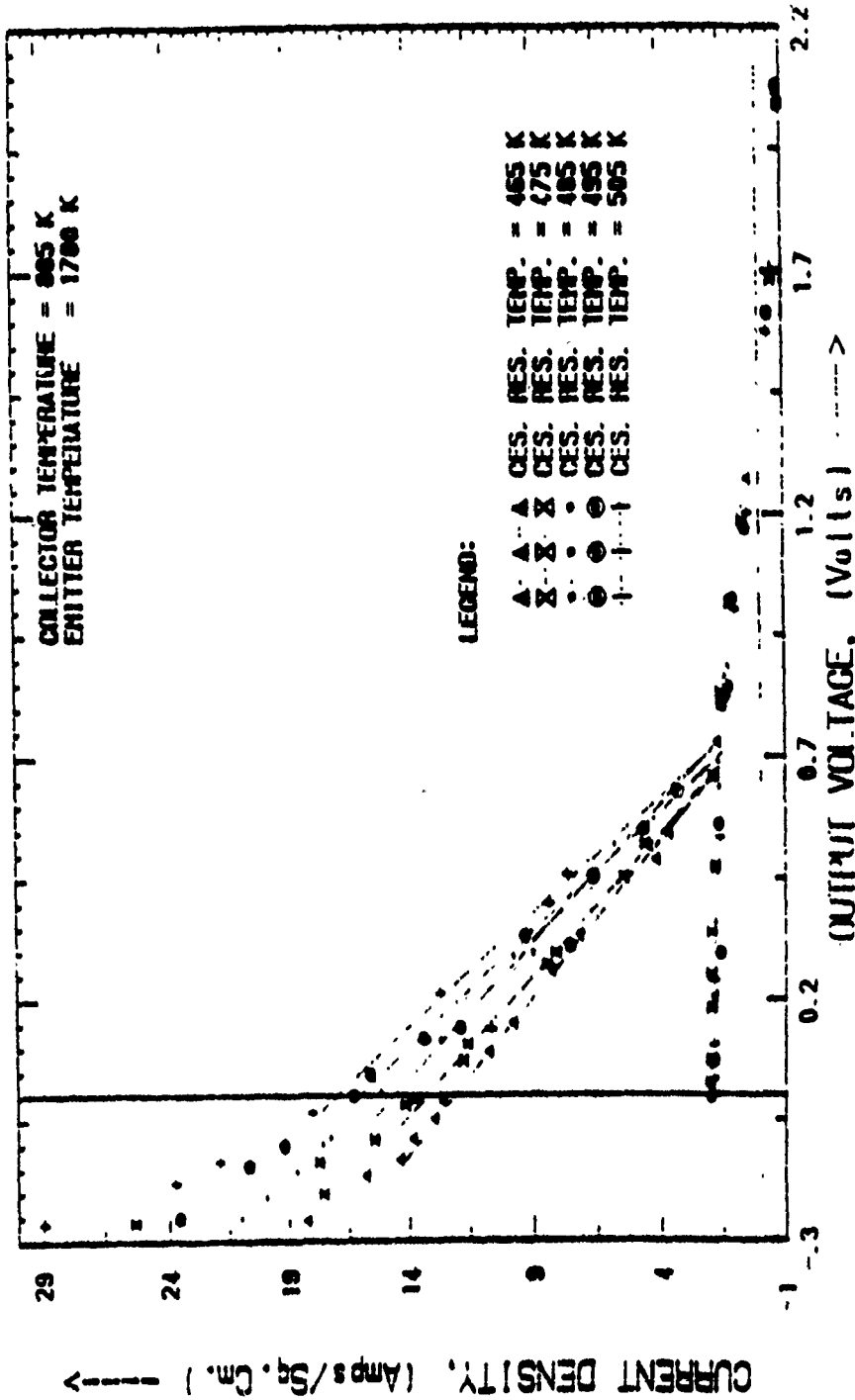


Figure 5.8 Final Stage Cesium Reservoir Temperature Optimized Output Current Density Characteristics.

# CES. RES. OPTIMIZED OUTPUT CHARACTERISTICS

(Second Stage Ces. Res. Temp. Optimization : LaB6)

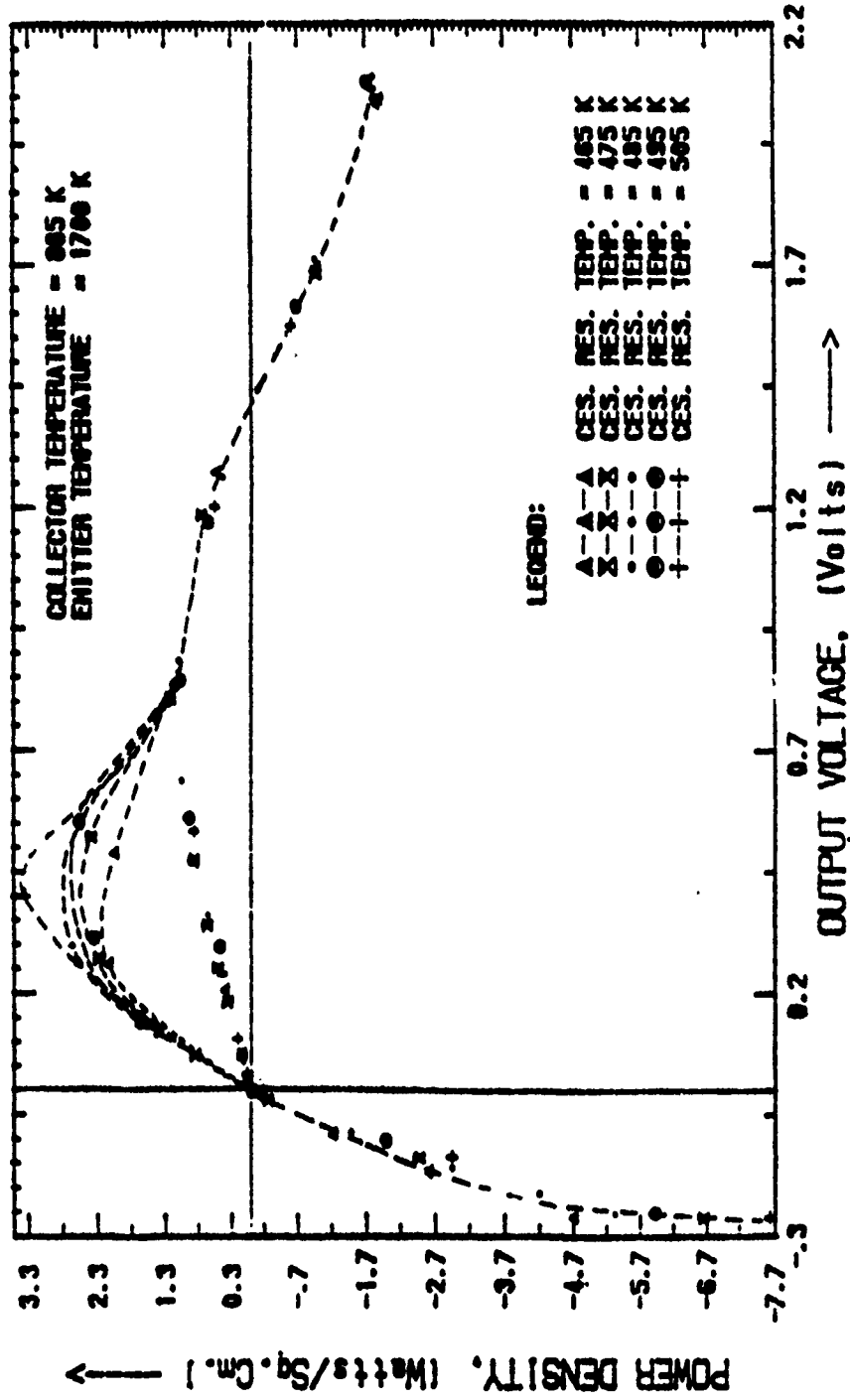


Figure 5.9 Final Stage Cesium Reservoir Temperature Optimized Output Power Density Characteristics.

# COLLECTOR OPTIMIZED OUTPUT CHARACTERISTICS

(Collector Temperature Optimization for LaB6 Diminide)

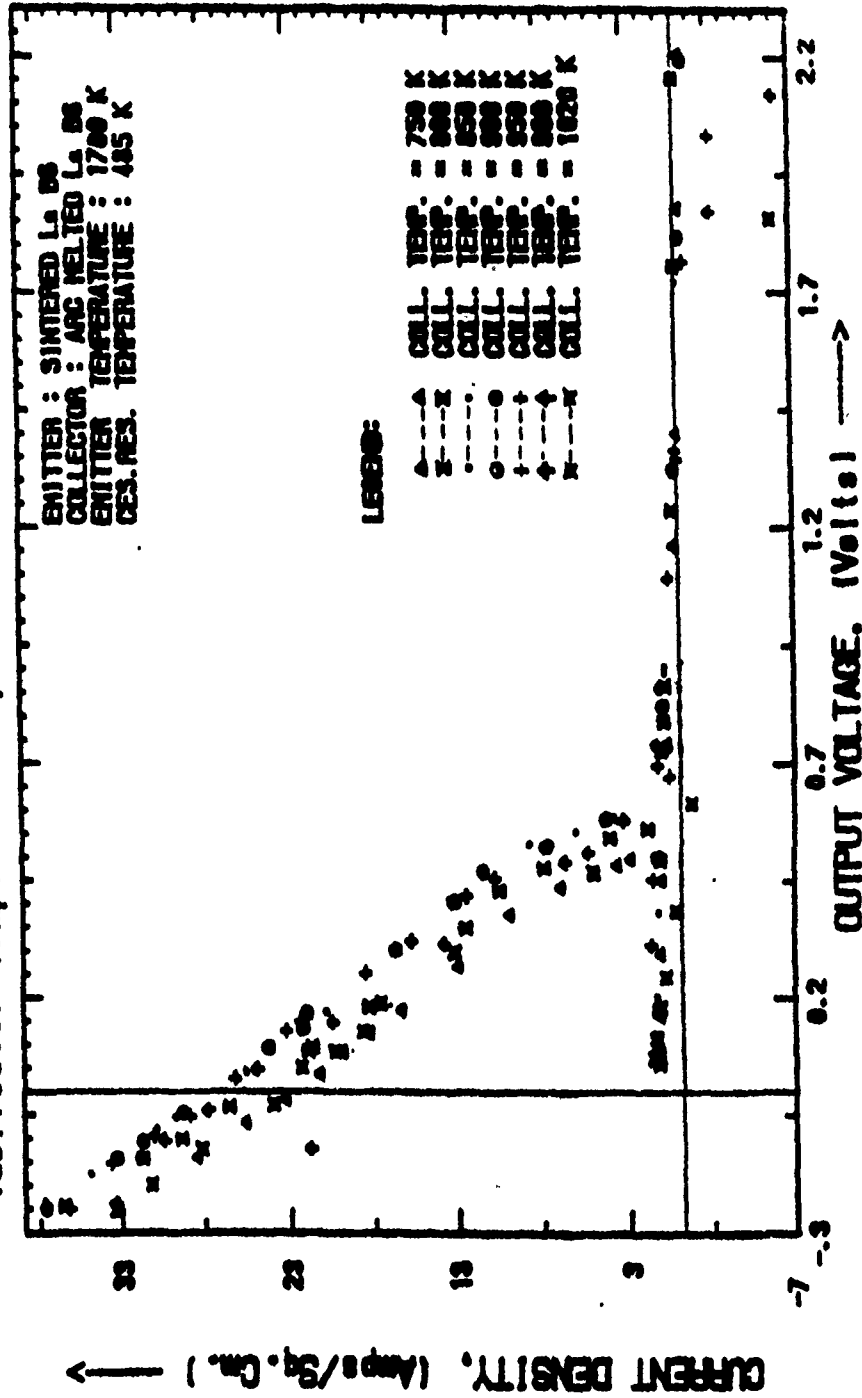


Figure 5.10 Output Current Density Characteristics for Various Collector Temperatures.

# COLLECTOR OPTIMIZED OUTPUT CHARACTERISTICS

(Collector Temperature Optimization for LaBB Diemidele)

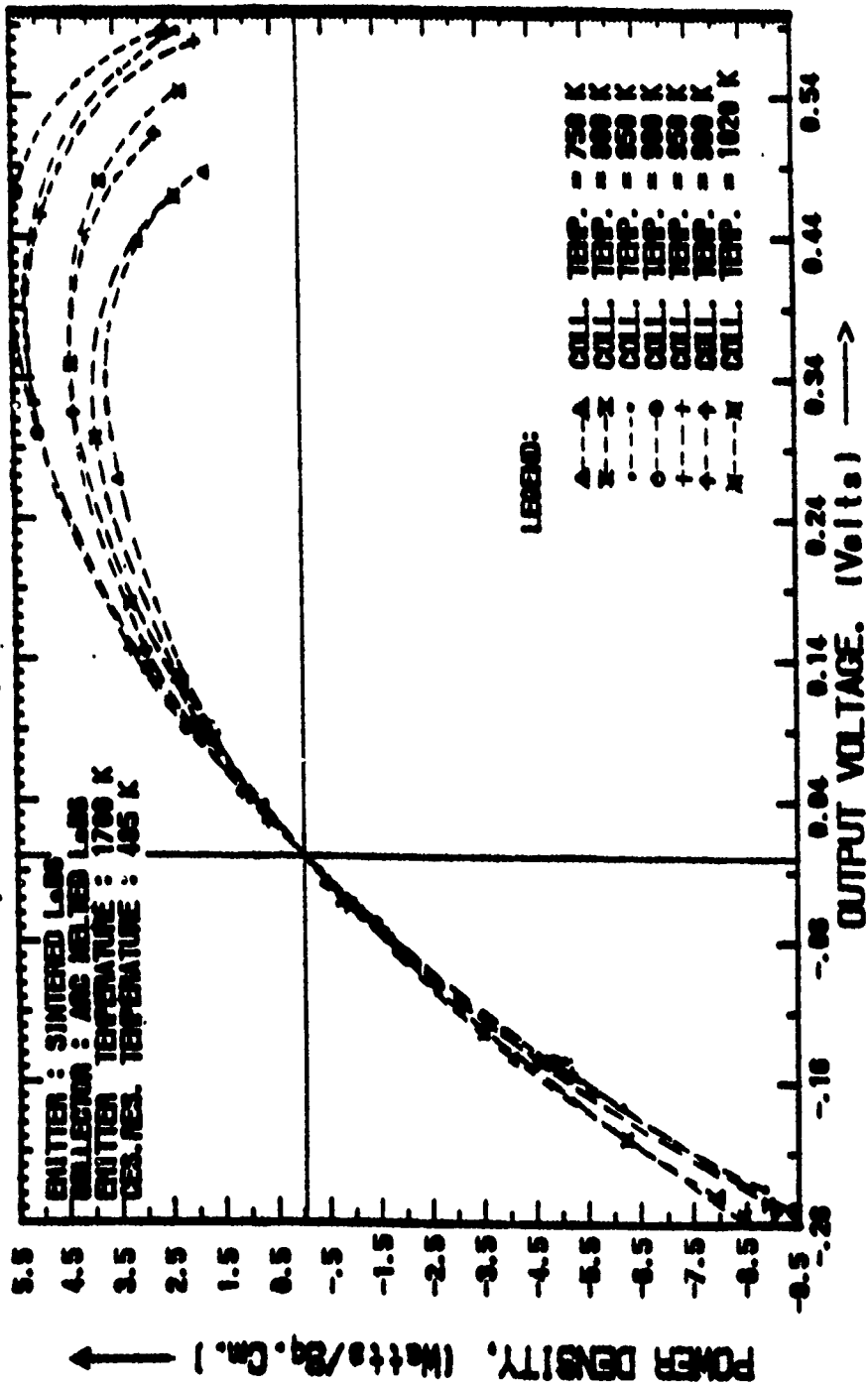


Figure 5.11 Output Power Density Characteristics for Various Collector Temperatures.

variation in the cesium reservoir temperature optimization. This implies that the cesium reservoir temperature has a great effect on the output characteristics of the diode in the concerned temperature range.

As seen in Figure 5.10 there is significant back emission for collector temperatures above 950 K. This back emission not only causes the difference in work functions between the emitter and collector to change but also reduces conduction of electrons due to the extra intermolecular/interparticle collisions. Thus there is a detrimental effect in increasing the collector temperature indefinitely in that the overall power output comes down significantly. The changes caused by changing the collector temperature for given values of emitter and cesium reservoir temperature are more easily discernible in Figure 5.11, in the region where the power density characteristics peak out.

The optimized electrode output current density characteristic envelope with respect to the collector temperature is shown in Figure 5.12. The corresponding optimized electrode output power density characteristic envelope with respect to the collector temperature is shown in Figure 5.13. Both these envelopes represent the best possible output parameters for a given emitter and cesium reservoir temperature. All possible operating points can only lie within the envelope regardless of how high the collector temperature could be increased. The collector optimized power density characteristic was found to peak at about 0.39 volt which would be the optimum design operating point for a Lanthanum Hexaboride diode with an emitter temperature of 1700 K and a cesium reservoir temperature of 485 K.

b) Optimum Collector Temperature

Figure 5.14 indicates the variation of the short circuit current density and the peak power density with the collector temperature which in this case has been built into a nondimensional temperature,  $T'$ . The nondimensional temperature is the ratio of the emitter temperature to the collector temperature. The short circuit current density was found to peak at a non-dimensional temperature of 2.356 while the peak power density peaked at 2.31. This

# COLLECTOR OPTIMIZED FAMILY ENVELOPE

(Collector Temperature Optimization for LeB6 Diminide)

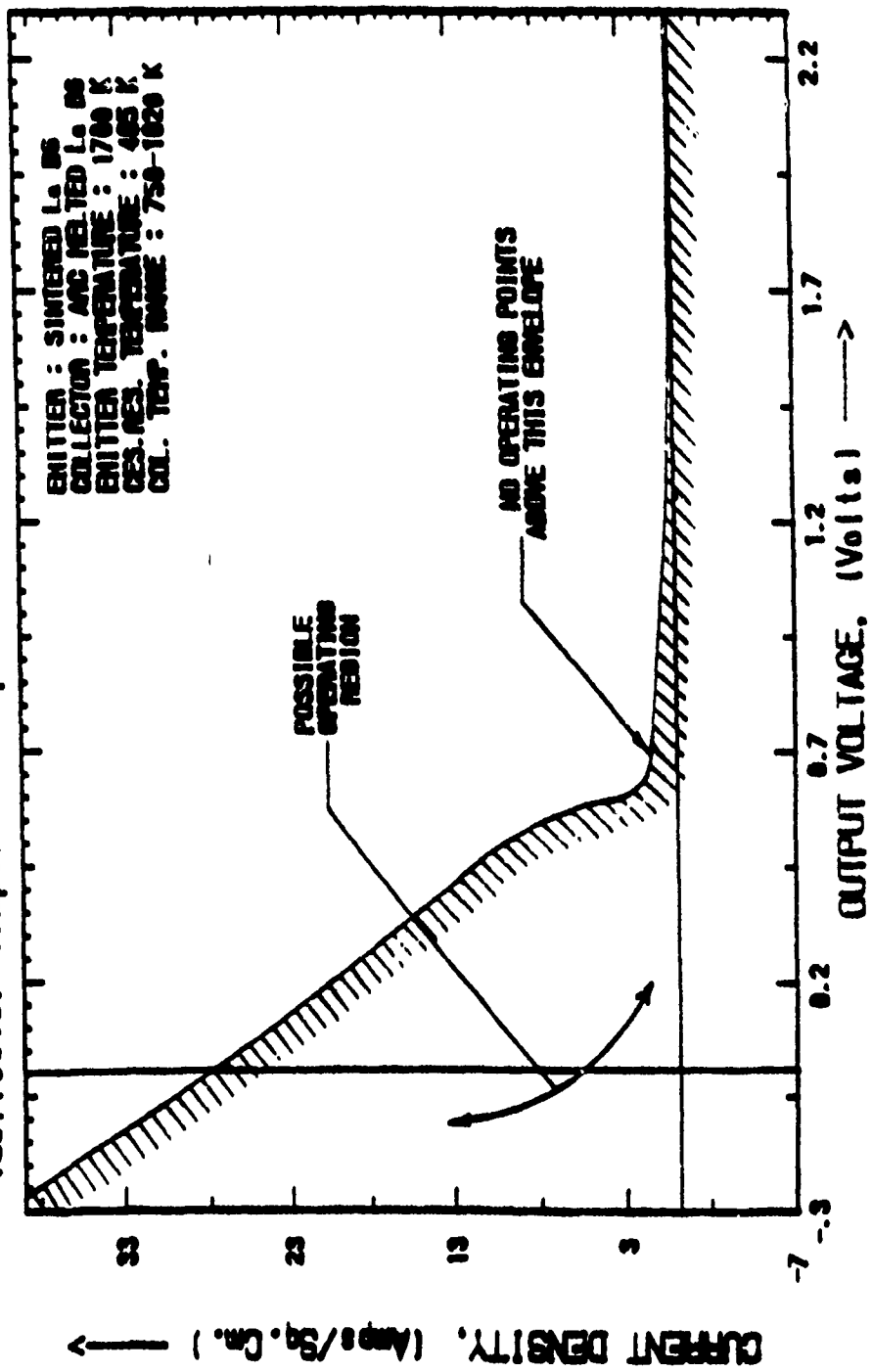


Figure 5.12 Optimized Electrode Output Current Density Characteristic Envelope for Collector Temperature.

# COLLECTOR OPTIMIZED FAMILY ENVELOPE

(POWER DENSITY ENVELOPE for LeB6 Diminide)

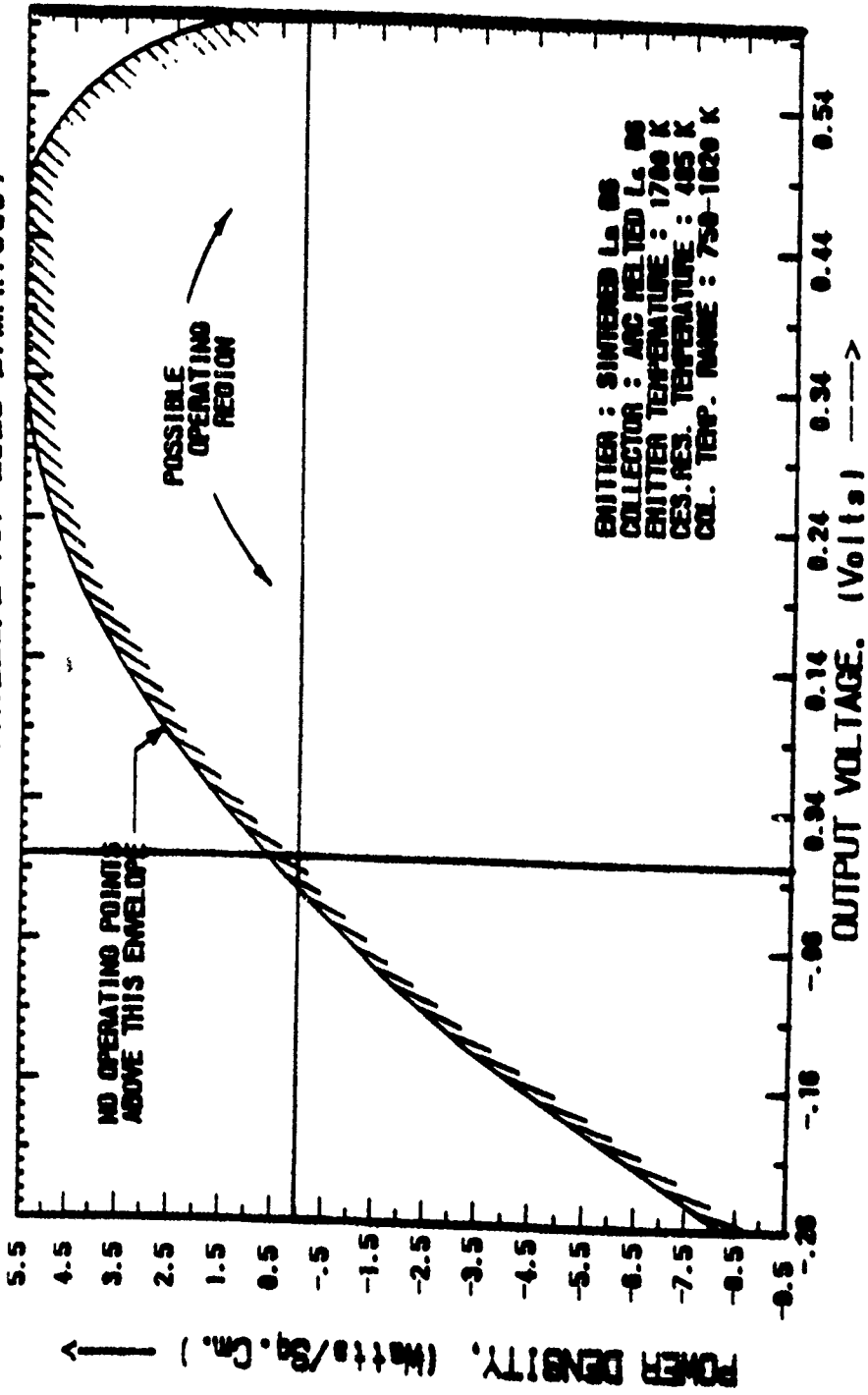


Figure 5.13 Optimized Electrode Output Power Density Envelope for Collector Temperature.

# SHT. CCT. CURRENT & PEAK POWER DEN. (COLLECTOR TEMPERATURE OPTIMIZATION)

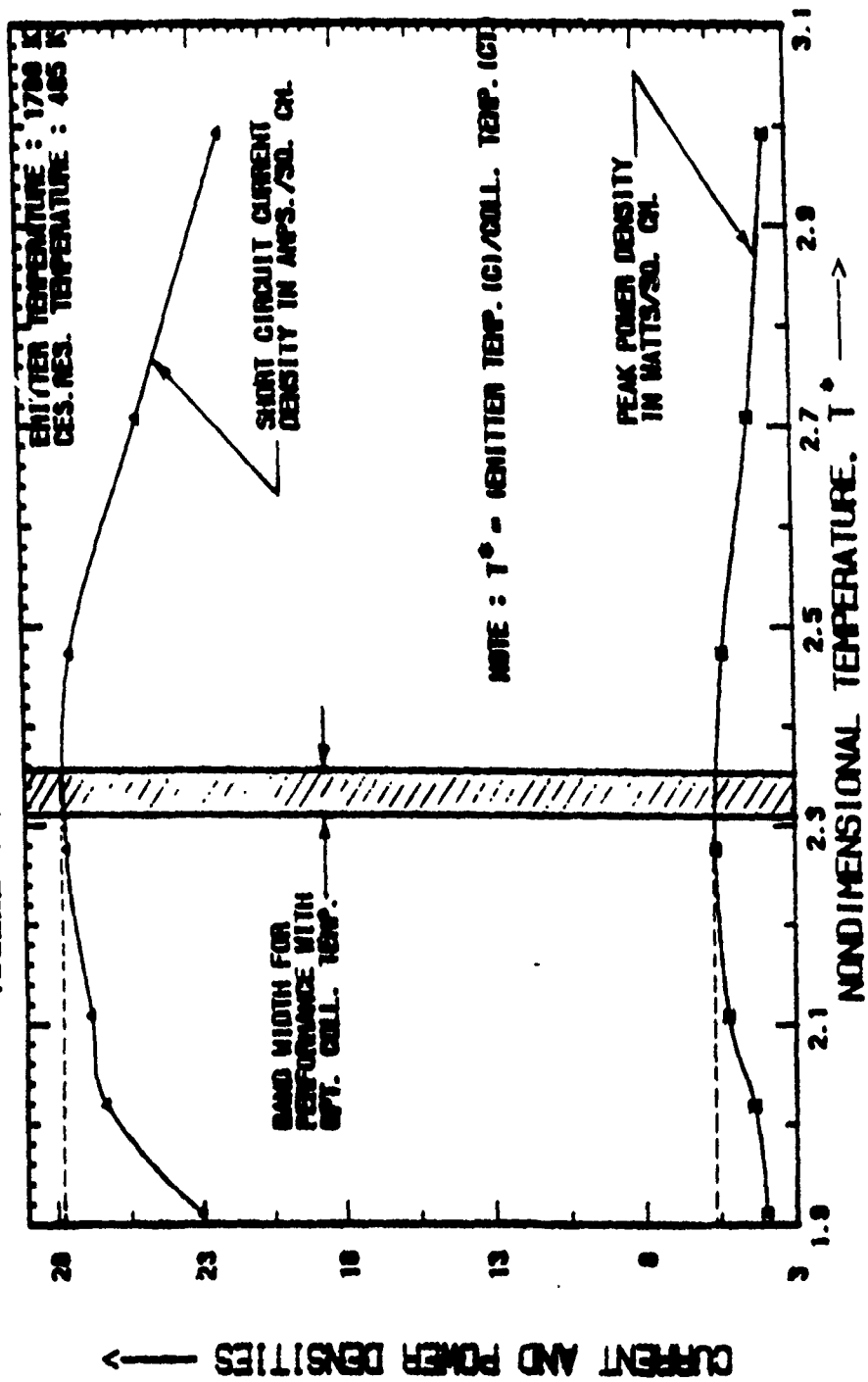


Figure 5.14 Effects of Collector Temperature on the Short Circuit Current Density and Peak Power Density.

translates to a collector temperature range of  $612 \pm 6^\circ\text{C}$ . The band width for performance with the optimum collector temperature is clearly shown in Figure 5.14.

c) Final Stage Collector Temperature Optimization

Figure 5.15 represents the output current density characteristics of the second stage collector temperature optimization tests. From the short circuit current density values for the various collector temperatures, the maximum short circuit current density occurs with the collector at 855 K. However, in Figure 5.16 there is a sharp drop in power density at this temperature above 0.4 volt. This sharp drop is not observed at higher temperatures and given the spread in the experimental data, the most likely value of optimum collector temperature would be 870 K. Any more accuracy in arriving at the optimum temperatures can only be obtained with high frequency data points generated with a 20-ms sweep.

5.1.4 Emitter Temperature Optimization

The emitter temperature optimization test on the Lanthanum Hexaboride diiminide was conducted with constant collector and cesium reservoir temperatures of 885 K and 477 K respectively. The emitter temperature was varied from 1450 K to 1700 K. The lower limit on this temperature was based on the fact that there was practically no positive output current below 1400 K, and the upper limit was based on the material bonding strength. The emitter is hot pressed to the tantalum target and the bonding is weakened above 1750 K partly because of the thermal expansion mismatch and partly because of the high reactivity of Lanthanum Hexaboride. Figure 5.17 represents the current density characteristics for the various emitter temperatures. As seen in the figure, the highest current densities were obtained with the emitter at 1700 K. On the way towards a negative bias voltage, ignition occurs earlier at a higher emitter temperature indicating that the emitter temperature plays an important part in the bulk or volume ionization of cesium atoms. The collector was maintained at 885 K and the cesium reservoir was maintained at 477 K, their respective optimized temperatures. Figure 5.18 represents the optimized electrode output current density characteristic envelope with respect to emitter temperature.

# COLLECTOR OPTIMIZED OUTPUT CHARACTERISTICS

(Second Stage Collector Temp. Optimization ; LaB6)

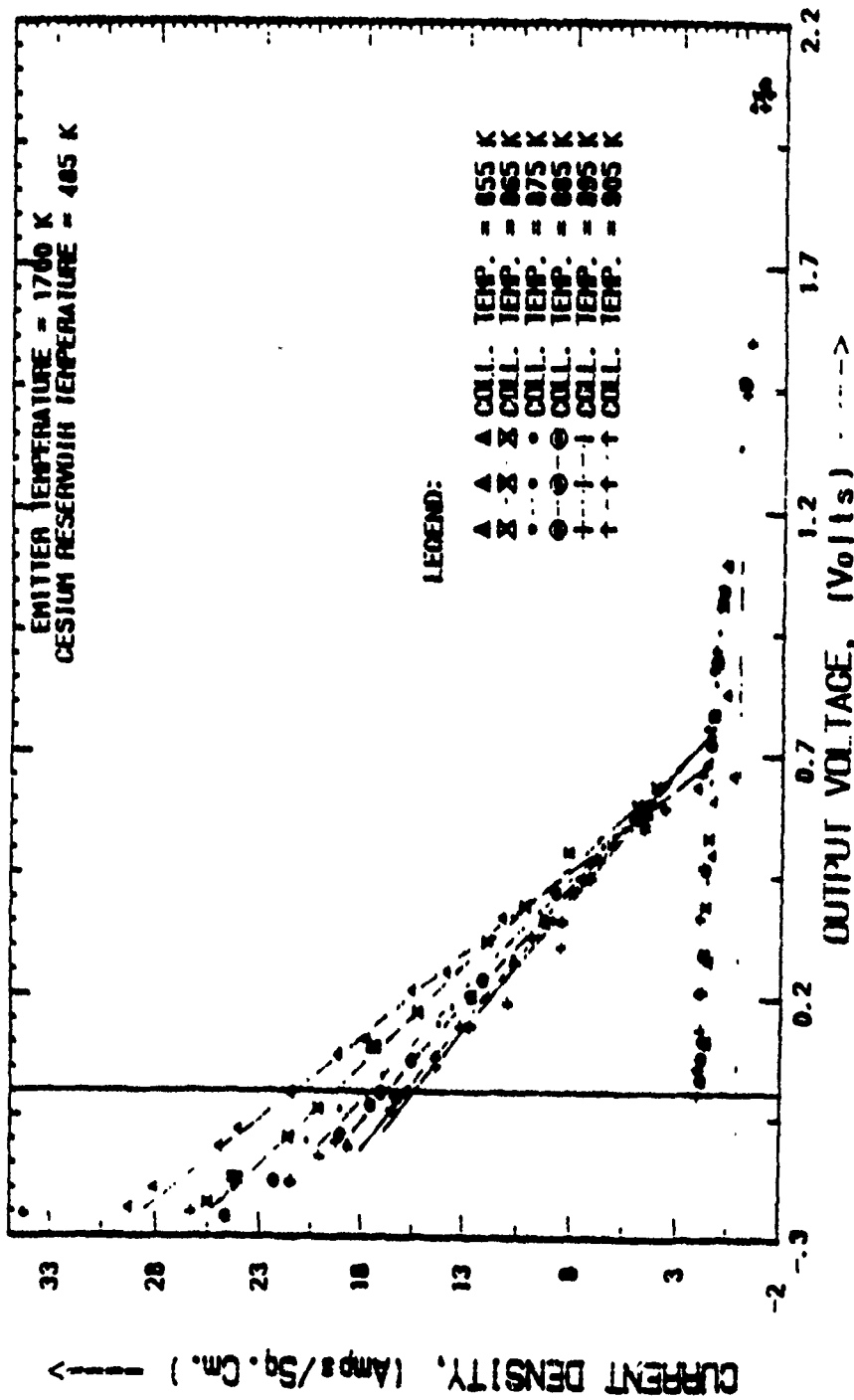


Figure 5.15 Final Stage Collector Temperature Optimized Output Current Density Characteristics.

# COLLECTOR OPTIMIZED OUTPUT CHARACTERISTICS

(Second Stage Collector Temp. Optimization ; Lab6)

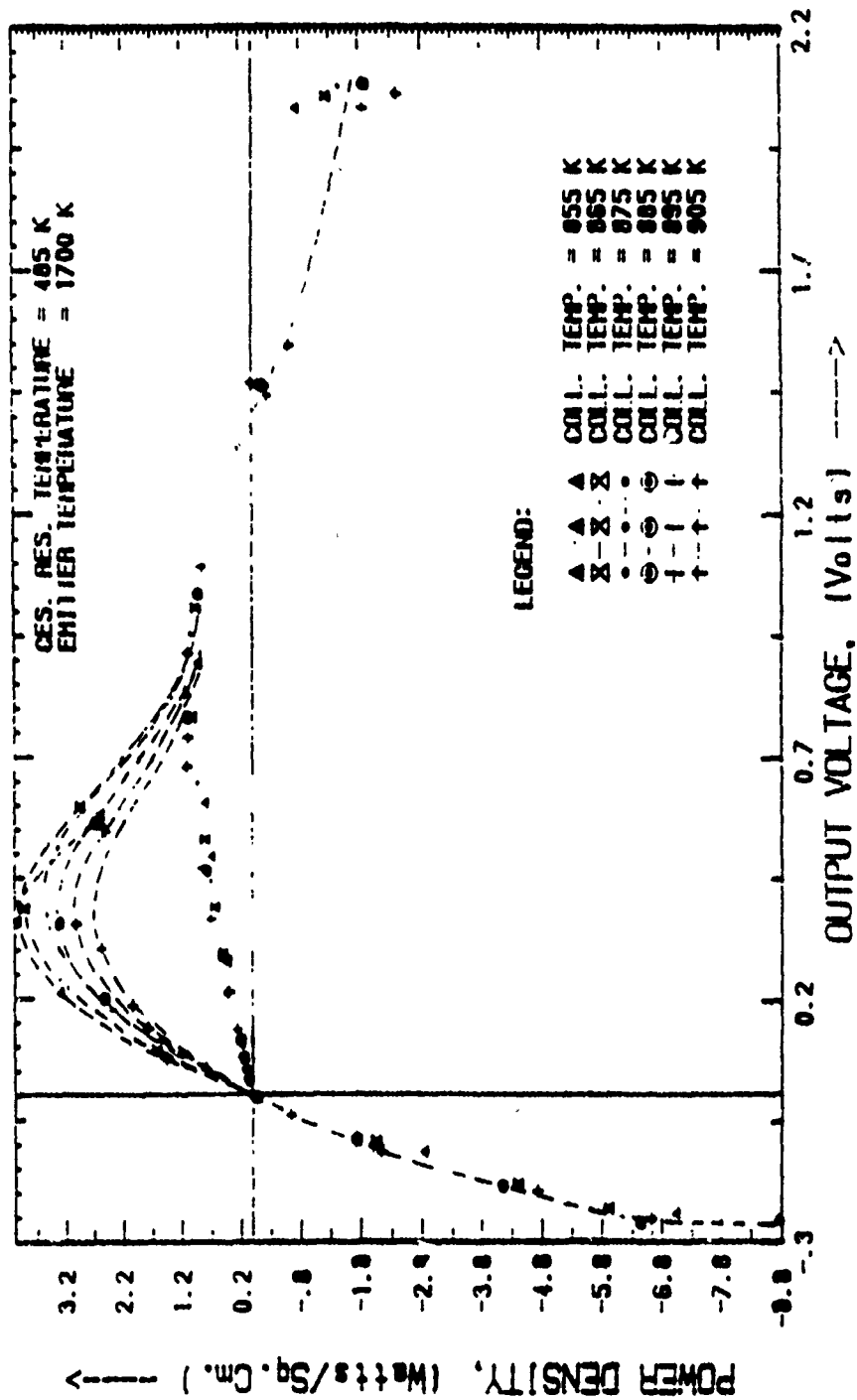


Figure 5.16 Final Stage Collector Temperature Optimized Output Power Density Characteristics.

# EMITTER OPTIMIZED OUTPUT CHARACTERISTICS

(Emitter Temperature Optimization for LeE6 Diminide)

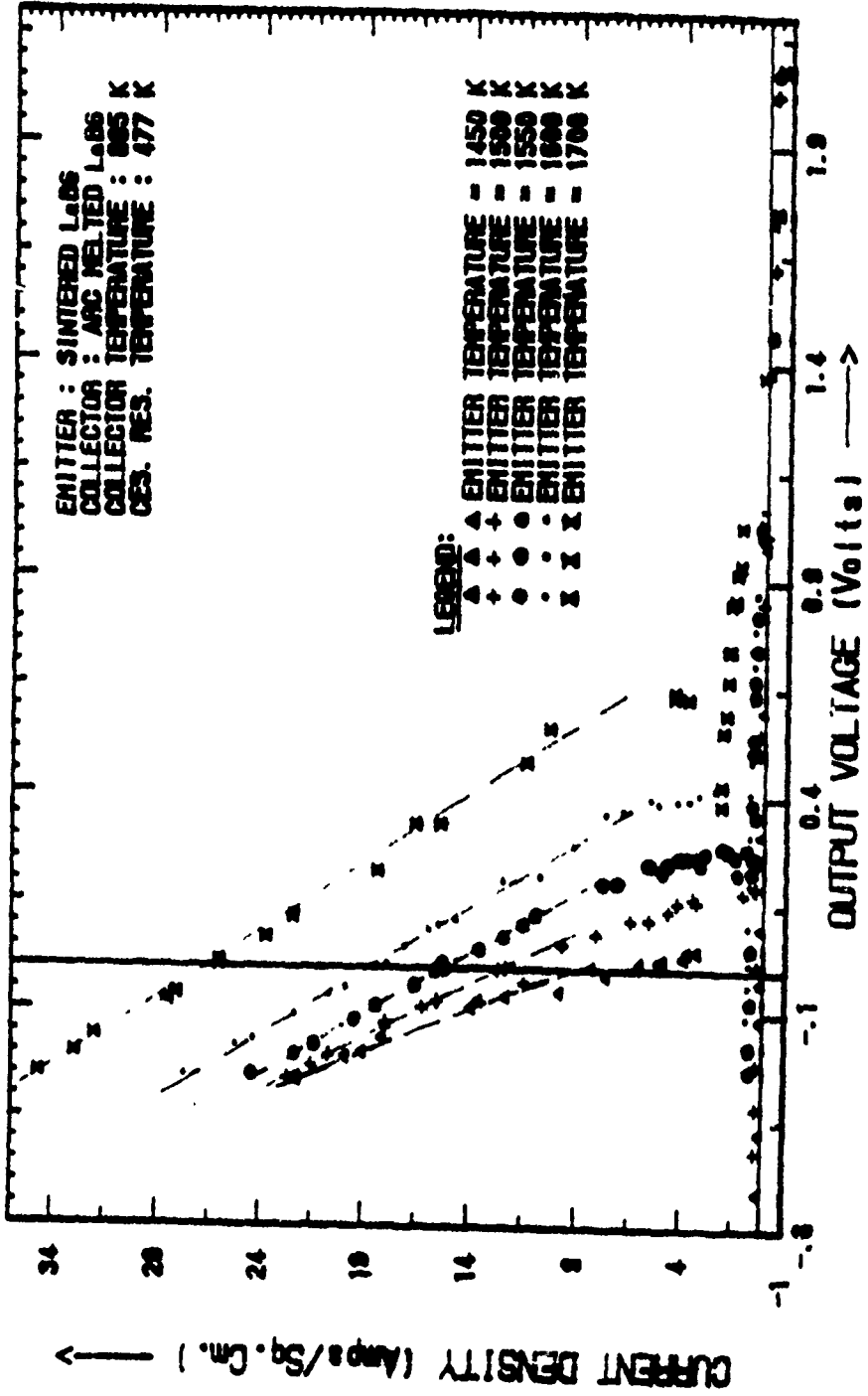


Figure 5.17 Output Current Density Characteristics for Various Emitter Temperatures

# EMITTER OPTIMIZED FAMILY ENVELOPE

(Emitter Temperature Optimization for LaB6 Diminide)

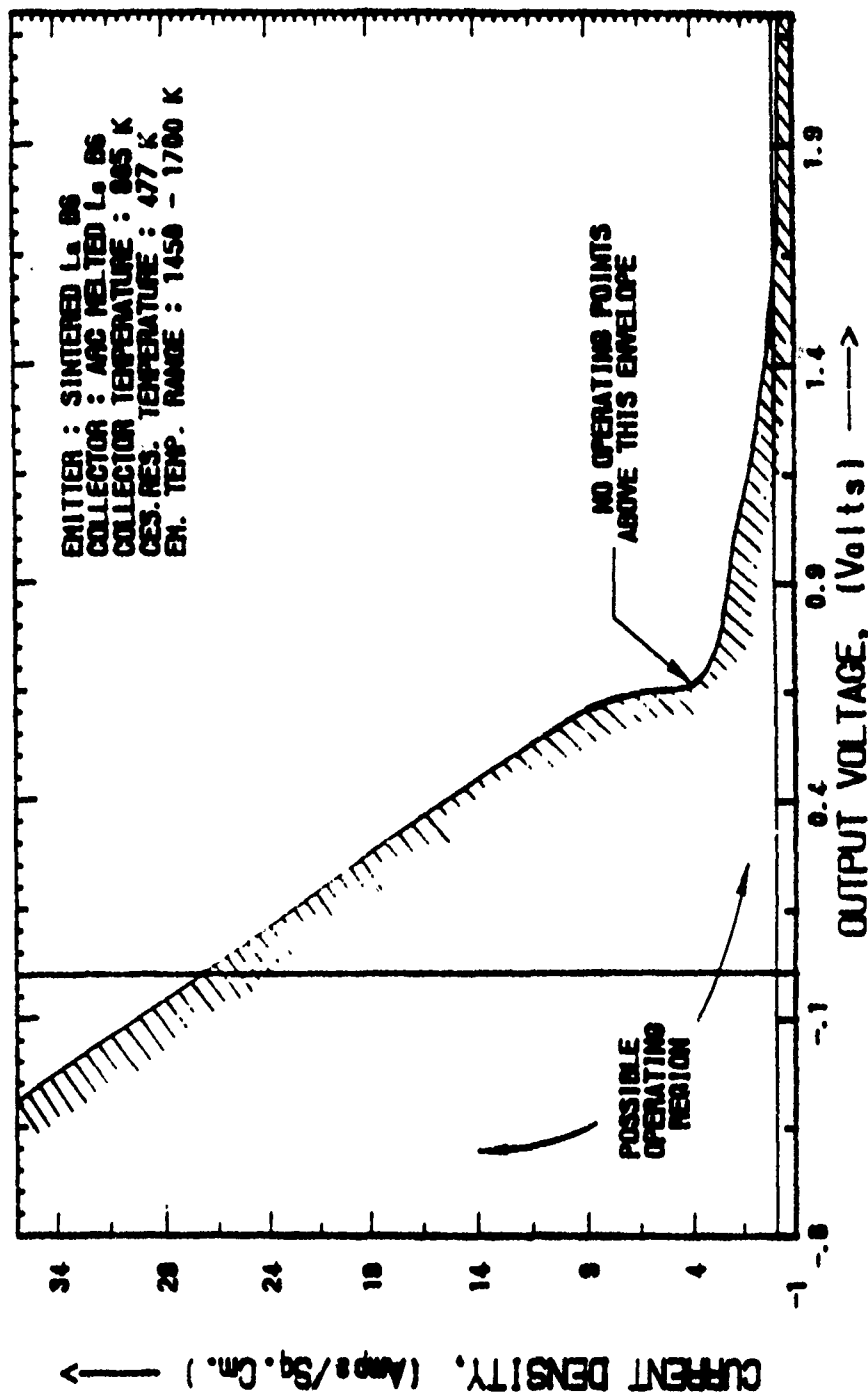


Figure 5.18 Optimized Electrode Output Current Density Characteristic Envelope for Emitter Temperature.

Figure 5.19 represents the output power density characteristics and Figure 5.20 represents the optimized electrode output power density characteristic envelope with respect to emitter temperature. These figures show that the peak power density occurs at about 0.45 volt. In an earlier series of collector temperature optimization tests, the peak occurred at 0.39 volt. By repeated iterations of optimization one can finally arrive at a design parameter for the diode output voltage at which peak emission occurs. The broken line in Figure 5.20 indicates that portion of the power density envelope that would have existed had ignition in all cases of emitter temperature, occurred above 0 volt.

Figure 5.21 indicates the variation of short circuit current density and peak power density as a function of the nondimensional temperature,  $T^*$ . The nondimensional temperature is the ratio of the maximum emitter temperature (1700 K) to the emitter temperature for a given test. The slopes of the two plots indicate that there might have been a peak at a temperature greater than 1700 K, but due to material bonding limitations, it was not advisable to go to higher temperatures. Thus, for all practical purposes the optimized emitter temperature was found to be 1700 K. Multi-stage optimization was not conducted in this case because of the temperature restraint above 1700 K.

#### 5.1.5 Ignition and De-Ignition Studies

Tests were conducted on the  $\text{LaB}_6$  diode in order to determine the current density and output voltage before and after ignition. The results of these tests are indicated in Table 5.2. Since the sequence of tests was not completed, no graphic representations have been provided. As seen in the table, the voltage at which ignition occurs increases with increase in emitter temperature which is expected and normal. The current density also increases with increase in emitter temperature but not as sharply as the rise in voltage.

Figure 5.22 gives the experimental data as well as the linear approximation for the variation of ignition voltage before and after ignition with variation in emitter temperature. The emitter temperature was varied from 1400 K to 1700 K. Higher temperatures could not be attained as a result of the bonding strength deterioration between the emitter and target. The

# EMITTER OPTIMIZED OUTPUT CHARACTERISTICS

(Emitter Temperature Optimization for LaB6 Diode)

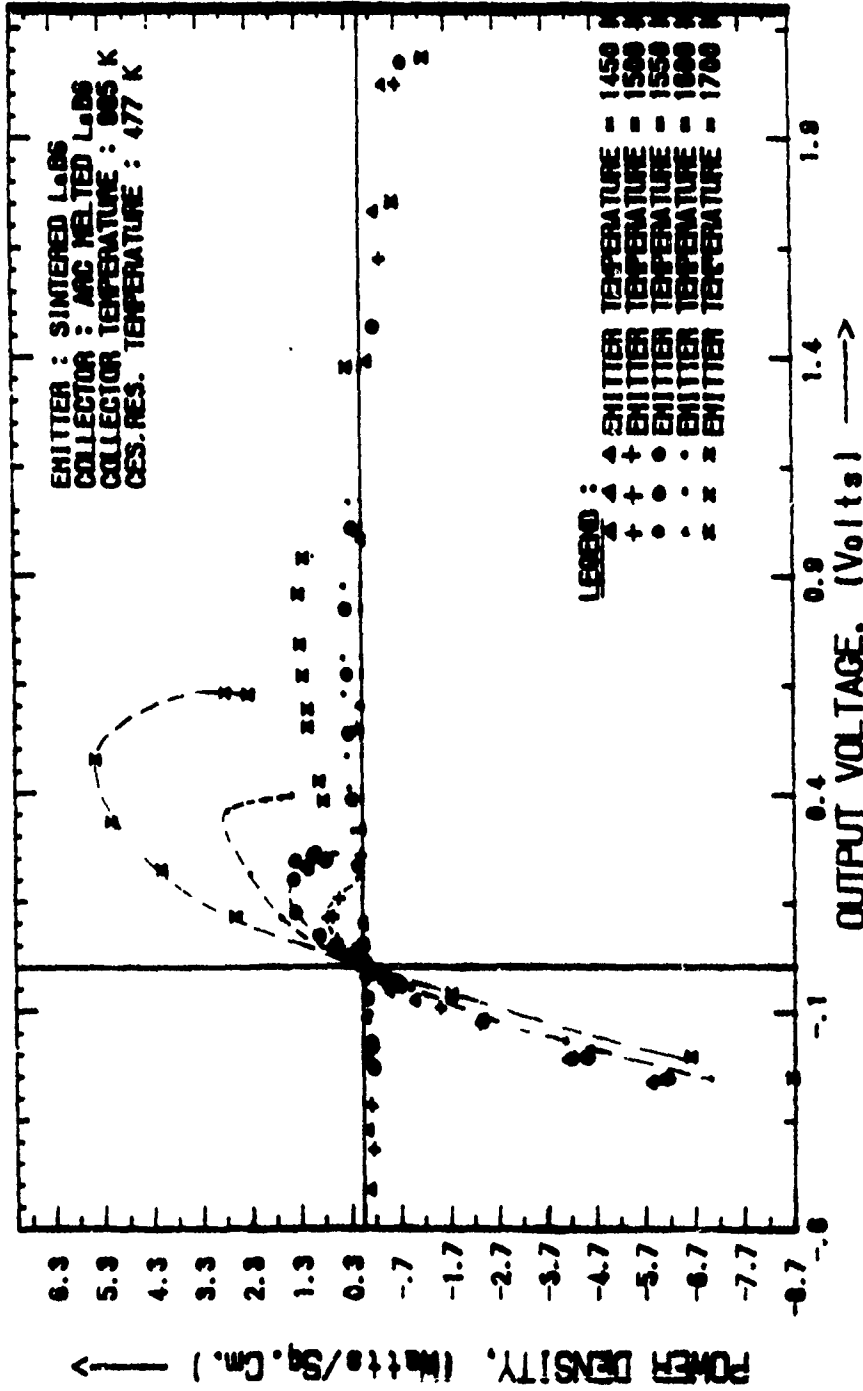


Figure 5.19 Output Power Density Characteristics for Various Emitter Temperatures.

# EMITTER OPTIMIZED FAMILY ENVELOPE (power)

(Emitter Temperature Optimization for LaB6 Diminide)

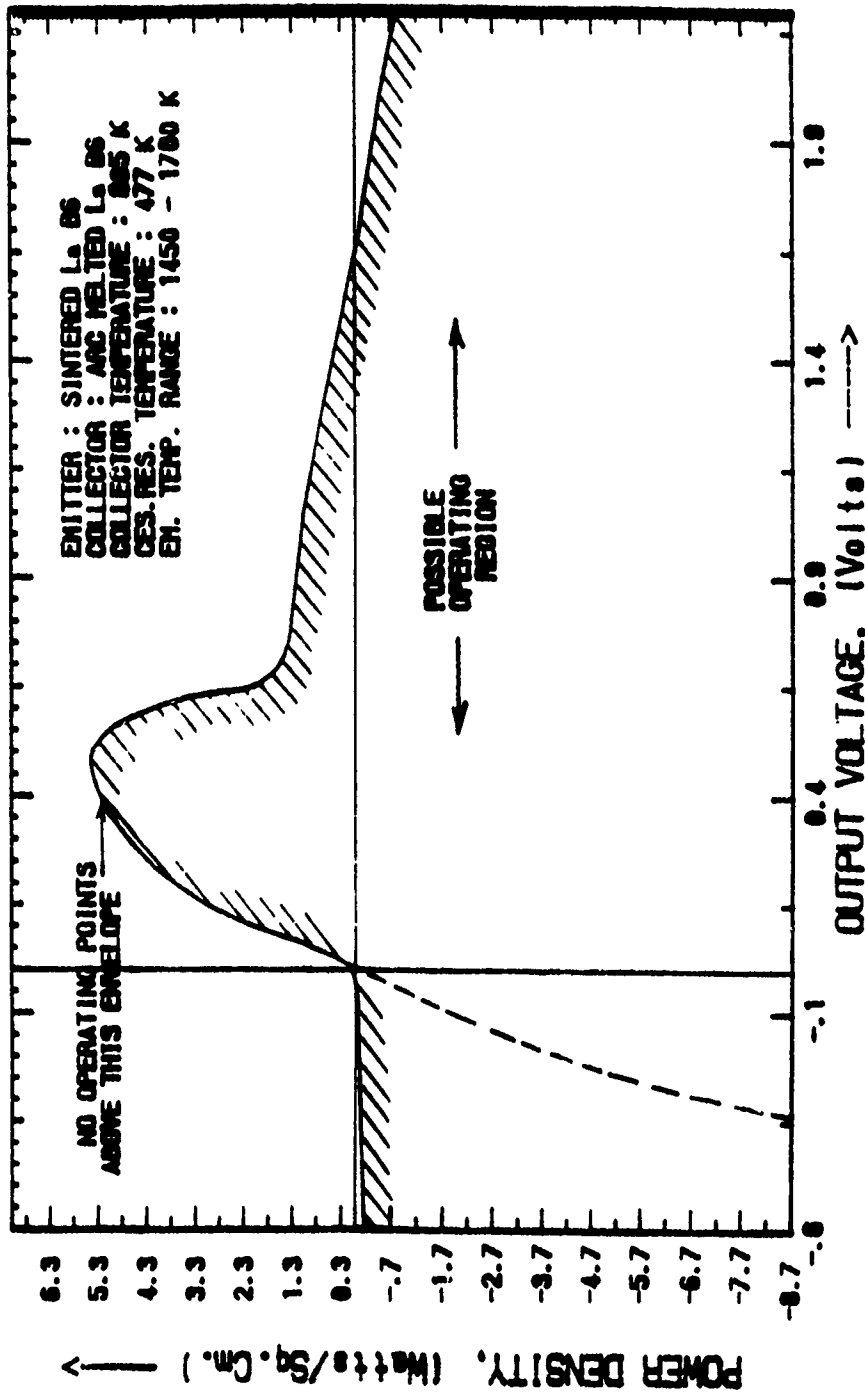


Figure 5.20 Optimized Electrode Output Power Density Characteristic Envelope for Emitter Temperature.

# SHT. CCT. CURRENT & PEAK POWER DEN. (EMITTER TEMPERATURE OPTIMIZATION)

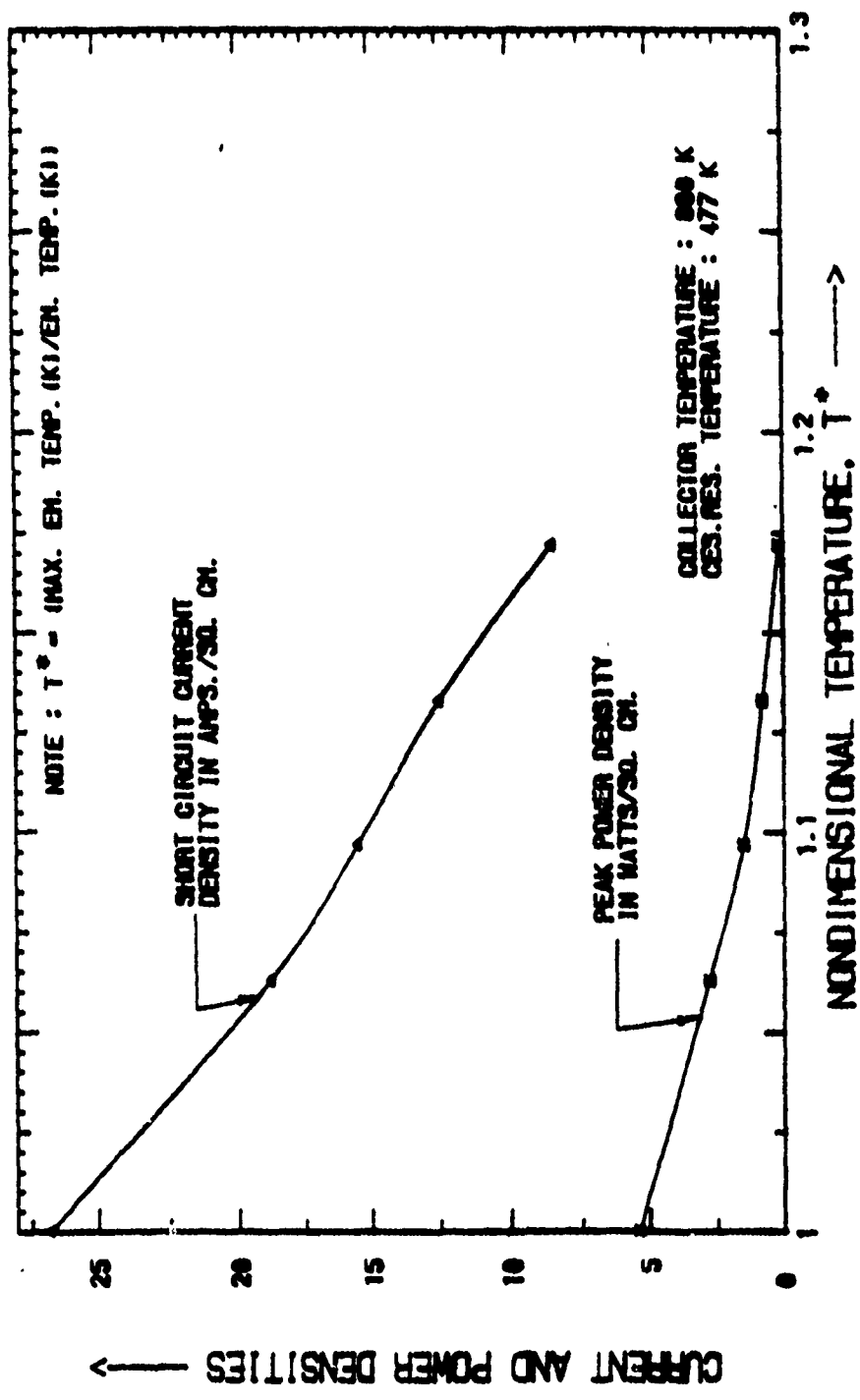


Figure 5.21 Effects of Emitter Temperature on the Short Circuit Current Density and Peak Power Density.

**Table 5.2 Ignition Point Current Densities and Output Voltages for Various Emitter Temperatures.**

| Sl. No. | Filename | Emitter Temperature<br>K | Ignition Point Results |        |                                      |       |
|---------|----------|--------------------------|------------------------|--------|--------------------------------------|-------|
|         |          |                          | Voltage (V)            |        | Current Density (A/cm <sup>2</sup> ) |       |
|         |          |                          | Before                 | After  | Before                               | After |
| 1       | BIASLD47 | 1400                     | -0.793                 | -0.096 | 0.018                                | 0.575 |
| 2       | BIASLD41 | 1450                     | -0.513                 | +0.047 | 0.035                                | 0.509 |
| 3       | BIASLD46 | 1500                     | -0.419                 | +0.136 | 0.061                                | 0.512 |
| 4       | BIASLD45 | 1550                     | -0.232                 | +0.260 | 0.116                                | 0.508 |
| 5       | BIASLD44 | 1600                     | -0.105                 | +0.399 | 0.136                                | 0.592 |
| 6       | BIASLD48 | 1650                     | +0.058                 | +0.480 | 0.198                                | 0.715 |
| 7       | BIASLD42 | 1700                     | +0.319                 | +0.630 | 0.343                                | 0.600 |

# IGNITION VOLTAGE CHARACTERISTICS (EMITTER TEMPERATURE OPTIMIZATION)

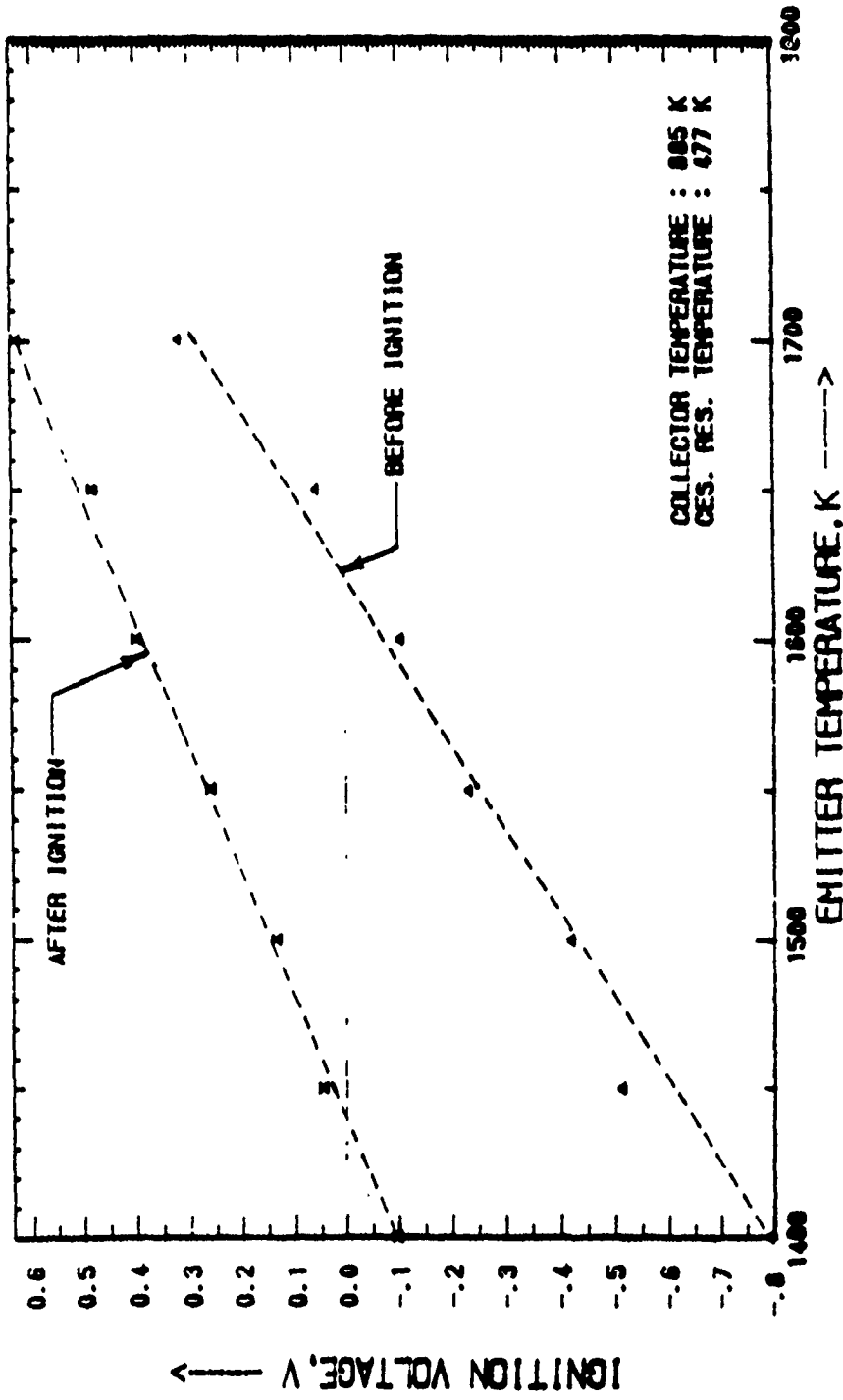


Figure 5.22 Experimental Data and Linear Approximation for Variation of Ignition Voltage with Emitter Temperature.

effect of bulk ionization is to increase both the output voltage as well as the output current immediately after ignition and this is clearly observed in the figure. Ignition occurs at negative voltages for all emitter temperatures below 1625 K. The effect of bulk ionization in obtaining higher power is greater at lower emitter temperatures as the difference between ignition voltages before and after ignition is greater. However as the emitter temperature is raised, the jump in the voltage level decreases indicating that bulk ionization as well as the high temperature contribute to the minimization of the negative space charge effect.

The broken lines connecting the experimental data points are linear approximations that best suit the trend in the behavior of experimental data points. An analytical curve fit revealed that the variation in ignition voltage before ignition can be represented by the relation.

$$V_{IOB} = 3.6455 \times 10^{-3}(T_E) - 3.8956 \quad (5.8)$$

and after ignition, the variation can be approximated by

$$V_{IOA} = 2.4203 \times 10^{-3}(T_E) - 3.4844 \quad (5.9)$$

where  $V_{IOB}$  = Voltage Before Ignition

$V_{IOA}$  = Voltage After Ignition

$T_E$  = Emitter Temperature

The results of the cesium reservoir and collector optimization ignition tests are provided in Tables 5.3 and 5.4 and Figures 5.23 and 5.24 respectively. The cesium reservoir temperature was varied from 350 K to 540 K at random intervals and the collector temperature was varied from 750 K to 980 K. In both series of tests, the emitter temperature was maintained at 1700 K. Since the emitter temperature remained constant it was hard to determine the effect of temperature on obtaining higher power output levels. As seen from the results, the output voltage after ignition, exhibited an expected trend with increase in cesium reservoir temperature.

Table 5.3 Cesium Reservoir Temperature Optimization Ignition Test Results.

| Test #    | Cesium Reservoir Temperature (K) | Ignition Output Parameters |             |             |         |        |       |
|-----------|----------------------------------|----------------------------|-------------|-------------|---------|--------|-------|
|           |                                  | Voltage (V)                |             | Current (I) |         | Before | After |
|           |                                  | Before                     | After       | Before      | After   |        |       |
| 81ASLD 49 | 350                              | -                          | No Ignition |             |         | -      | -     |
| 81ASLD 50 | 390                              | -                          | No Ignition |             |         |        |       |
| 81ASLD 52 | 420                              | -0.16097                   | +0.46112    | 0.36923     | 0.86255 |        |       |
| 81ASLD 53 | 440                              | -0.00143                   | +0.54282    | 0.35974     | 0.75557 |        |       |
| 81ASLD 58 | 450                              | 0.13028                    | 0.55019     | 0.32416     | 0.63445 |        |       |
| 81ASLD 54 | 460                              | 0.05559                    | 0.56983     | 0.35123     | 0.74187 |        |       |
| 81ASLD 59 | 470                              | 0.05551                    | 0.56229     | 0.30925     | 0.68428 |        |       |
| 81ASLD 55 | 480                              | 0.07626                    | 0.52199     | 0.30994     | 0.69303 |        |       |
| 81ASLD 56 | 500                              | 0.06968                    | 0.49078     | 0.27316     | 0.58618 |        |       |
| 81ASLD 57 | 520                              | 0.18510                    | 0.46600     | 0.31862     | 0.54803 |        |       |
| 81ASLD 60 | 540                              | 0.04373                    | 0.37876     | 0.22743     | 0.53121 |        |       |

Table 5.4 Collector Temperature Optimization Ignition Test Results.

| Test #    | Collector Temperature (K) | Ignition Output Parameters |         |             |         |
|-----------|---------------------------|----------------------------|---------|-------------|---------|
|           |                           | Voltage (V)                |         | Current (I) |         |
|           |                           | Before                     | After   | Before      | After   |
| 81ASLD 61 | 750                       | 0.39080                    | 0.45379 | 0.07821     | 0.12506 |
| 81ASLD 62 | 800                       | 0.29590                    | 0.40170 | 0.24458     | 0.56392 |
| 81ASLD 63 | 825                       | 0.08466                    | 0.60328 | 0.27425     | 0.65961 |
| 81ASLD 64 | 850                       | 0.07350                    | 0.60120 | 0.27706     | 0.66994 |
| 81ASLD 65 | 875                       | 0.00463                    | 0.38862 | 0.29202     | 0.60070 |
| 81ASLD 66 | 900                       | 0.03724                    | 0.57417 | 0.33709     | 0.73105 |
| 81ASLD 67 | 925                       | -0.01138                   | 0.53250 | 0.33139     | 0.73039 |
| 81ASLD 68 | 950                       | -0.03034                   | 0.51314 | 0.25424     | 0.73039 |
| 81ASLD 69 | 980                       | -0.04228                   | 0.46906 | 0.26591     | 0.69387 |

# IGNITION VOLTAGE CHARACTERISTICS (CESIUM RESERVOIR OPTIMIZATION)

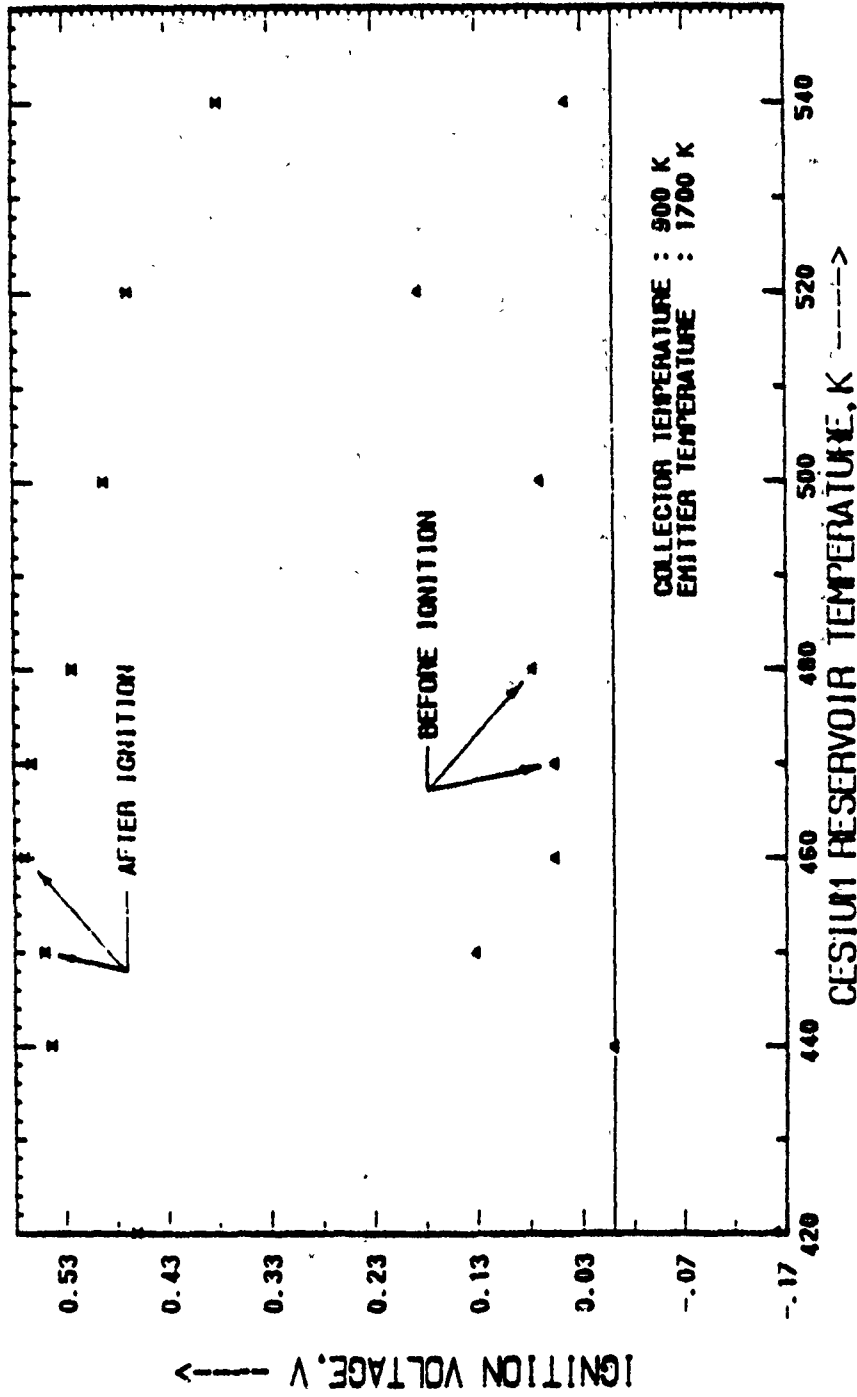


**Figure 5.23** Ignition Characteristics for Cesium Reservoir Temperature Optimization.

# IGNITION VOLTAGE CHARACTERISTICS (COLLECTOR OPTIMIZATION)

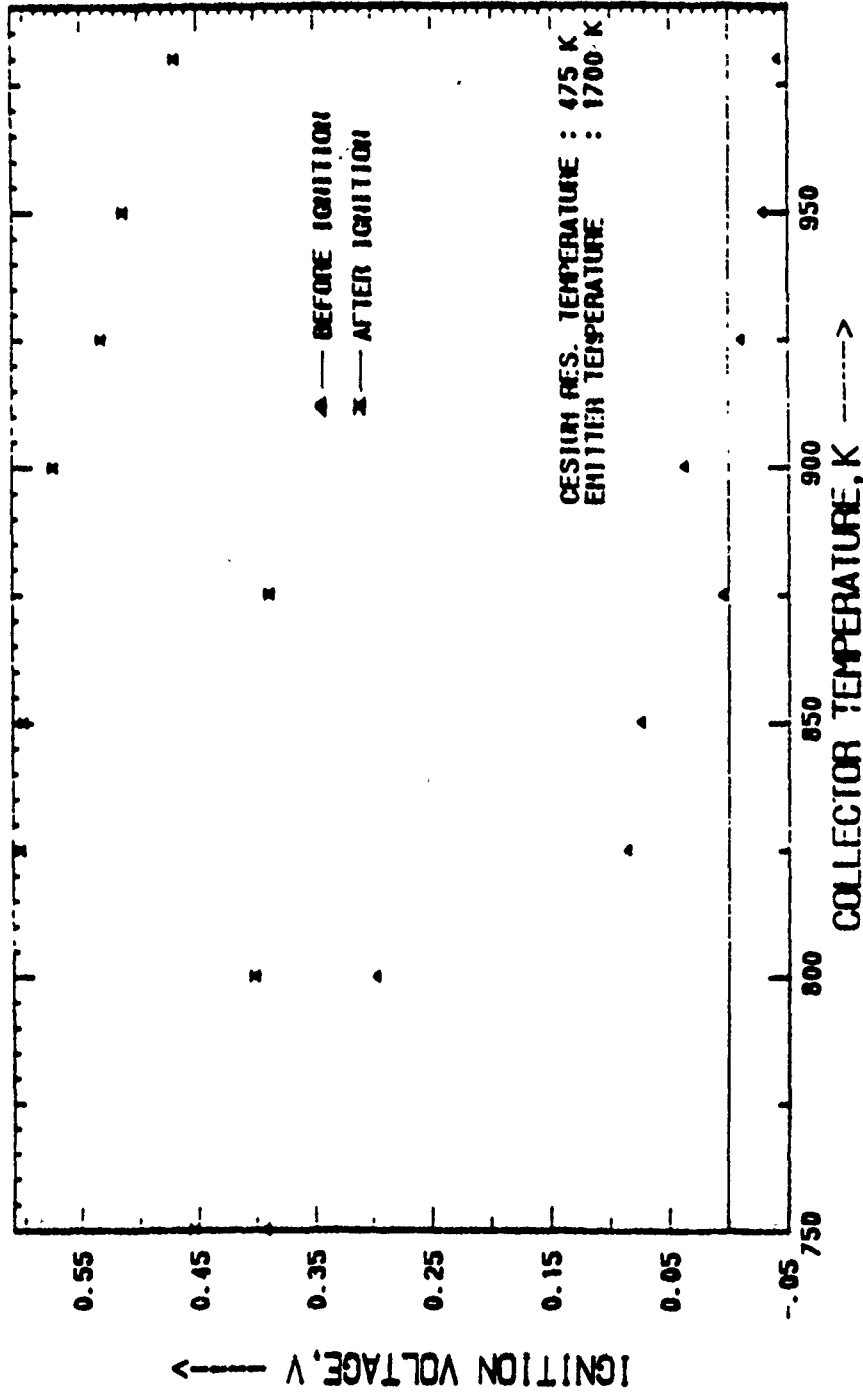


Figure 5.24 Ignition Characteristics for Collector Temperature Optimization.

The voltage peaked at about 470 K indicating that the optimum power levels can be obtained in this vicinity.

However, the trend exhibited by the ignition characteristics for the variation in collector temperature was not uniform but fluctuating thereby giving an indication that the ignition output parameters were not strong functions of the collector temperature. However, it was found that a strong driving force was necessary to cause bulk ionization as ignition was initiated at negative voltages above a collector temperature of 925 K. Since the same effect was observed at low cesium reservoir temperatures, it can be concluded that the optimum power levels for the  $\text{LaB}_6$  diminiode can only be obtained by operating it with a cesium reservoir temperature  $< 450$  K and a collector temperature  $> 900$  K.

## 5.2 ASTAR-811C Diminiode Performance

The emitter for this fixed space planar miniature diode is a tantalum alloy termed ASTAR-811C. This alloy has a nominal composition consisting of 90 at.% Ta, 8 at.% W, 0.7 at.% Hf, 1 at.% Re and 0.025 at.% C. The collector is a Niobium - 1 at.% Zirconium alloy which is separated from the emitter by 0.254 mm.

The tests were conducted with an emitter temperature of 1800 K, a collector temperature of 1040 K and a cesium reservoir temperature ranging from 604 K to 708 K. The tests were a repeat of those conducted at NASA and reported by James F. Morris and others [12]. The purpose of these tests was to verify the performance of the diminiode with identical operating conditions. Each test was conducted by bringing the diminiode up to the specified primary parameters and then varying the bias supply from a positive voltage through zero, to a negative voltage and back to the positive voltage. One complete sweep with the bias power supply ensures the occurrence of ignition, de-ignition and coincidence of current densities before and after de-ignition for the same output voltage. For the externally driven diminiode, the corresponding output voltage varied from +1.2 volts to -0.25 volt and then back to +1.2 volts.

### 5.2.1 Current and Power Density Characteristics

The output current and power density characteristics of the ASTAR-811C diode for a cesium reservoir temperature of 651 K is indicated in Figure 5.25. Superimposed on the plot is the corresponding plot obtained at NASA, LeRC. As represented in the figure, a number of differences were observed between the plots obtained at AFWAL and those published in the NASA report. The back emission was considerably higher at all cesium reservoir temperatures. This indicated that either the collector temperature at which the tests were conducted was too high or the characteristics of the collector surface had changed by deposits of the emitter material. This can be checked by repeating some of the key tests at lower collector temperatures.

The tests conducted, exhibited a general trend with cesium reservoir temperature. The short circuit current densities and the open circuit voltages constantly decreased with increase in cesium reservoir temperature unlike the trend exhibited by the NASA plots where the power density peaked at a cesium reservoir temperature of 651 K. From an optimization point of view, this might indicate that with the change in surface characteristics, the optimum cesium reservoir temperature for efficient ionization has dropped to 600 K or lower.

The test results published in the NASA report and presented in Figure 5.25 had clearly defined Ignition and De-ignition points while the corresponding plots for the tests conducted recently, did not show any indication of operating in the ignited mode. Neither ignition nor de-ignition points were identifiable on any of the plots. The main reason for this behavior is the high back emission and low forward emission at lower voltages. This characteristic prevents the diode from operating in a space charge limited mode which transitions into the ignited mode of operation after ignition occurs. Cesium depletion is yet another possibility that could be responsible for the lack of an ionizing plasma to cause ignition or neutralization of the negative space charge accumulation at the emitter surface.

**CURRENT AND POWER DENSITY CHARACTERISTICS**  
 (Current Densities for the ASTAR-811C Diminide.)

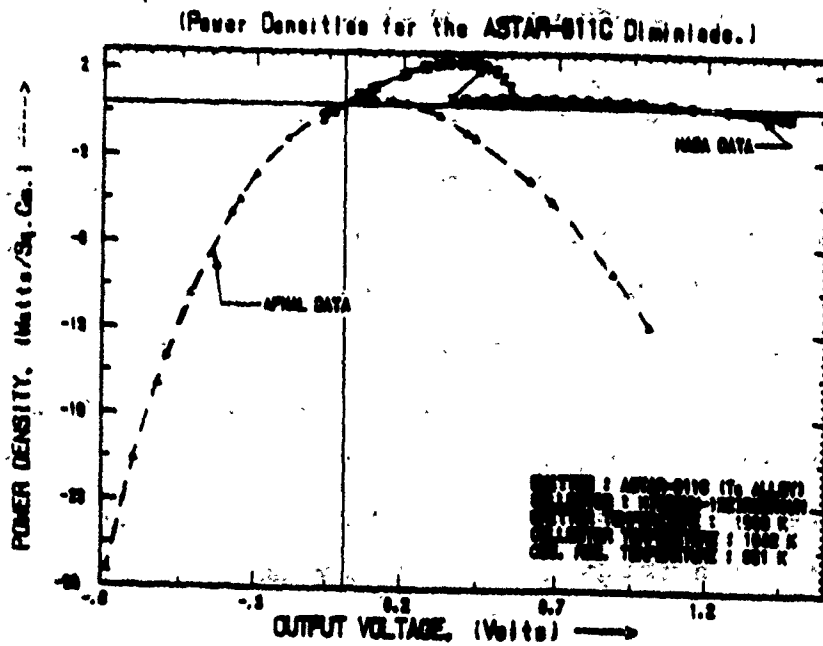
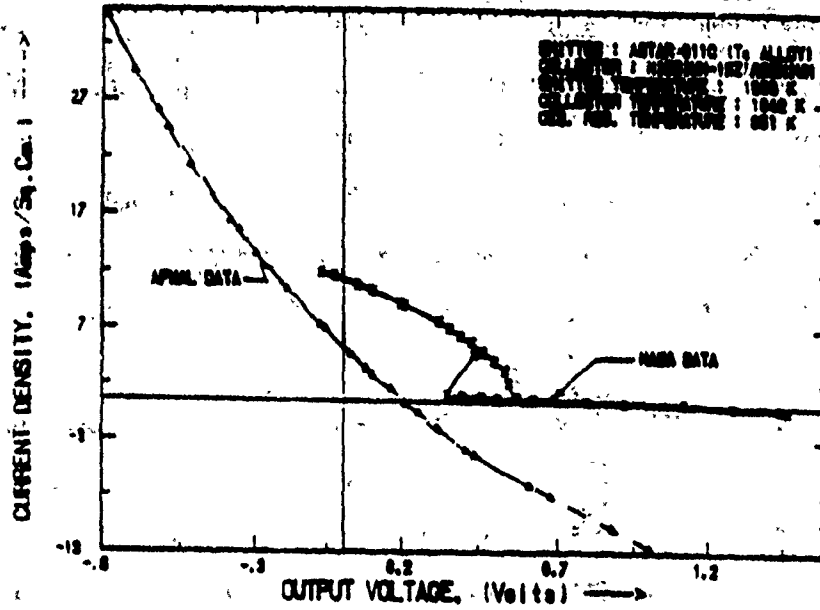


Figure 5.25 Output Characteristics of ASTAR-811C Diminide for a Cesium Reservoir Temperature of 651 K.

### 5.3 Performance of the Etched Rhenium - Niobium Diode

#### 5.3.1 General Performance

The planar diode with a Rhenium Emitter and Niobium collector was tested for the first time in diode Station #3. The cesium reservoir temperature and collector temperature were maintained constant at 473 K and 773 K respectively. However, the emitter temperature was varied from 1273 K to 1773 K. The corresponding output current and power density characteristics for an emitter temperature of 1723 K is shown in Figure 5.26. As observed from these characteristics, the diode continued to operate in the space charge limited mode till the emitter temperature was raised to 1723 K, when ignition occurred and current densities moved up rapidly. The points of ignition and de-ignition are clearly indicated in the characteristics corresponding to an emitter temperature of 1723 K. Ignition did occur at 1673 K but the overall current densities were lower than those at 1623 K indicating that the optimum emitter temperature was between 1573 K and 1673 K. Any further increase in emitter temperature did not enhance the current densities but eventually led to a form of unstable operation as represented by the characteristics corresponding to an emitter temperature of 1773 K. These tests represent a preliminary series to affirm the performance capacity of the diode station.

#### 5.3.2 Peak Power Density as a Function of Emitter Temperature

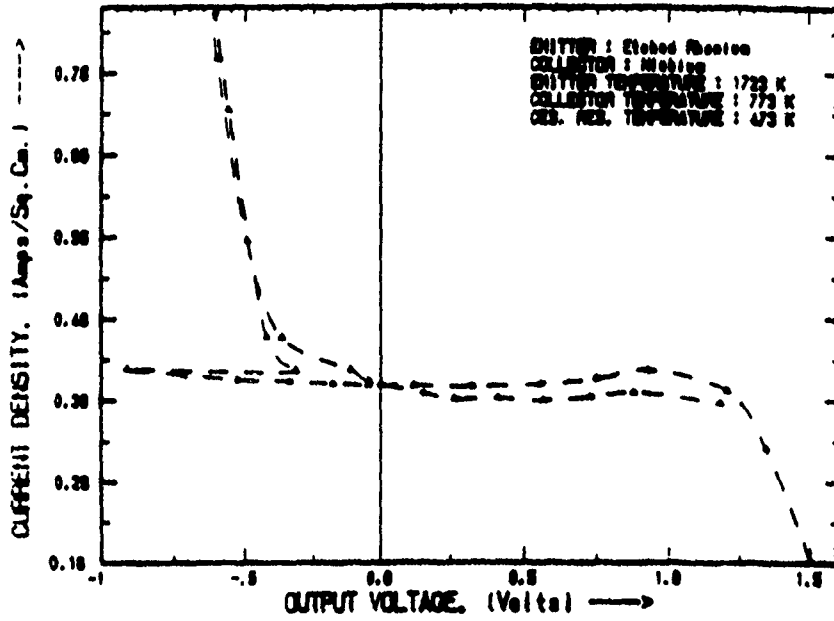
Figure 5.27 is a plot of peak power density as a function of emitter temperature for the Rhenium-Niobium diode. This is a result of the various tests conducted on the diode with constant collector and cesium reservoir temperatures. As seen in the characteristics, the power density was a maximum at an emitter temperature of 1723 K, even though ignition occurred at negative voltages. Ignition was found to occur only at emitter temperatures of 1623 K, 1673 K and 1723 K because of the low Cesium Reservoir Temperature. It is proposed to conduct extensive tests on this diode for mapping its performance.

#### 5.4 Characterization of the Lanthanum Hexaboride Diode with a 1-D Code

A one-dimensional Thermionic Energy Conversion (TEC) computer code has been utilized to provide a theoretical basis of comparison for experimentally derived data obtained from a lanthanum hexaboride cesium vapor thermionic diode. Although the code generated predictions

# CURRENT AND POWER DENSITY CHARACTERISTICS

(Current Densities for the Re - Nb Diode)



(Power Densities for the Re - Nb Diode)

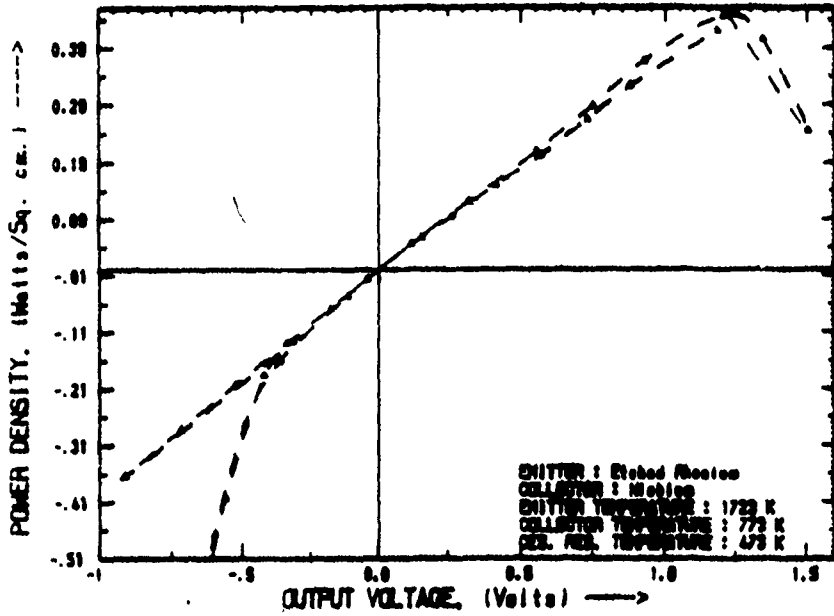


Figure 5.26

Output Characteristics of Re-Nb Diode for a Cesium Reservoir Temperature of 473 K.

# VARIATION OF PEAK POWER DENSITY (Re-Nb Emitter Optimization)

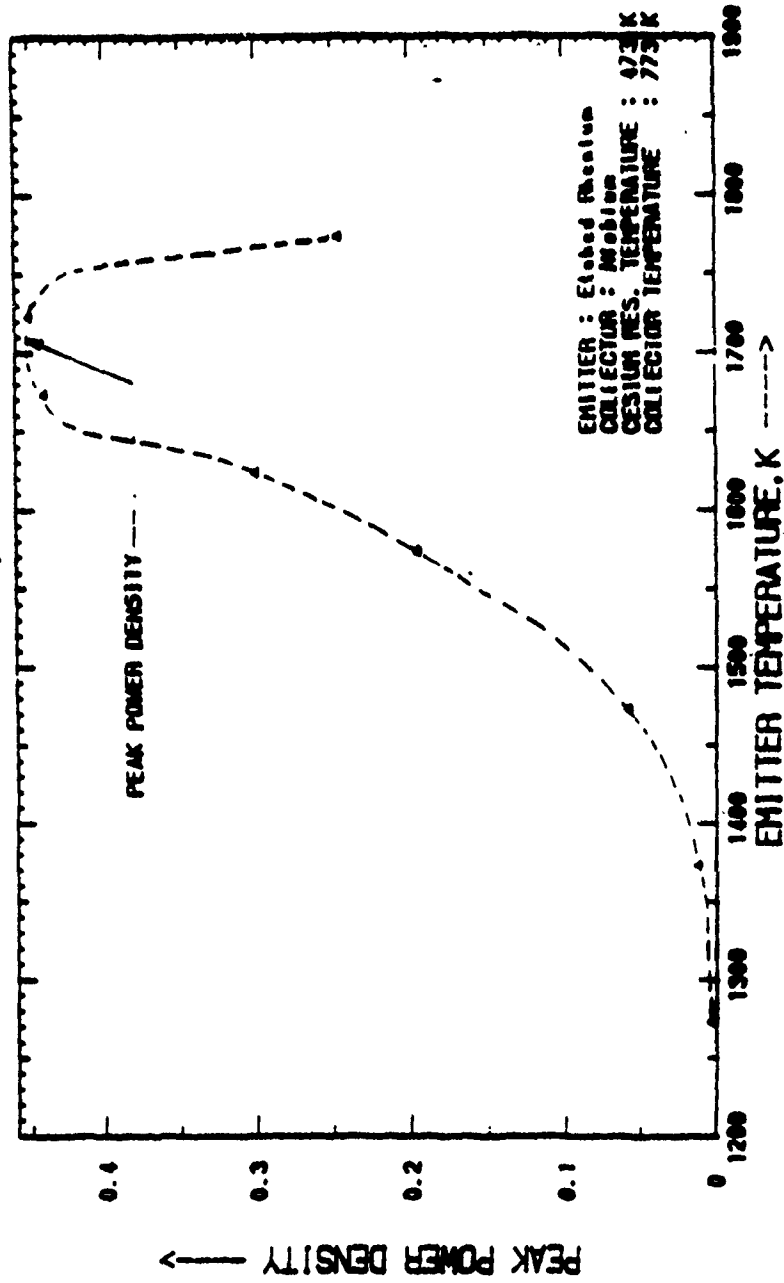


Figure 5.27 Variation of Peak Power Density as a Function of Emitter Temperature.

obtained were not in precise agreement with the experimental results, they do provide a basis for establishing the validity of the experimental results from an analytical framework. Certain discrepancies are thus identified and are attempted to be accounted for in terms of code inaccuracies and/or possible experimental error.

M. Ramalingam and M. Morgan produced experimental lanthanum-hexaboride ( $\text{LaB}_6$ ) cesium-vapor TEC diode characteristics which are compared to those predicted by the TEC code [13]. The diode used was activated by electron bombardment (EB) heating in a rejuvenated diode testing facility, originally acquired from the National Aeronautics and Space Administration (NASA) Lewis Research Center (LeRC), Cleveland, OH [1,2].

A Disk Operating System (DOS) loop (Figure 5.28) and auxiliary fortran program (Figure 5.29) were used in conjunction with the original TEC code to generate both general and ( $\text{LaB}_6$ ) simulated diode current density vs. output voltage (J-V) characteristics. The effects of changing the emitter & collector work functions, as well as the operating cesium-vapor pressure, were studied for both cases. All results are shown in terms of J-V characteristics.

#### 5.4.1 Code Description and Simulation Procedure

The Fortran code is a time-dependent analysis code which was used by Main [14] and Lawless [15] to compute the TEC plasma conditions over discrete time intervals. When running on a desk-top PC, the code first prompts the user for the basic TEC parameters: emitter and collector work functions ( $\phi_e$  &  $\phi_c$ ), emitter and collector temperature ( $T_e$  &  $T_c$ ), cesium vaporpressure (p) inter-electrode gap (d), and operating current density (J). In addition, the user can specify the time between iteration steps and several program output control conditions as well. The program calculates the plasma densities, electron temperatures, sheath heights, and many other pertinent thermionic parameters. If the iterations are continued for a sufficient length of time, in some cases, a convergence will occur, the plasma will ignite, and a "steady-state" condition of the diode will be observed.

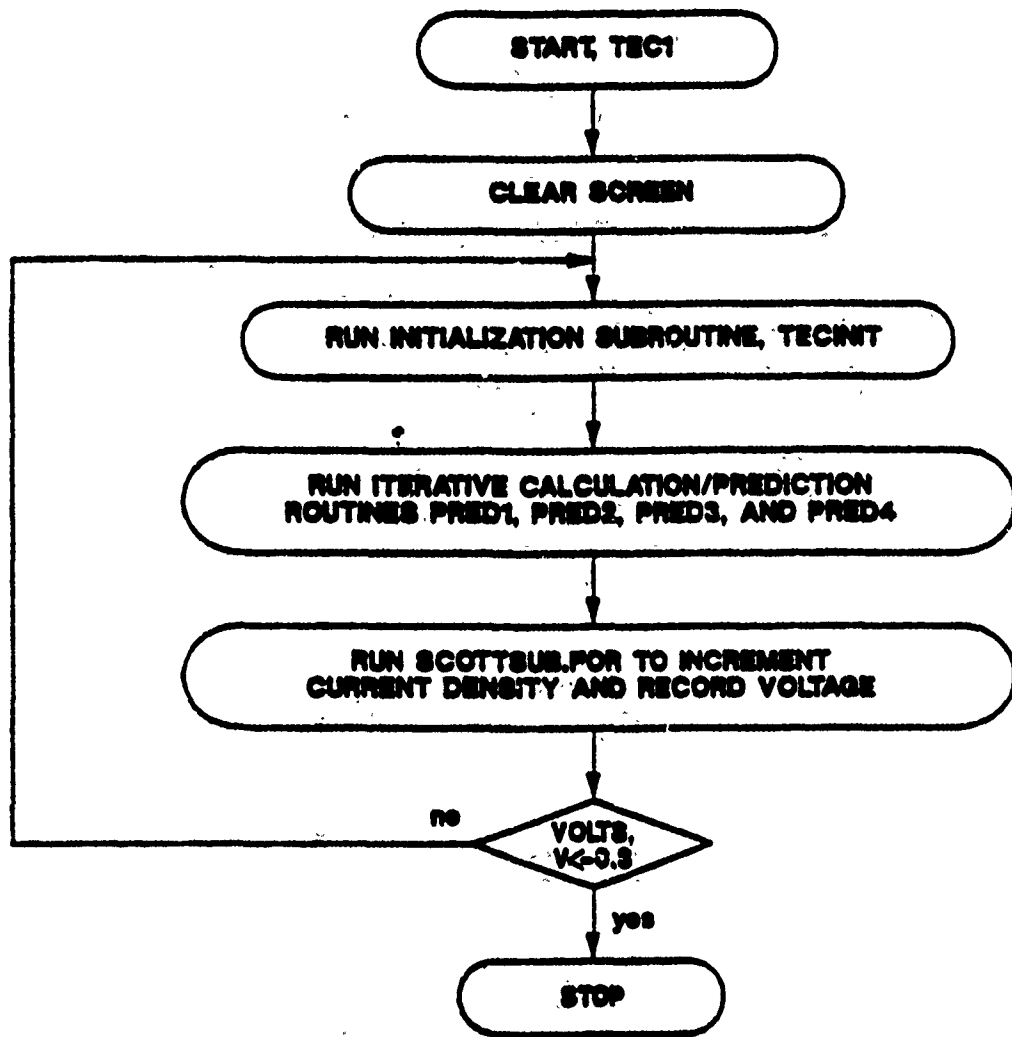


Figure 5.28 Flow Chart for Repeated Runs of the TEC Program.

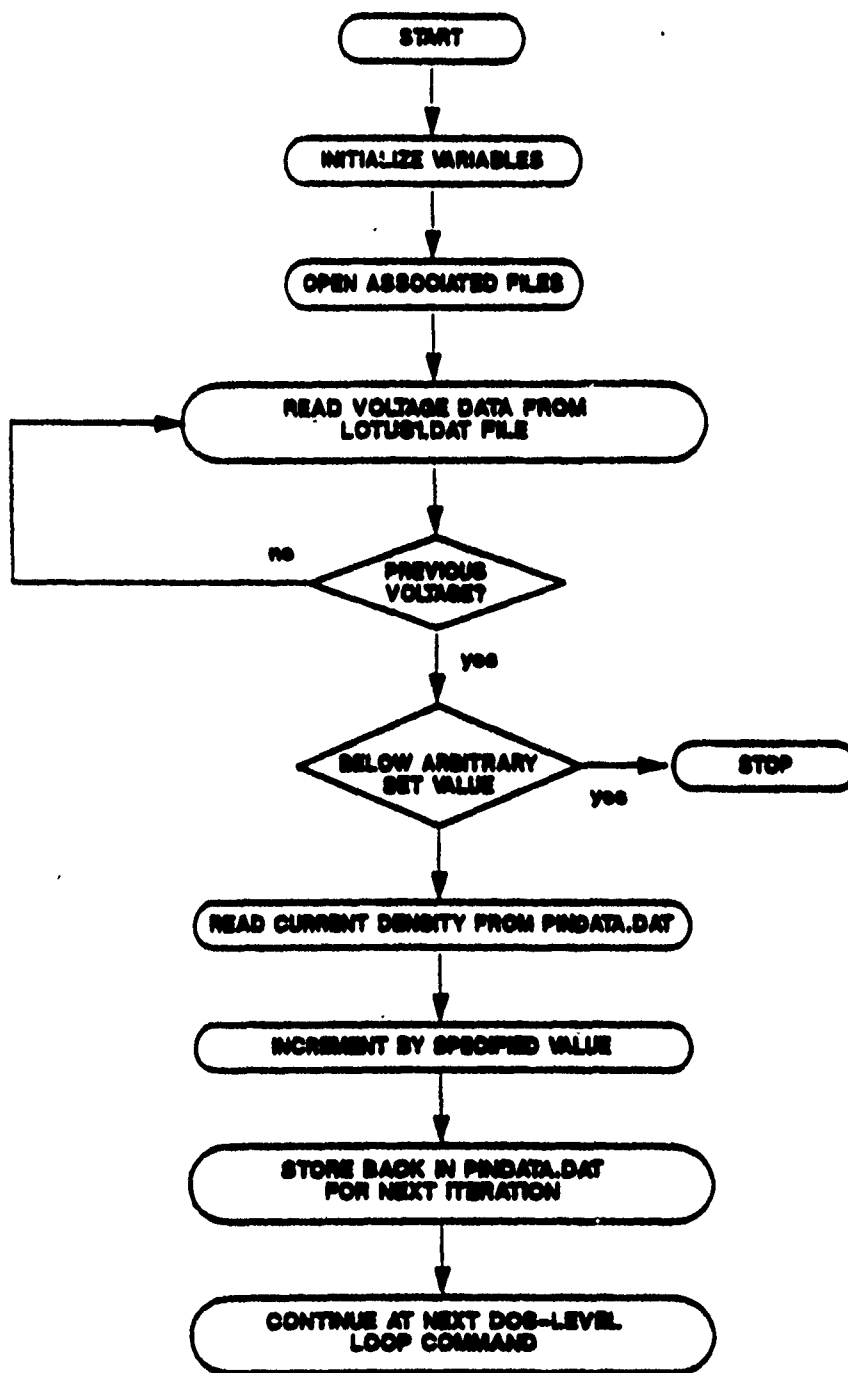


Figure 5.29 Flow Chart for the One-Dimensional TEC Program.

At the Aerospace Propulsion and Power Laboratory, another Fortran program and an associated DOS level loop was developed to provide the capability of graphing the program's output into the typical diode J-V characteristic. This allowed the simulated results to be easily compared with those generated experimentally. Many J-V characteristics were thereby produced, some of which are discussed below. Other characteristics were generated only to verify and observe the code's performance. In attempting to simulate the LaB<sub>6</sub> diode, the first requirement was that of insuring that a converged (or ignited) characteristic was produced from the parameters chosen. T<sub>s</sub>, T<sub>e</sub>, d, and p (derived from known cesium reservoir temperature and spacing) were known from experiment. However, both φ<sub>s</sub> and φ<sub>c</sub> could only be approximated. These values were therefore estimated based on the literature and previously measured LaB<sub>6</sub> experimental J-V curves. The φ<sub>s</sub> was first approximated from the experimental J-V slope and maximum observed current density, as 2.25 eV or less. The φ<sub>c</sub> was then estimated based on the zero-voltage crossing point for the experimental curves and a rough calculation using coulombic resistance:

$$J_{ideal} = AT_e^2 [\exp -(V + \phi_s) 11600/1700] \quad (5.10)$$

$$V_{ideal} = \frac{1700}{11600} \ln \left[ \frac{120.T_e^2}{J_{ideal}} \right] - \phi_s \quad (5.11)$$

with coulombic resistance,

$$\phi_c = 0.14655 \ln \frac{120.T_e^2}{J} - e[V_{out} - (Rc)(d)(J)] \quad (5.12)$$

assuming Rc = 0.75 ohm.cm from the slope of the experimental J-V curve, with other variables known, yielded φ<sub>c</sub> 1.81 eV.

After the  $LaB_6$  work functions were approximated, various combinations of emitter, collector, and cesium temperatures were thus simulated. The results were plotted and are discussed in the following section.

#### 5.4.2 Performance of the Code

The code is an extremely useful method of estimating TEC characteristics for materials, temperatures, pressures, etc. as yet untried experimentally. As previously stated, the code allows an examination of a TEC diode's characteristics on a transient, time-scale basis.

This transient TEC diode J-V characteristic can easily be noted in Figure 5.30 where TEC code parameters were chosen arbitrarily. As the number of iterations increases, the characteristic moves to the left, eventually converging on the Boltzmann portion of the curve. It is observed that the initial mode is basically that of unignited, space-charge limited operation, but as  $N$  is increased, ignition occurs and the Boltzmann slope becomes more pronounced. In Figure 5.30, ignition is clearly observed for  $N=1000$ . The "knee" between the Boltzmann slope and semi-saturation portions of the curve is not entirely understood but it appears to be an artifact of the computer algorithm.

Figure 5.31 is similar to that of Figure 5.30 except that it represents half the cesium vapor pressure. Lower pressures are observed to be less predictable with the code. This is exemplified by the  $N=2000$  curve. Notwithstanding, all plots converge at the highest saturation current density as would be expected. As in Figure 5.30, the TEC diode operated partially ignited for  $N=100$  where the ions in the diode plasma have not yet achieved sufficient concentration.

Figure 5.32 is again similar to Figures 5.30 and 5.31 except that it represents a further reduction in cesium vapor pressure. The current density is seen to decay over time and with increasing numbers of iterations until the curve for  $N=2500$  is reached where a converged characteristic or "pseudo-ignited" mode is observed. The inaccuracies of the program at low pressures are again observed. The reasons for this could be several, including approximations

# THEORETICAL OUTPUT SIMULATION CHARACTERISTIC

( One dimensional code )

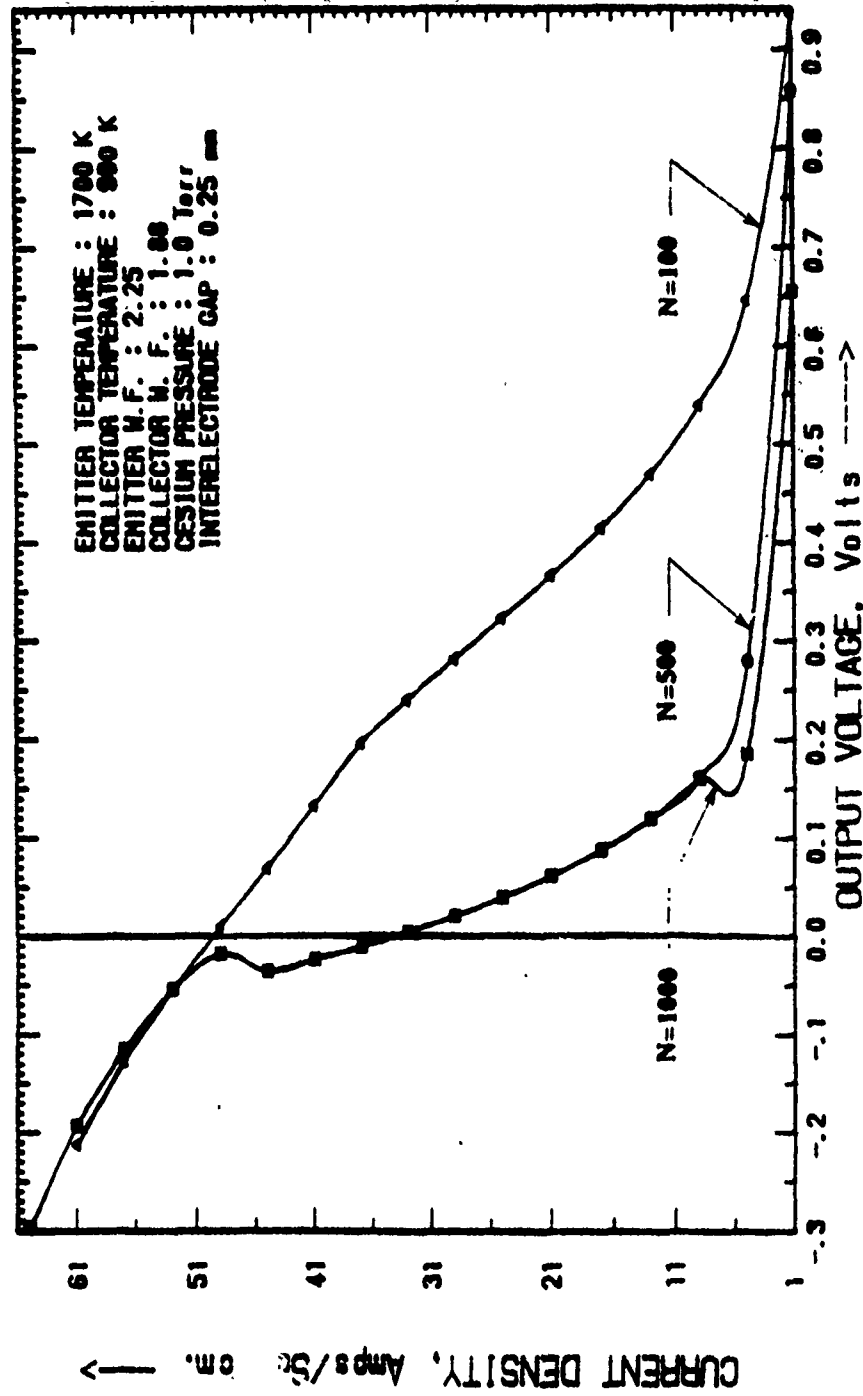


Figure 5.30 Simulated Characteristics for Various Iterations and a Cesium Pressure of 1.0 Torr.

# THEORETICAL OUTPUT SIMULATION CHARACTERISTIC

( One dimensional code )

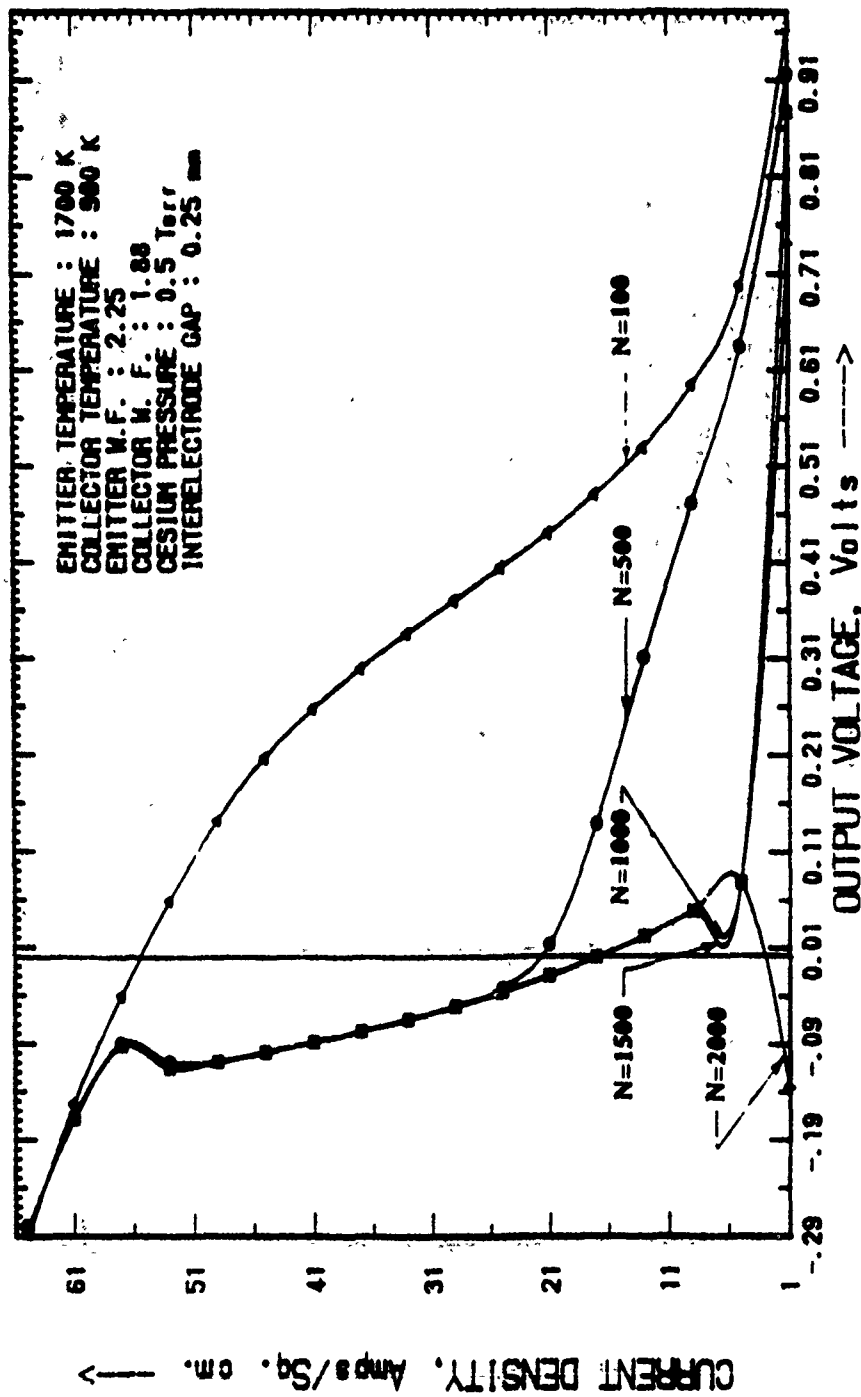


Figure 5.31 Simulated Characteristics for Various Iterations and a Cesium Pressure of 0.5 Torr.

# THEORETICAL OUTPUT SIMULATION CHARACTERISTIC

( One dimensional code )

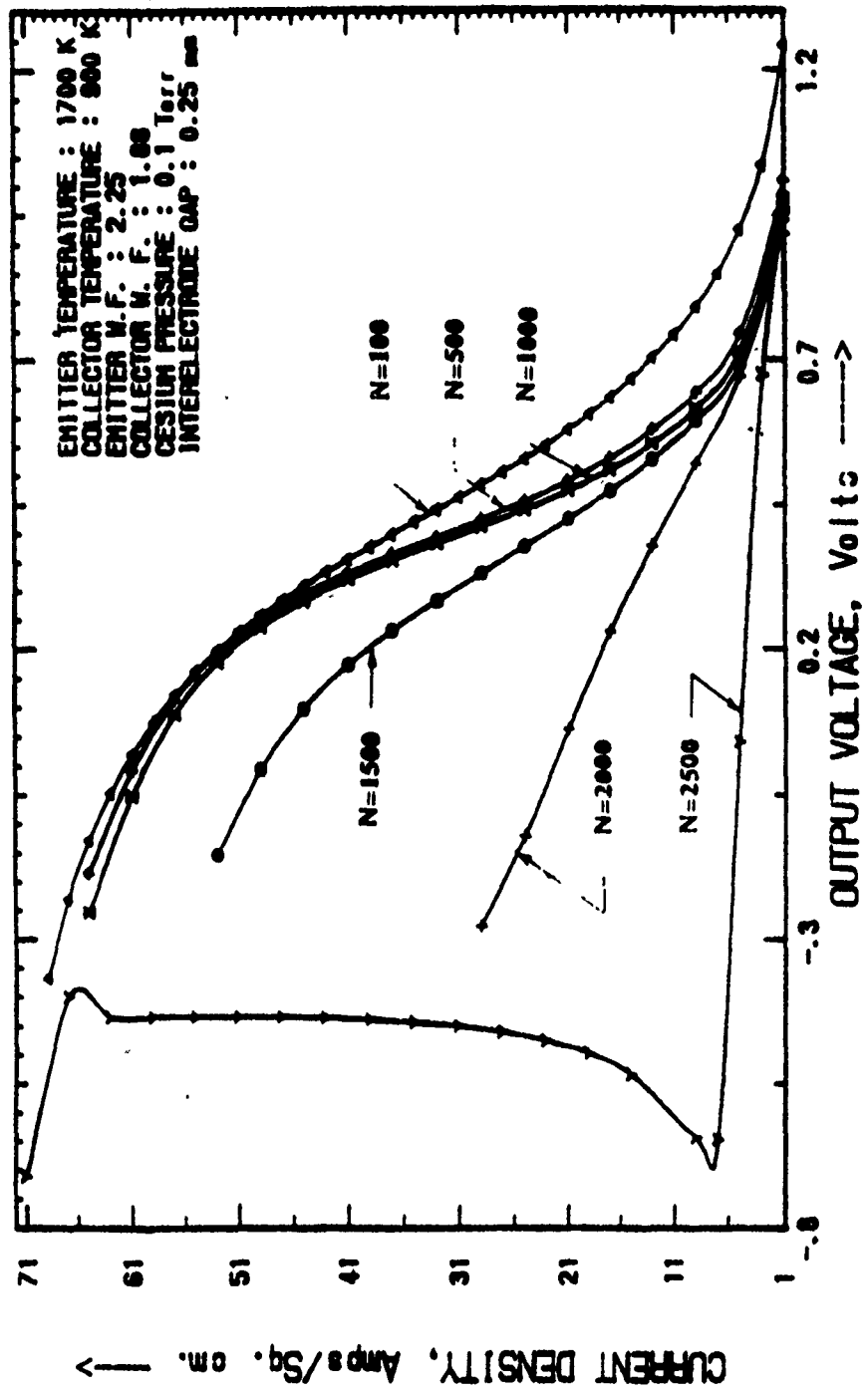


Figure 5.32 Simulated Characteristics for Various Iterations and a Cesium Pressure of 0.1 Torr.

of the ion/electron collision cross-section are too rough or the neglect of ion inertia in the conservation of momentum equations. In any case, low mean free paths associated with low pressures, are very difficult to be mathematically modeled with utmost precision.

In Figure 5.33, TEC operation under varied emitter temperature conditions for "high" pressure is simulated. As expected, large variations in current density with modest changes in emitter temperature are observed. The dependence on the  $T_e$  squared term in the Richardson-Dushman equation verifies the appropriateness of this result:

$$J = AT_e^2[\exp(-\phi_e/kT_e)] \quad (5.13)$$

Note that the  $T_e=1900$  K curve was not operated to show saturation.

Figure 5.34 shows a theoretical simulation representation of TEC diode operation for a high cesium reservoir pressure but varying collector temperatures. It is noted that collector temperature variations in the range shown play a minor role in moderating the TEC diode performance. Only slight variations in the characteristic are observed for changes of  $\pm 200$  K. The largest variations are predicted in the previously mentioned "knee" region. In a similar fashion, Figure 5.35 shows the results of a varied emitter temperature but under lower cesium vapor pressure conditions. (The  $\phi_e$  was changed slightly to enable a LaB<sub>6</sub> comparison in the next section.) In this case, the current-density behaves again as expected, with a seemingly greater proportionate increase at the higher temperature than that observed previously in Figure 5.33.

J-V characteristic discontinuities indicating ignition are also noted in each curve of Figure 5.35 whereas they were not observed in Figure 5.33. Also, the Boltzmann slopes of the two curves of Figure 5.35 are basically parallel whereas they appear skewed in Figure 5.33.

# THEORETICAL OUTPUT SIMULATION CHARACTERISTIC

( Emitter Temperature Variation )

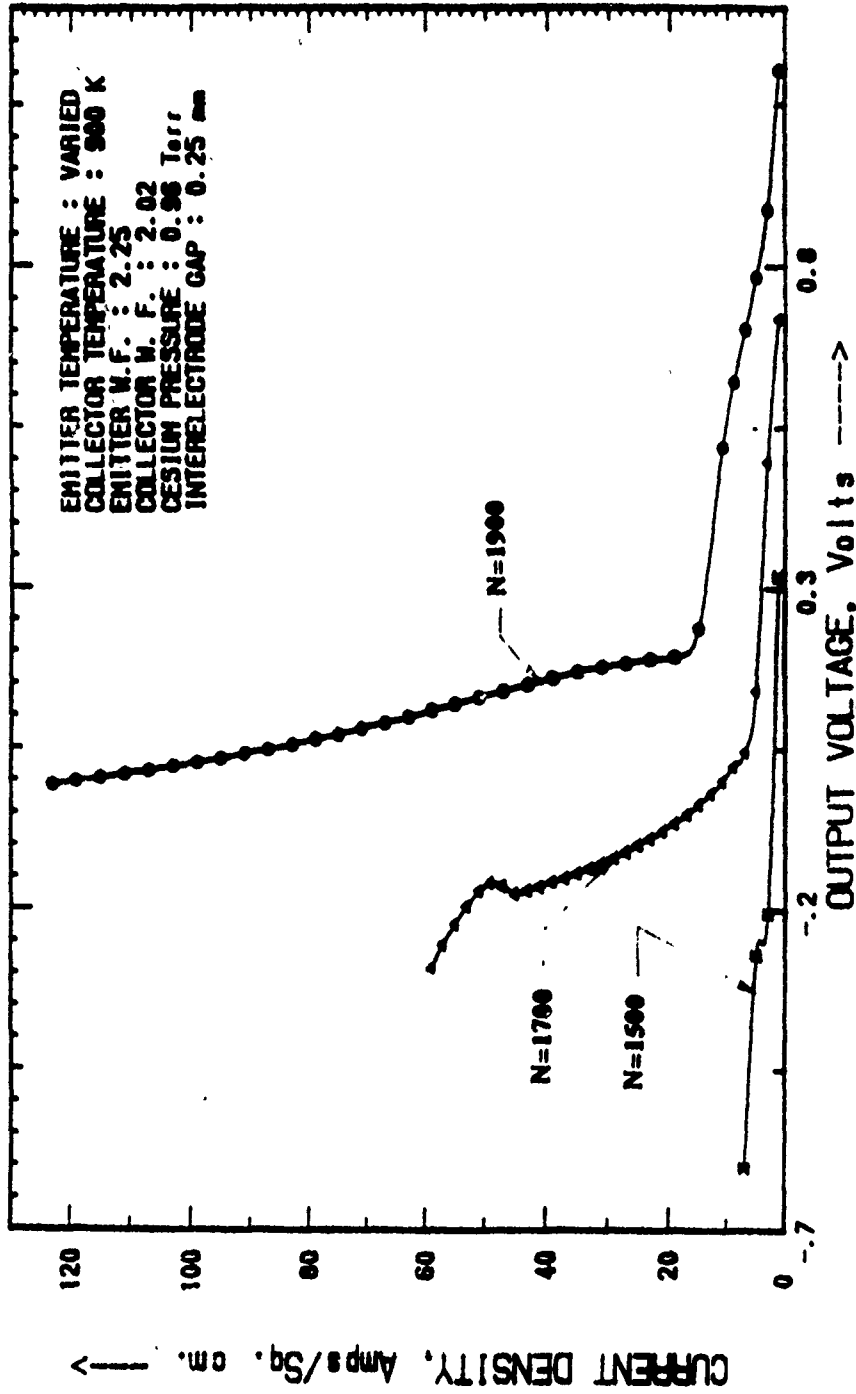


Figure 5.33 Operation Under Various Emitter Temperatures for High Cesium Vapor Pressures.

# THEORETICAL OUTPUT SIMULATION CHARACTERISTIC

( Collector Temperature Variation )

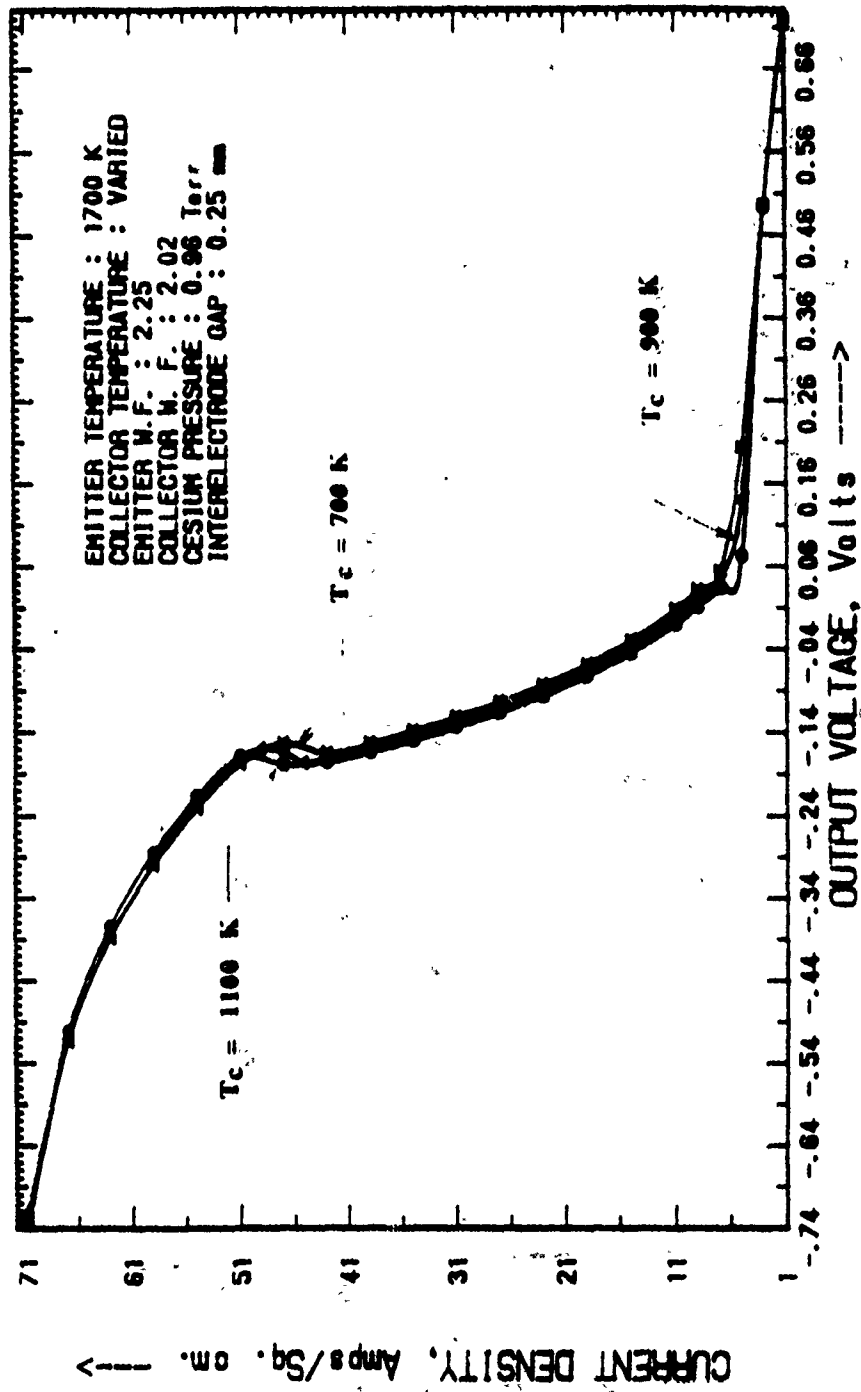


Figure 5.34 Operation Under Varied Collector Temperatures for High Cesium Vapor Pressures.

# THEORETICAL OUTPUT SIMULATION CHARACTERISTIC

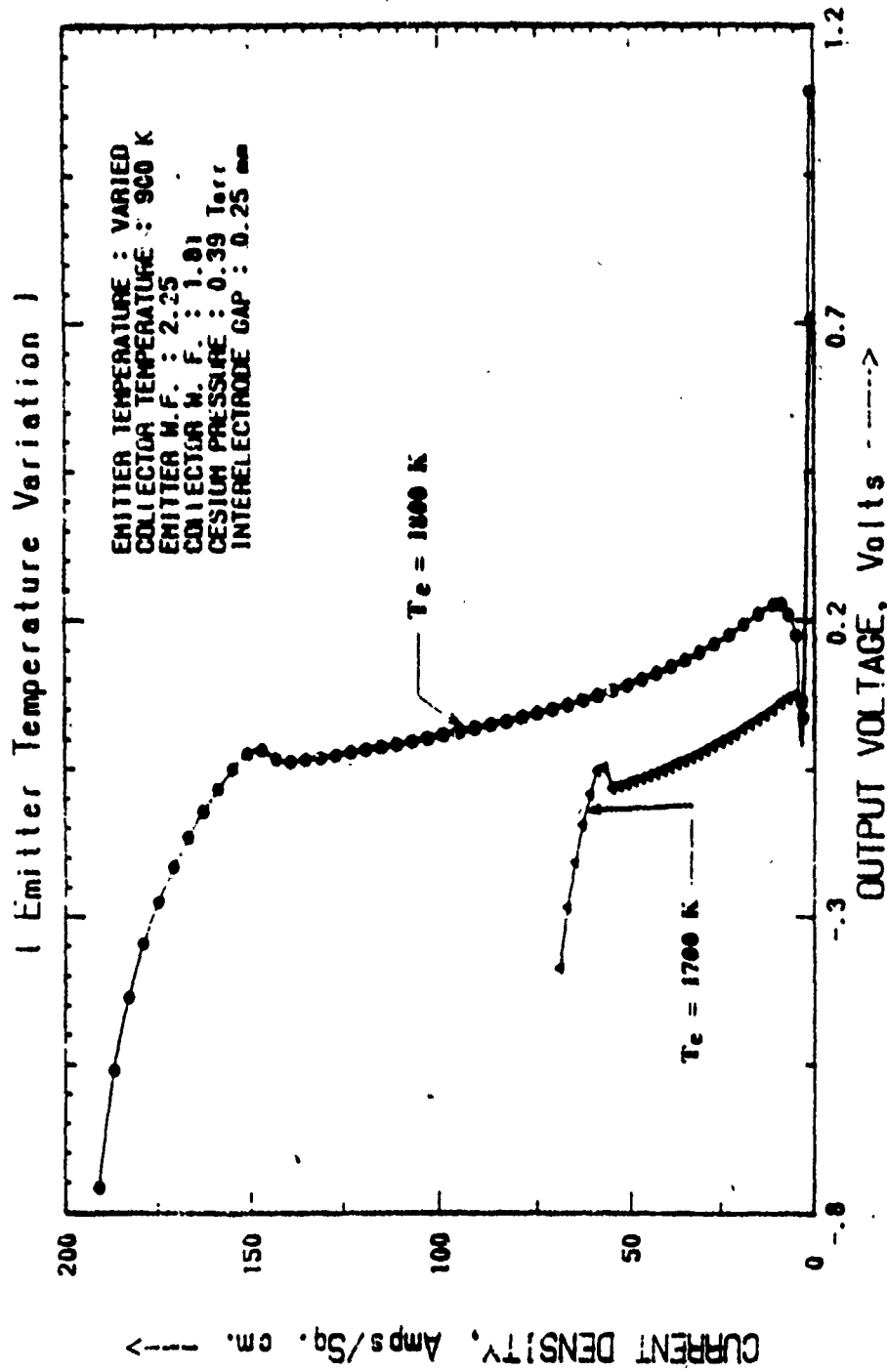


Figure 5.35 Operation Under Varied Emitter Temperatures and Lower Cesium Pressures.

Finally, Figure 5.36 illustrates the same results seen in Figure 5.34 except that the cesium vapor pressure has been decreased and the  $\phi_e$  has been changed slightly as discussed previously. Again, only small changes in the J-V characteristic would be incurred as the result of relatively large collector temperature changes. As in Figure 5.34 saturation values and Boltzmann slopes are similar with Figure 5.36 having more pronounced "Boltzmann" and "Saturation" features.

#### 5.4.3 Application of the Code

Experimentally obtained optimized LaB<sub>6</sub> results are shown in Figures 5.3, 5.10 and 5.17 [16]. The apparatus used allowed the measurement of fairly low pressures but not sufficiently high currents. The code was able to approximately simulate these curves by employing estimated emitter and collector work functions. Other TEC parameters were known from the experimental setup. The LaB<sub>6</sub> emitter work function was assumed to be 2.25 eV based on the magnitudes and slopes of current densities observed from various tests. The LaB<sub>6</sub> collector work function was approximated between 1.81 and 2.02 eV based on the aforementioned calculations and other experimental observations.

Experimentally obtained results for a LaB<sub>6</sub> diode showing characteristic variations due to changes in collector temperature are provided in Figure 5.10. It is noted that no major distinction can be made between curves, supporting the previous results achieved by simulation. In like manner, experimentally obtained results for the same diode showing the impact of emitter temperature changes on the diode characteristic are shown in Figure 5.17.

Figure 5.37 presents the TEC code simulated LaB<sub>6</sub> J-V characteristics with respect to variation in cesium vapor pressure. Obviously, again as in Figure 5.32, the lowest pressure plot (p=0.1 torr) does not seem appropriate, hence the program inadequacy at relatively low pressures is demonstrated. In this case, the best TEC operating condition is obviously that of the highest emitter temperature. In comparison with Figures 5.33 and 5.35, this result is also

# THEORETICAL OUTPUT SIMULATION CHARACTERISTIC

( Collector Temperature Variation )

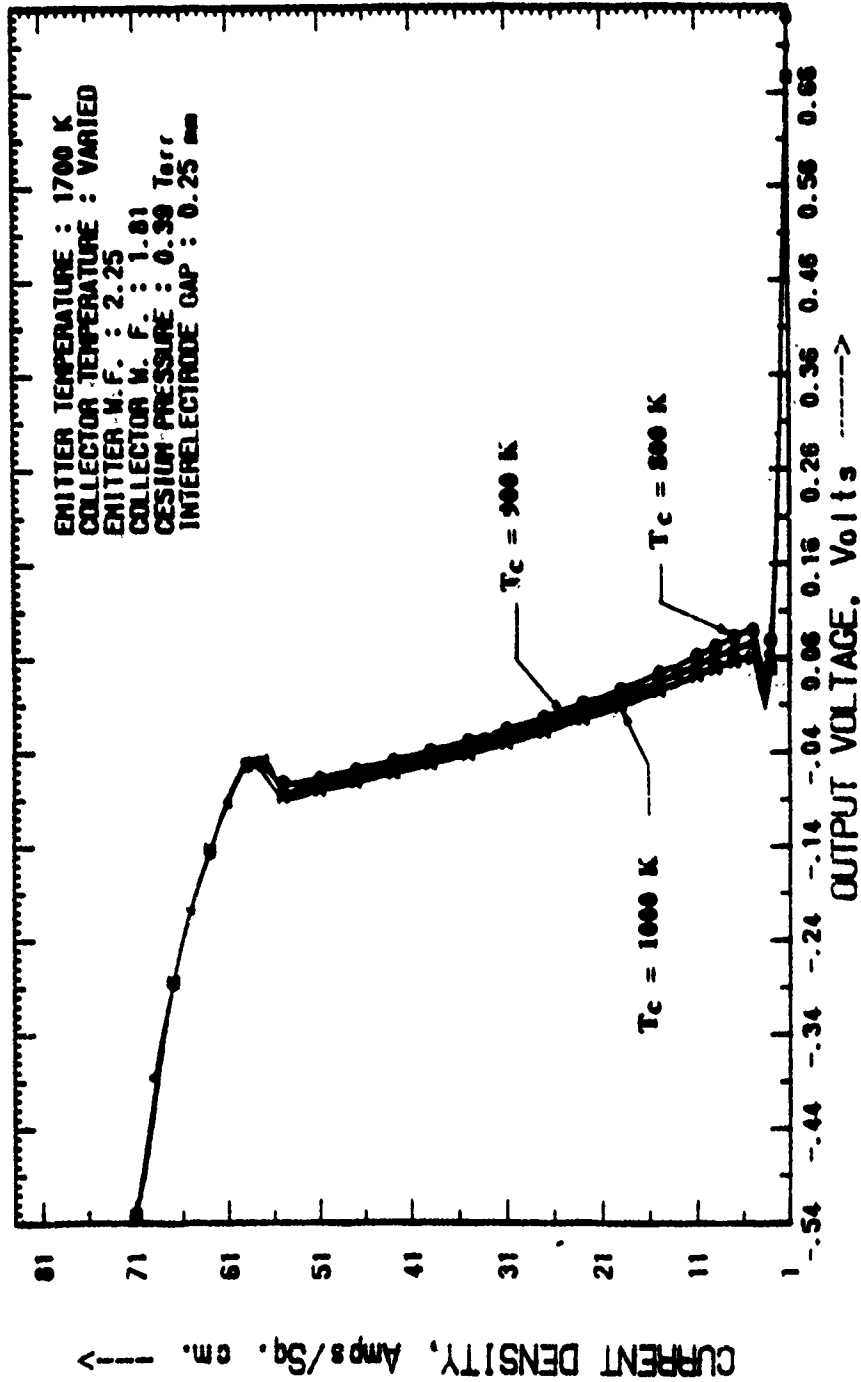


Figure 5.36 Operation Under Varied Collector Temperatures for Lower Cesium Pressures.

# THEORETICAL OUTPUT SIMULATION CHARACTERISTIC

( Cesium Reservoir Temperature Variation )

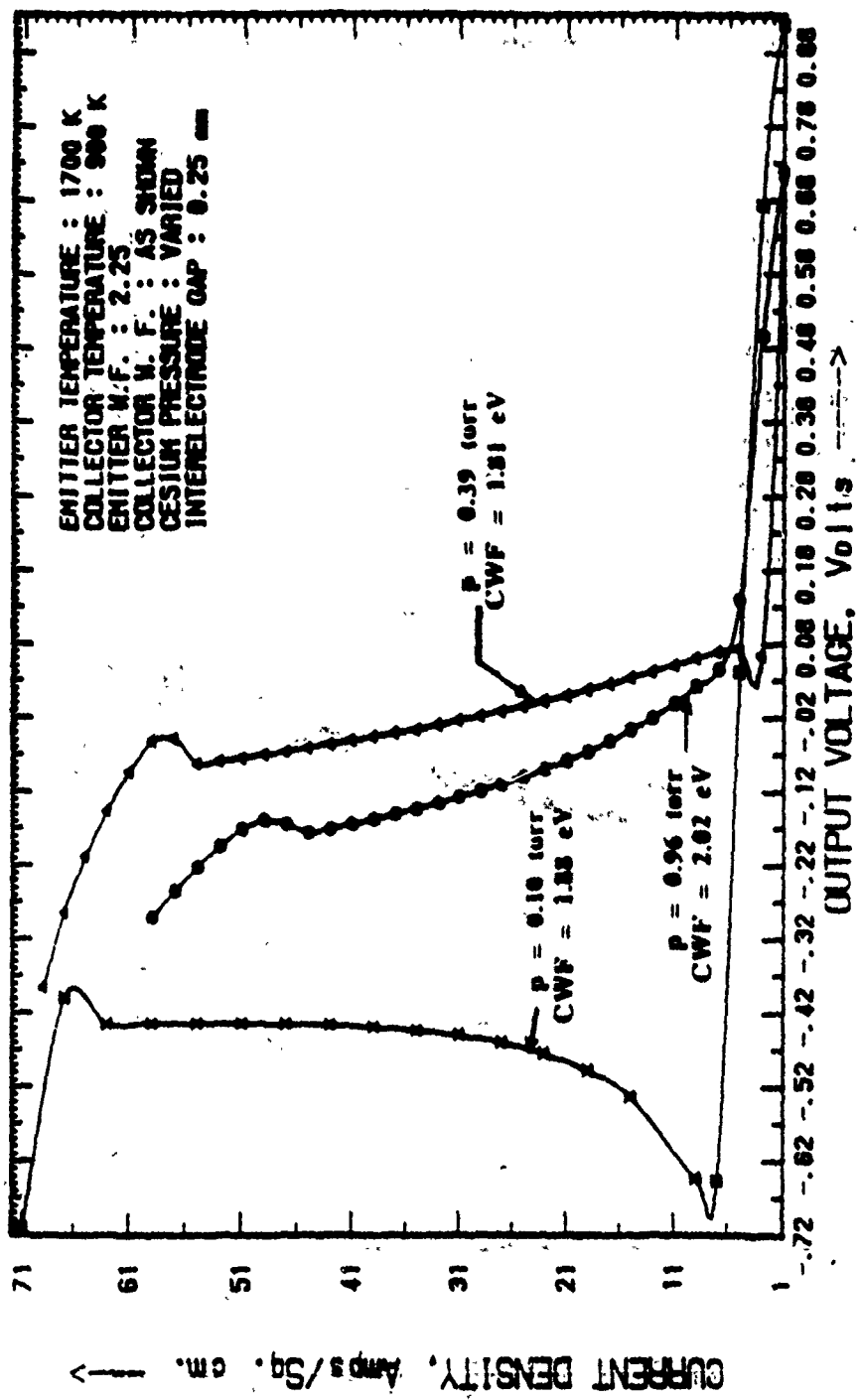


Figure 5.37 Simulated Characteristics Corresponding to Experimental Cesium Reservoir Temperature Optimization.

substantiated in that an increment in emitter temperature results in an increase in current density, with that increase not necessarily being roughly proportional to the square of the emitter temperature as might be expected from fundamental theory.

## SECTION VI

### CONCLUSIONS AND FUTURE ACTIVITIES

The section has been divided into the conclusions and future activities for five different topics of research encountered in the entire program.

#### 6.1 Diminiode Test Stations and Lanthanum Hexaboride Diode

The facilities and equipment acquired from NASA LeRC through Arizona State University (ASU) were successfully set up and tested with a Lanthanum Hexaboride diminiode at the APL of AFWAL/WPAFB. Both performance verification and optimization tests were conducted to establish the performance of the instrumentation, data acquisition/processing systems and other accessories. There was excellent correspondence of the results obtained formerly at NASA LeRC and presently at AFWAL. The entire exercise was a valuable experience for all the scientists and technicians involved in the project and a morale booster for future, more innovative research activities in Thermionic Energy Conversion.

The major problem involving the testing of the diode/diminiode was the lack of a sweep generator system to bias the diode. With manual biasing, it takes the best part of 3 hours to complete one sweep going from an output voltage of +2.0 volts to -1.0 volts. The reason for this is that all the cooling adjustments have to be made prior to increasing or decreasing the bias supply. However, by using a 5- or 10-V pulse to sweep the diode, the entire duration can be brought down to less than 20 msec as we are now able to capitalize on the thermal inertia properties of the metal that facilitate the maintenance of constant temperature. This addition together with an oscilloscope to view the J-V characteristic should bring the stations close to having the state of the technical art in instrumenting a diode test station.

#### 6.2 The ASTAR-811C Diode and the Diode Processing Station

The ASTAR-811C Diode did not seem to possess any significant current even when the emitter was heated up to 1800 K. The back emission seemed to be considerably high at all cesium reservoir temperatures. This indicates that either the collector temperature at which the

tests were conducted was too high or the characteristics of the collector surface had changed by deposits of the emitter material. This can be checked by repeating some of the tests at lower collector temperatures.

The diode processing station is almost 90 percent insulated. It would be a good idea to replace the existing power supplies with more sophisticated temperature controllers and power supplies. A welding filament has to be designed and several tantalum tubes should be welded in order to optimize the weld parameters.

### 6.3 TECO Test Station and the Rhenium-Niobium Diode

Preliminary test on the etched Rhenium-Niobium diode did indicate that the diode was performing with ignition and de-ignition but at low current densities. It would take several different test procedures to map the performance of the diode completely and then come to any conclusions regarding its operating efficiency. Again, the biasing of the diode was done manually, and unless a sweep generator and oscilloscope are included as a part of the instrumentation, the thermal inertia properties of the material cannot be exploited.

### 6.4 Computer Characterization of Diode Performance

The TEC code J-V characteristic simulations were significant in their use as a comparison for actual characteristics generated experimentally. In addition, they were useful in demonstrating the transient nature of the characteristics themselves over time.

Figure 5.30 indicates that a cesium vapor pressure of 1 torr represents approximately what might be expected under experimental conditions. The "knees" in the curves, however, are not consistent with experimental results and might be attributed to different rates of decay of the plasma parameters in the code for the region between the "Boltzmann" and "saturation" portions of the curve.

Other unexpected ambiguities in the code's results include the  $N=2000$  curve in Figure 5.31. This is considered to be an artifact occurring at low pressures (low number of mean free paths) and due to a combination of either inaccurate collision cross section modeling and/or the neglect of ion inertia in the conservation of momentum equations as used, in calculating the plasma profile in the code.

Differences in plasma ignition characteristics were also observed between the experimental results and the code's predictions. As ignition of the plasma is dependent on many variables (electron temperature, mean free paths, ion concentration, etc.), it was expected that this portion of the curve might be less accurate. In the steady-state mode, calculated values for a moderate pressure of 0.39 torr, agreed with experimental results within 5 percent but at lower pressures ( $< 1.0$  torr), the analytical results deviated considerably from experimental results. The simulations for collector temperature variation were reasonably good as this does not affect the performance appreciably as observed from experimental results. The emitter temperature simulations yielded exaggerated current densities. Furthermore, the code predicted "knee" as observed in some of the results, was not measured experimentally, as the equipment used was not capable of measuring higher current densities than that shown (Figure 5.3). This portion of the curve requires additional attention from both the simulation (code) and experimental directions.

The TEC code used demonstrates the capability of current computer programs to produce significant results and provide reasonably accurate TEC predictions. With the advent of improved computational facilities, it is expected that this and possible other codes will be further advanced, thereby providing continued insight into rapid analytical verification of experimental work in the field.

Areas requiring improvement in the particular code examined in this paper include:

- 1) improved modeling accuracy at relatively low cesium vapor pressures,
- 2) better ignition/de-ignition definition,
- 3) possible flattening of the "knee" portion of the curve, and

- 4) numerical operations within the code might be reformulated to allow for a faster program execution time. The program might also be recompiled to run on more powerful mainframe systems.

#### 6.5 Goals of Thermionic Research at WRDC

The overall goal of the WRDC in-house thermionic conversion research in the future will be to support Air Force needs in 6.1, 6.2, and 6.3 research. Specifically, this means supporting efforts such as the Advanced Thermionic Initiative (ATI) being undertaken cooperatively between SDIO/IST and WRDC. There will be close interfacing with universities and businesses providing technical assistance and leadership as appropriate. Accordingly, the design philosophy in developing in-house facilities is to use standard, inexpensive equipment and software wherever possible, so as to facilitate smooth interactions with universities and businesses, thereby making the universal contribution to the thermionic technology, more effective.

A high-priority goal is to fabricate diodes in-house using the "Diminiode" fabrication equipment acquired from Arizona State university. There are several reasons for doing this. One is that it will allow quick examination of novel surfaces and configurations (i.e., grooved surfaces, diamond-like surfaces, oxygenated surfaces, etc.). A second advantage is that it would support very high temperature thermionics (VHTT), where tests resulting in damage or destruction can be undertaken without fear of crippling the in-house capability. A third advantage is that it will allow the interaction with universities and businesses, leading to a broader US technology base. The goal is to produce a diminiode as soon as possible and modify the setup to more closely replicate added features such as variable gap, sapphire windows to view plasma conditions and so on.

With the existing diminiodes or similar converters, the phenomena of ignition/de-ignition in converters will be studied. These are of crucial importance in devising a stable startup procedure for a thermionic reactor. The reason is that the formation of an arc in cesium may

cool the emitter so much that the arc may extinguish itself, which has an adverse effect on the startup process and on the nucleonics. To date these phenomena have not been addressed in great detail by the US thermionic community.

## **REFERENCES**

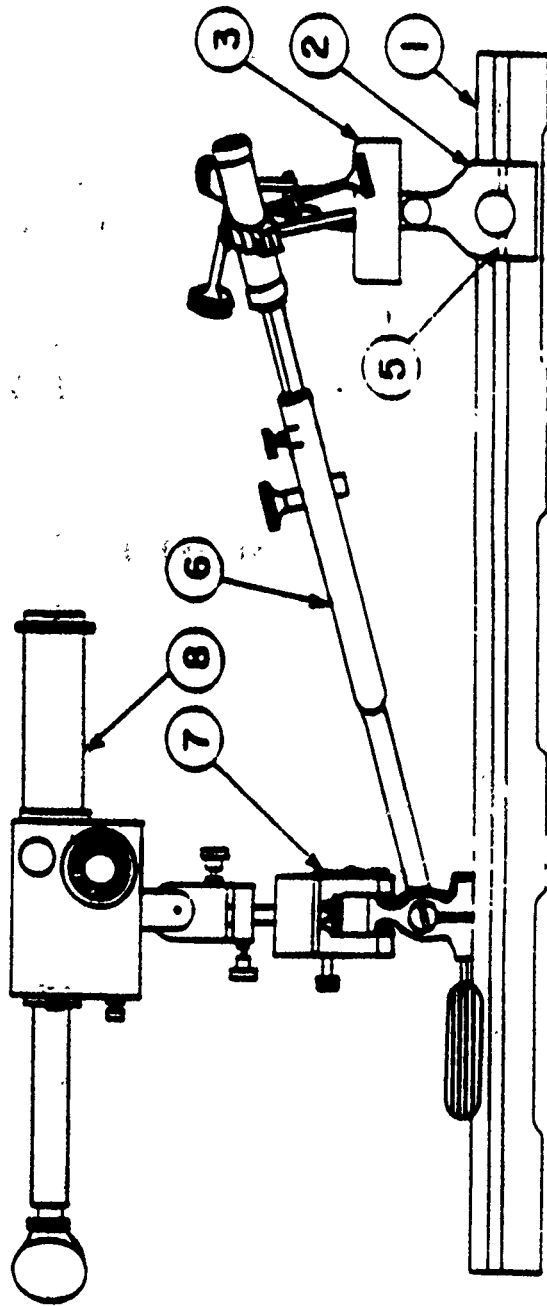
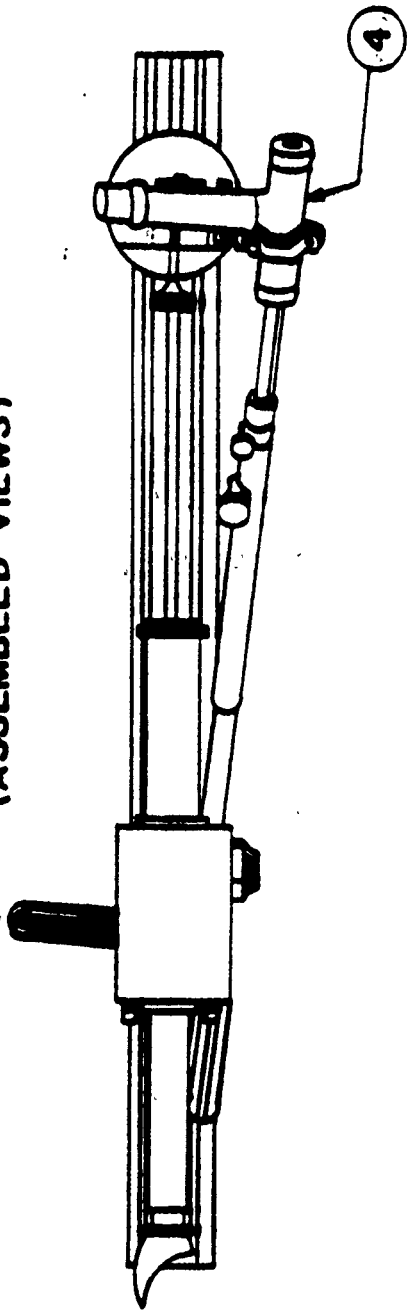
1. Kroeger, E.W., Bair, V.L., and Morris, J.F., "Diminiode Thermionic Energy Conversion with Lanthanum Hexaboride Electrodes," NASA TM-78887, Lewis Research Center, 1978.
2. Morris, J.F., "High Efficiency, Low Temperature Cesium Diodes with Lanthanum Hexaboride Electrodes," NASA TMS-71549; IEEE 1974, International Conference on Plasma Science, Conference Record Abstracts; IEEE, pp. 7-8, 1974.
3. Johnson, R.W., and Danne, A.h., "The Lanthanum - Boron System," Journal of Physical Chemistry, 65, 6, pp. 909-915, 1961.
4. Lundholm, J.G., Morris, J.F., and Stearns, J.W., "NASA Thermionic Converter Research and Technology Program," IEEE Thermionic Conversion Specialist Conference, Eindhoven, The Netherlands, 1975.
5. Pawlik, E.V., and Phillips, W.M., "A Nuclear Electric Propulsion Vehicle for Planetary Exploration," Journal of Spacecrafts and Rockets, 14, 9, pp. 518-525, 1977.
6. Morris, J.F., "High Temperature, High Power Density Thermionic Energy Conversion for Space," NASA TMX-73844, 1977.
7. Morris, J.F., "The Diminiode: A Research and Development Tool for Nuclear Thermionics," NASA TMX-2586, 1972.
8. Morris, J.F., "Vacuum-Packaged Cesium for Nuclear Thermionic Diodes," NASA TMA-2152, 1971.

9. Lancashire, R.B., Manista, E.J., Morris, J.F., and Smith, A.L., "Emitter Surface Temperature Distribution for a Miniature Thermionic Diode," NASA TMX-2588, 1972.
10. Morris, J.F., "A Freeze, Melt Valve and Dispensing System for Cesium," NASA TMX-2126, 1970.
11. Smith, A.L., Manista, E.J., and Morris, J.F., "Thermionic Performance of a Cesium Diminiode with Relatively Impure 110-Tungsten Electrodes," NASA TMX-3021, 1974.
12. Smith, A.L., Lancashire, R.B., Manista, E.J. and Morris, J.F., "Diminiode Performance Data with an ASTAR-811C, Emitter and a Nb-1Zr Collector," NASA TMX-2587, 1972.
13. Ramalingam, M.L., Kennel, E.B., and Morgan, M., "The Experimental Thermionic Diode Research Development Program at Wright-Patterson Air Force Base," Thermionic Conversion Specialist Conference, Sunnyvale, CA, October 1989.
14. Main, G.F., "Emitter Sheath Effects on Thermionic Converter Performance," Doctoral dissertation at Princeton University, October 1984.
15. Lawless, Jr. J.L., and Lam, S.H., "The Plasma Dynamics and Ionization Kinetics of Thermionic Energy Conversion," Doctoral dissertation at Princeton University, Feb. 1982.
16. Ramalingam, M.L., and Morgan, M., "Optimization of Lanthanum Hexaboride Electrodes for Maximum Thermionic Power Generation," IAF Space Power Conference, Cleveland, OH, June 1989.

**APPENDIX A**

**DESIGN DRAWINGS FOR THE PYROMETER SUPPORT STAND**

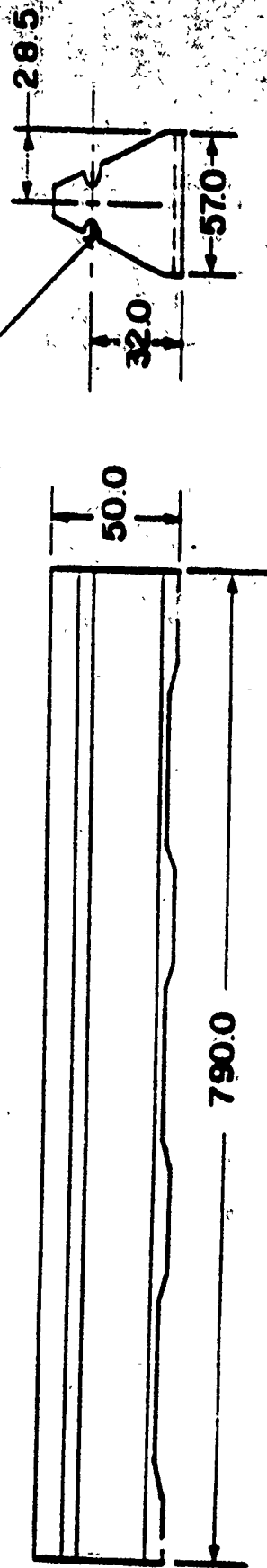
PYROMETER SUPPORT STAND  
(ASSEMBLED VIEWS)



NOTE: ALL DIMENSIONS IN MM.  
(DRAWINGS ARE NOT TO SCALE)

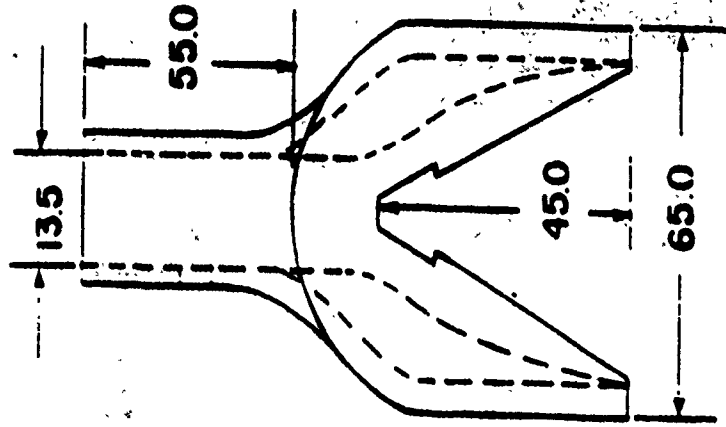
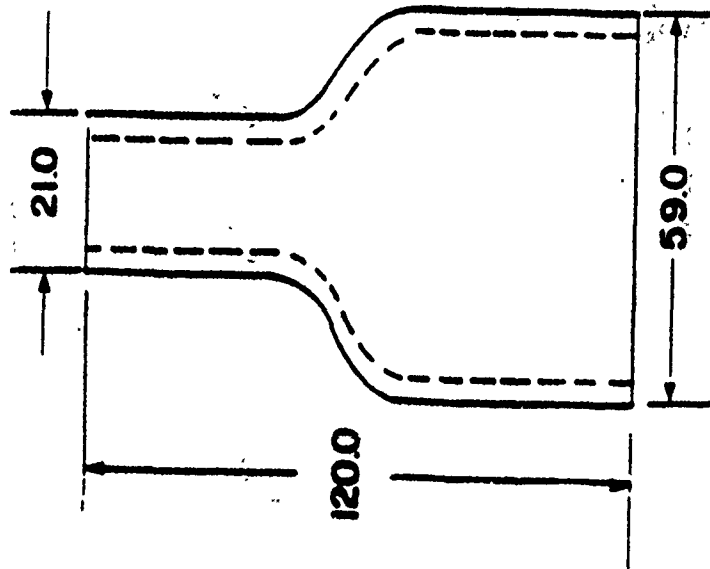
|          |            |
|----------|------------|
| PART #   | 1          |
| NAME     | GUIDE WAYS |
| MATERIAL | CAST IRON  |
| QUANTITY | 1          |

ACTUAL  
GUIDE WAYS



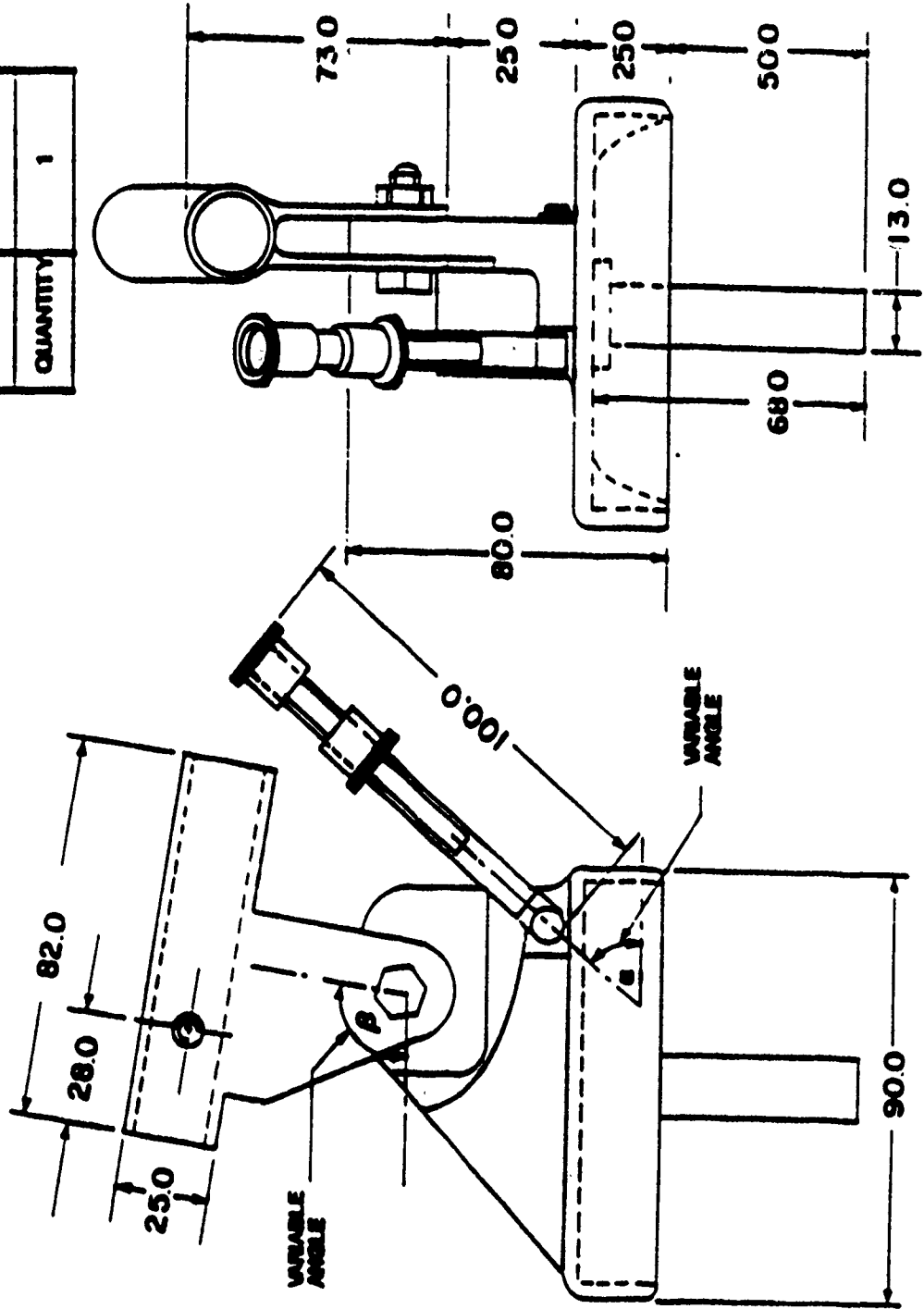
NOTE: ALL DIMENSIONS IN mm  
(DRAWINGS ARE NOT TO SCALE)

|          |              |
|----------|--------------|
| PART #   | 2            |
| NAME     | SUPPORT BASE |
| MATERIAL | ALUMINUM     |
| QUANTITY | 1            |



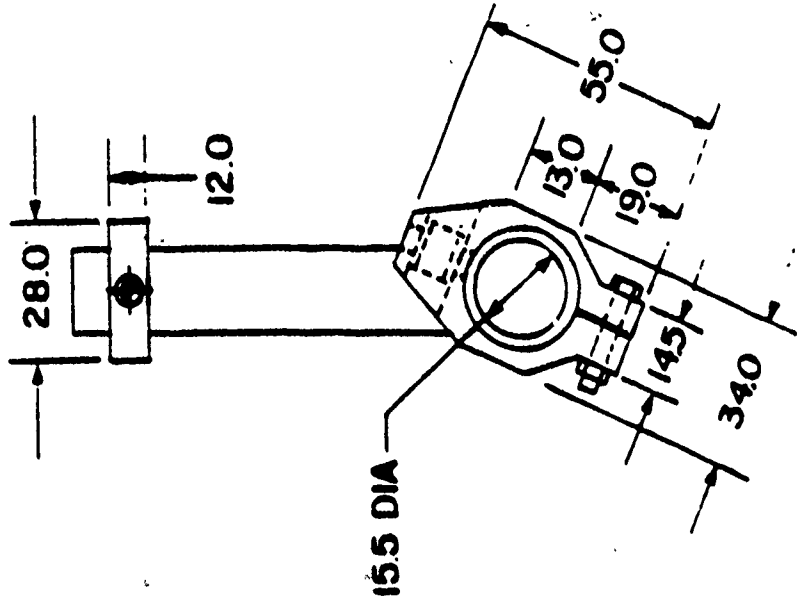
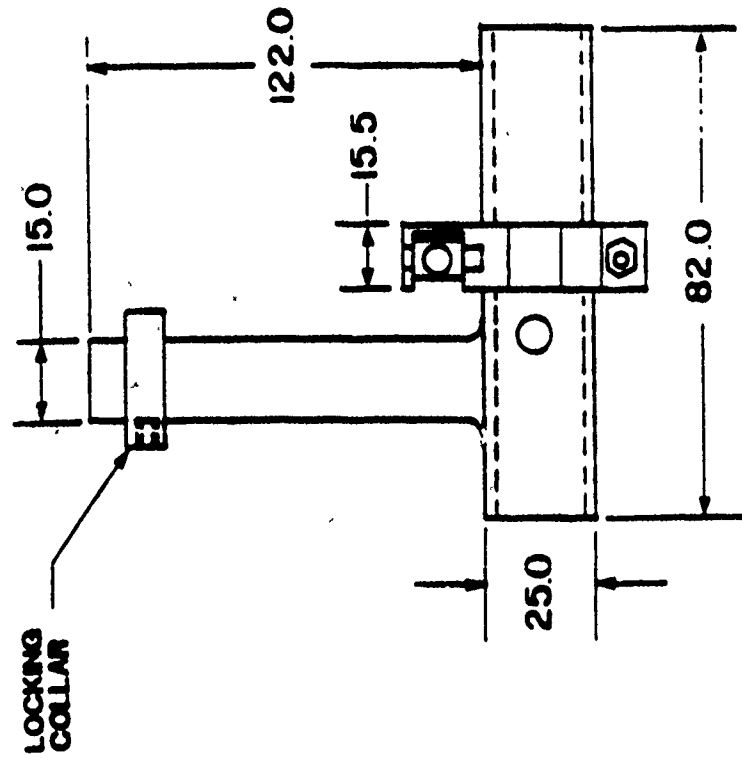
|          |                     |
|----------|---------------------|
| PART #   | 3                   |
| NAME     | SWING ARM MECHANISM |
| MATERIAL | N + CI              |
| QUANTITY | 1                   |

NOTE: ALL DIMENSIONS IN MM  
(DRAWINGS ARE NOT TO SCALE)



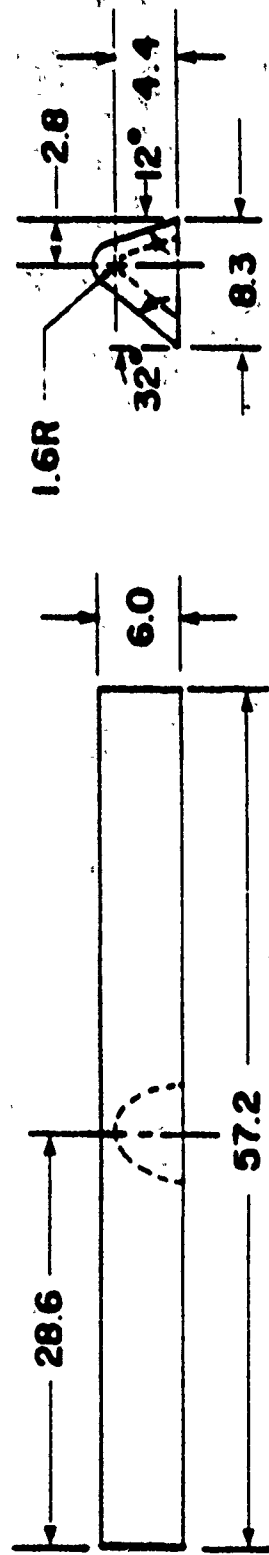
|          |               |
|----------|---------------|
| PART #   | 4             |
| NAME     | REVOLVING ARM |
| MATERIAL | CAST IRON     |
| QUANTITY | 1             |

NOTE: ALL DIMENSIONS IN MM  
(DRAWINGS ARE NOT TO SCALE)



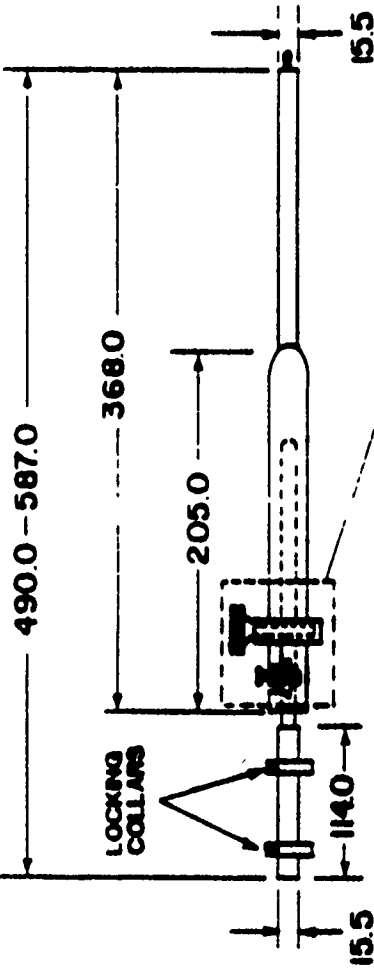
|          |                |
|----------|----------------|
| PART #   | 5              |
| NAME     | DRIFTING WEDGE |
| MATERIAL | CAST IRON      |
| QUANTITY | 1              |

NOTE: ALL DIMENSIONS IN mm.  
(DRAWINGS ARE NOT TO SCALE)

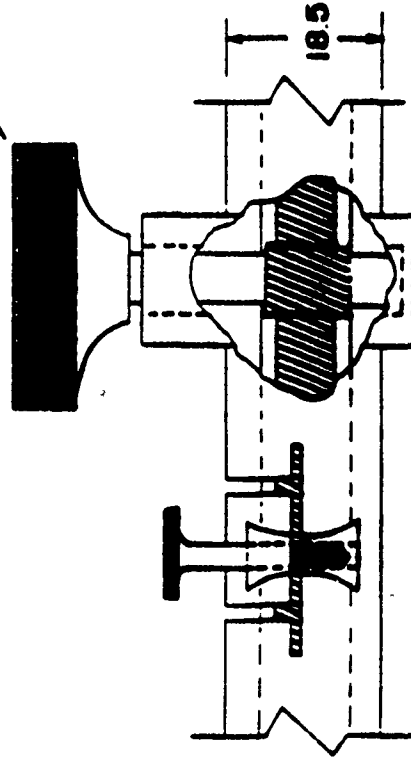
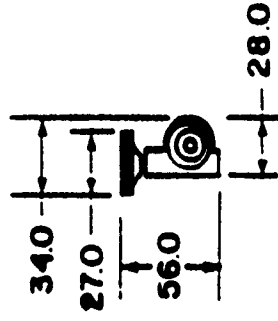


NOTE: ALL DIMENSIONS IN MM  
(DRAWINGS ARE NOT TO SCALE)

ADJUSTABLE

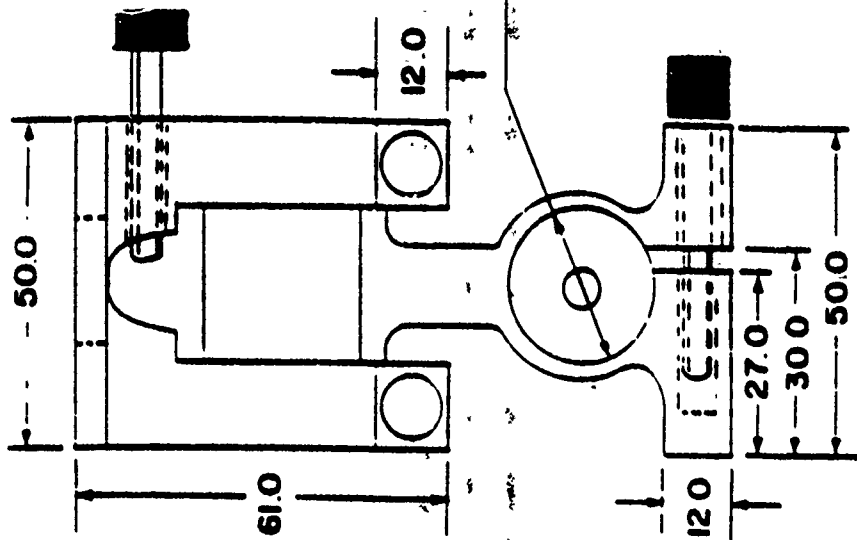
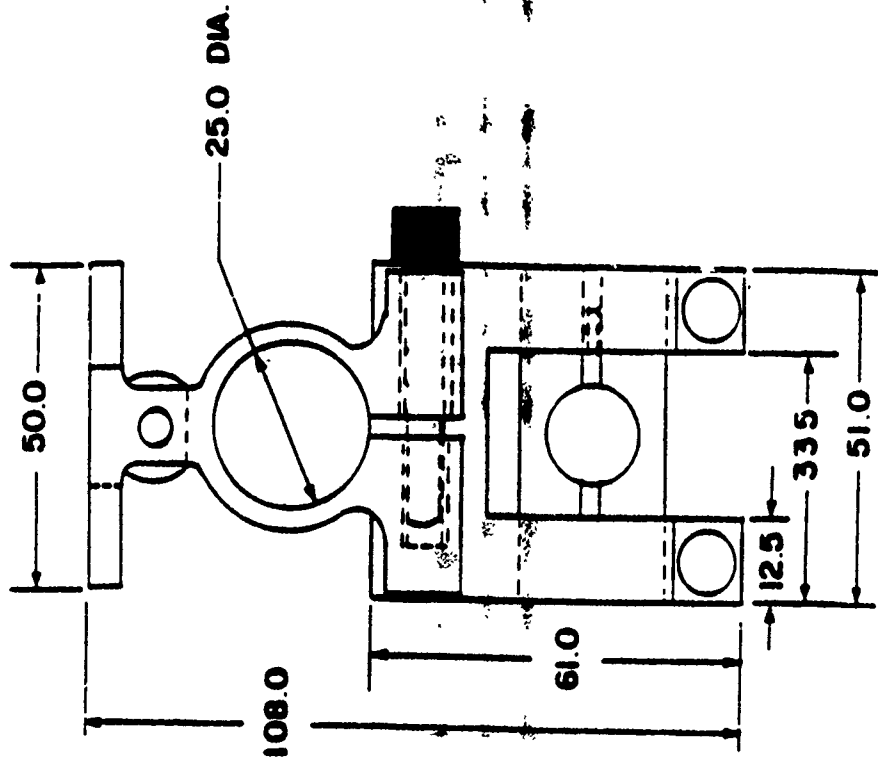


|          |                 |
|----------|-----------------|
| PART #   | 6               |
| NAME     | EXTENSION ARM   |
| MATERIAL | STAINLESS STEEL |
| QUANTITY | 1               |



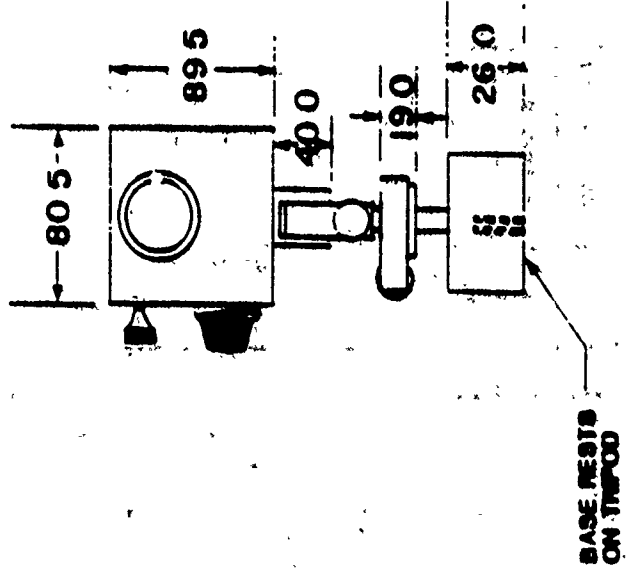
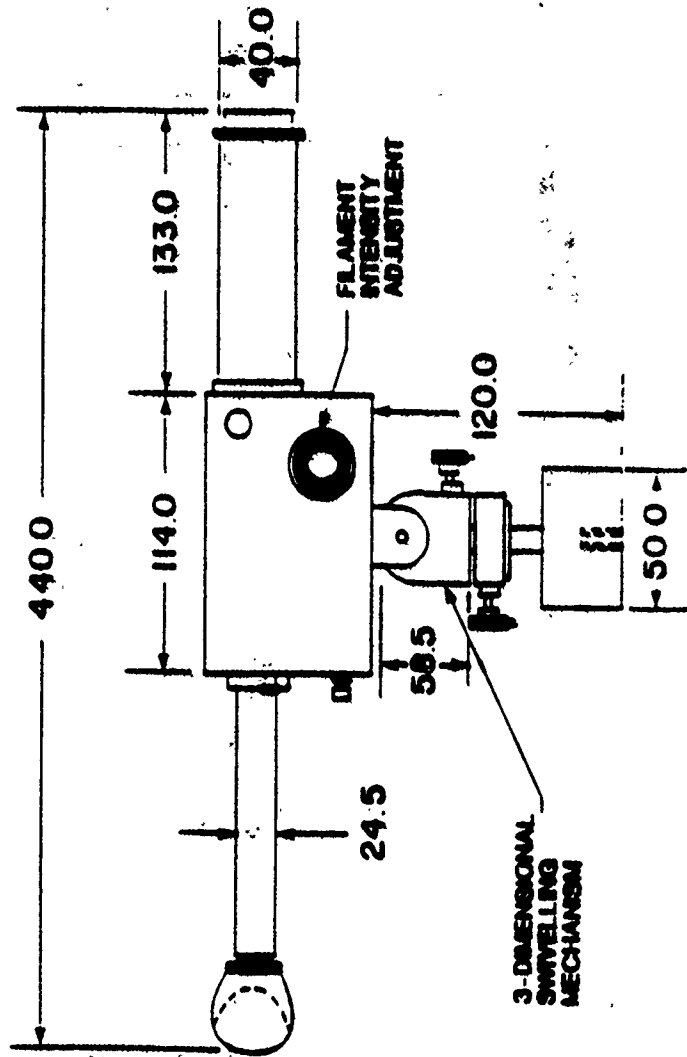
|          |              |
|----------|--------------|
| PART #   | 7            |
| NAME     | SWIVEL MOUNT |
| MATERIAL | ALUMINUM     |
| QUANTITY | 1            |

NOTE ALL DIMENSIONS IN MM.  
(DRAWINGS ARE NOT TO SCALE)



|          |                         |
|----------|-------------------------|
| PART #   | 6                       |
| NAME     | MICRO-OPTICAL PYROMETER |
| MATERIAL | ASSORTED                |
| QUANTITY | 1                       |

NOTE: ALL DIMENSIONS IN mm.  
(DRAWINGS ARE NOT TO SCALE)

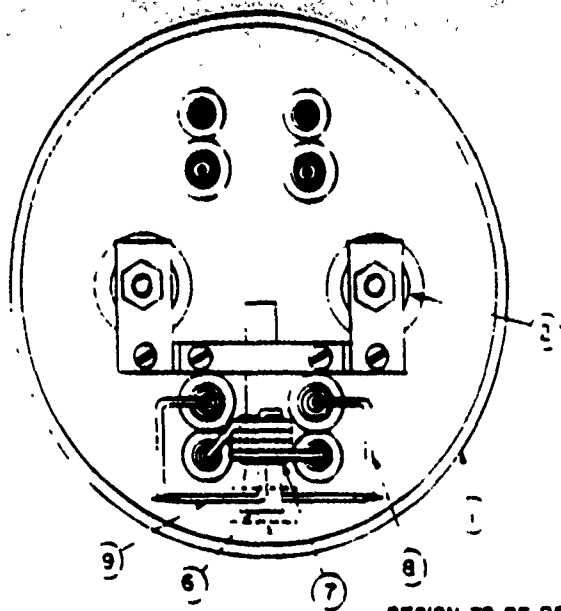


**APPENDIX B**

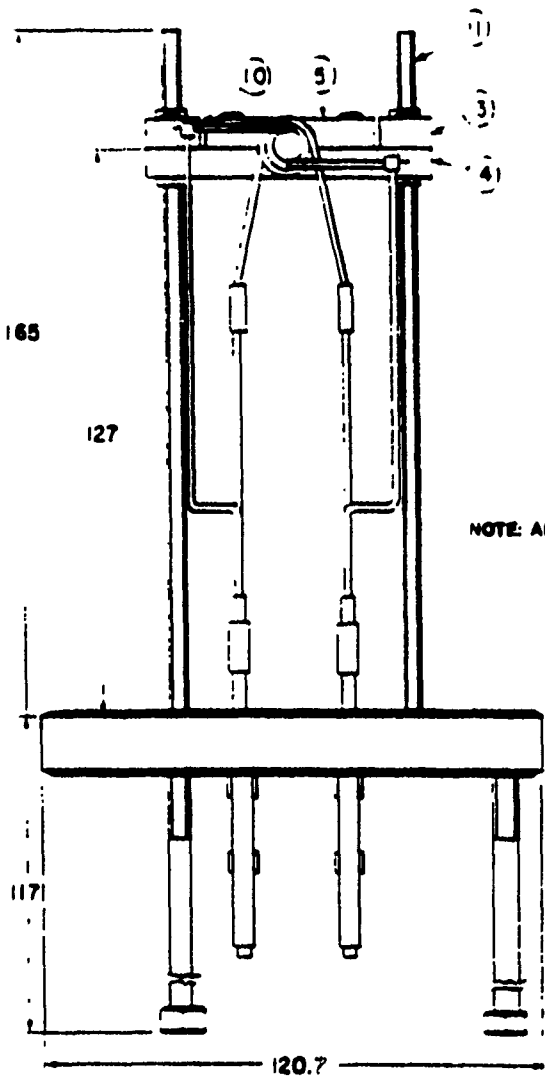
**DESIGN DRAWINGS OF THE SIMULATED STRUCTURE FOR  
CESIUM CYLINDER BRAZING**

DETAILS FOR PARTS OF SIMULATED STRUCTURE FOR CESIUM CYLINDER BRAZING

| PART # | DESCRIPTION                  | MATERIAL          | QTY. |
|--------|------------------------------|-------------------|------|
| 1      | Base Flange                  | S.S.304           | 1    |
| 2      | Flange Insert                | S.S.304           | 2    |
| 3      | Support Strip - 1            | S.S.304           | 2    |
| 4      | Support Strip - 2            | S.S.304           | 1    |
| 5      | Support Strip - 3            | S.S.304           | 1    |
| 6      | Cesium Capsule Container     | Tantalum          | A.R. |
| 7      | Base for Cesium Cooling Coil | S.S.304           | A.R. |
| 8      | Nichrome Heater Connection   | -                 | -    |
| 9      | Nichrome Heater              | Nichrome          | -    |
| 10     | Ceramic Insulating Bead      | Aluminum<br>Oxide | 2    |
| 11     | Allthread (6-32)             | S.S.              | -2   |



REGION TO BE BRAZED  
BY ELECTRON BOMBARDMENT

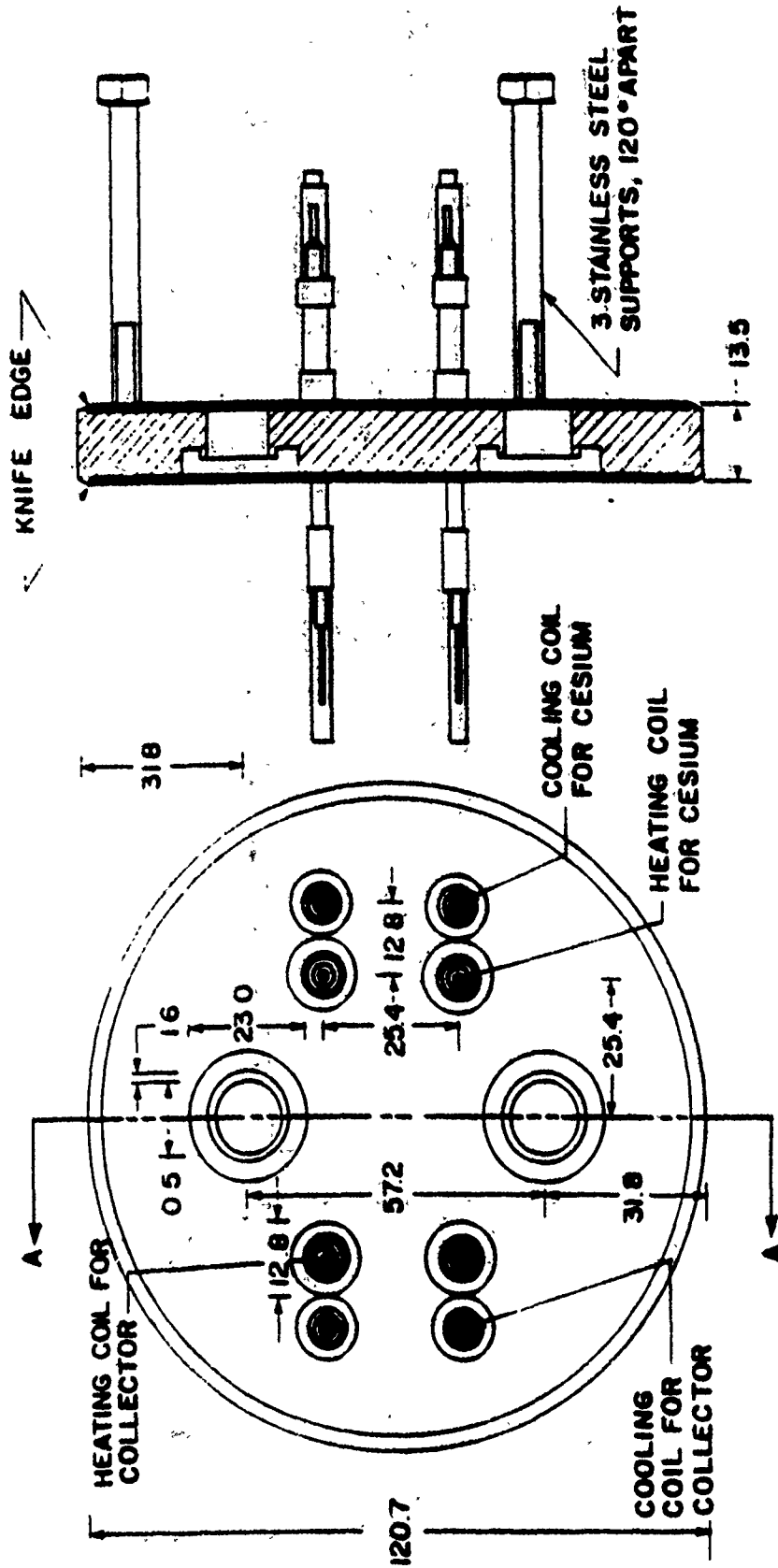


NOTE: ALL DIMENSIONS IN MM.

SHIELDED STRUCTURE FOR CESIUM CYLINDER BRAZING

TITLE: BASE FLANGE  
 PART NO.: 1  
 MATERIAL: STAINLESS STEEL  
 QUANTITY: 1

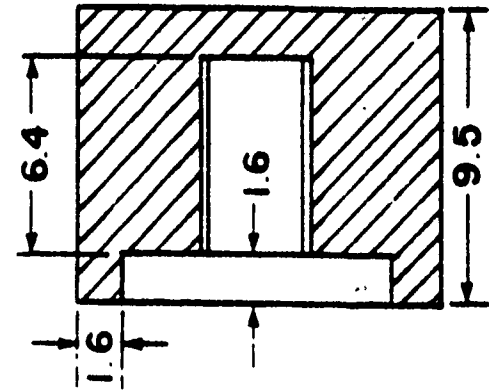
NOTE: ALL DIMENSIONS IN MM.



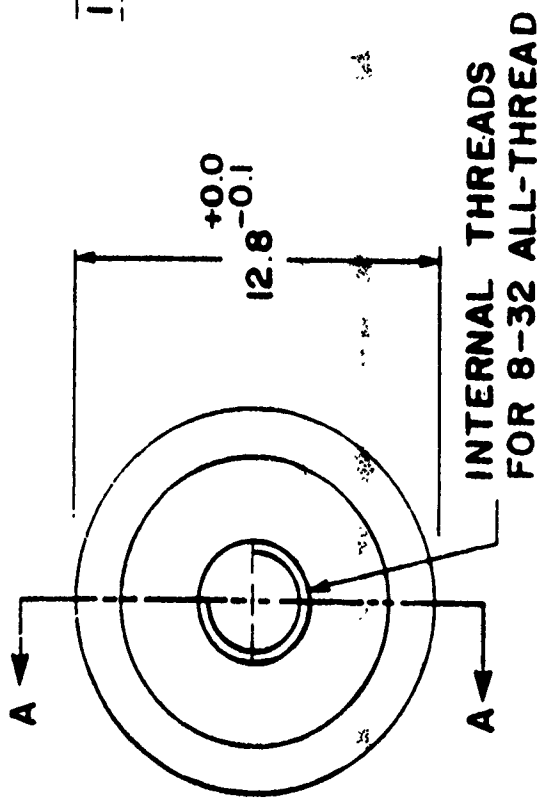
SECTION A-A

**TITLE: FLANGE INSERT  
PART NO: 2  
MATERIAL: S.S. 304  
QUANTITY: 2**

**NOTE: ALL DIMENSIONS IN MM.**

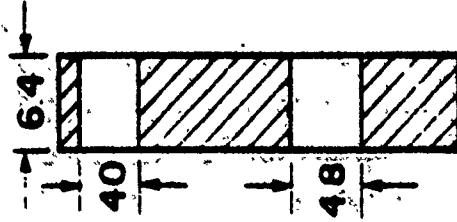
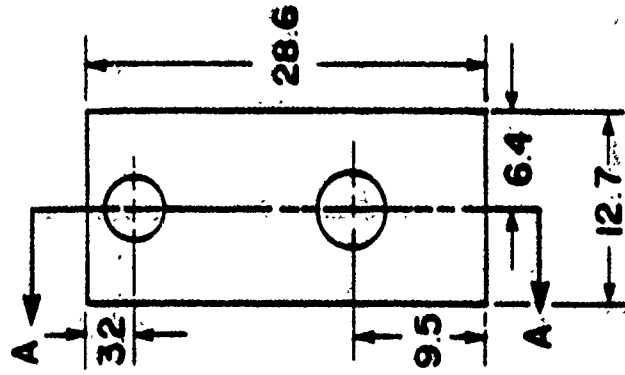


**SECTION A-A**



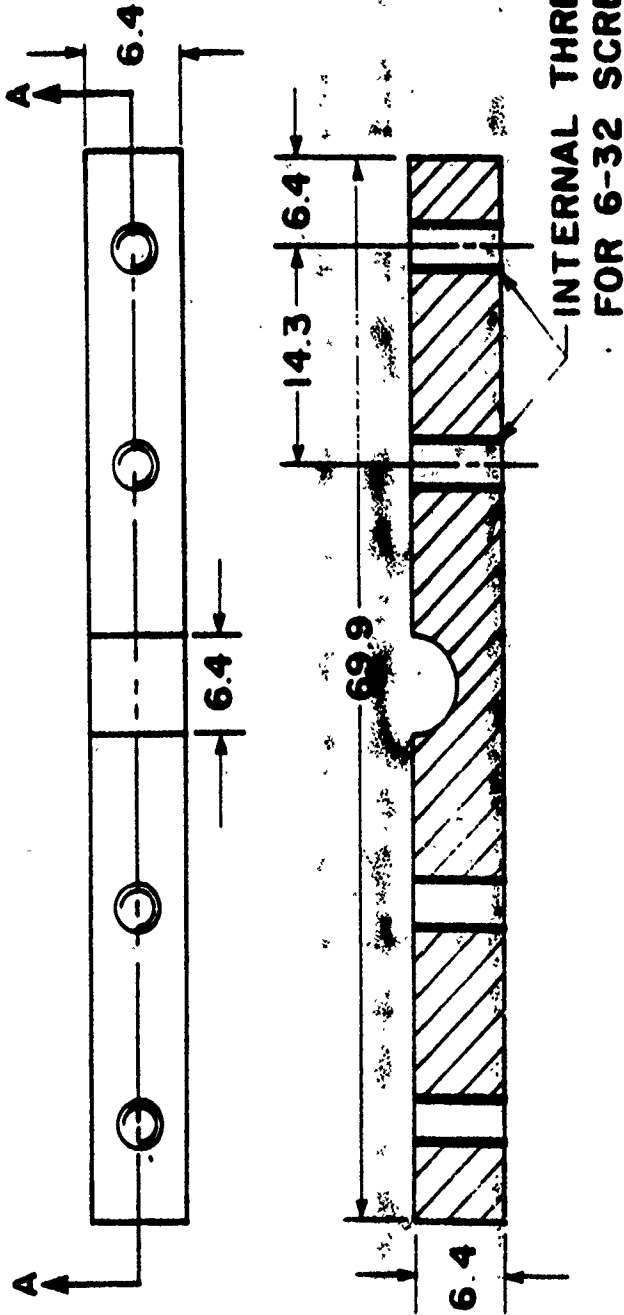
**TITLE: SUPPORT STRIP 1**  
**PART NO.: 3**  
**MATERIAL: S.S. 304**  
**QUANTITY: 2**

**NOTE: ALL DIMENSIONS IN MM.**



TITLE: SUPPORT STRIP 2  
PART NO.: 4  
MATERIAL: S.S. 304  
QUANTITY: 1

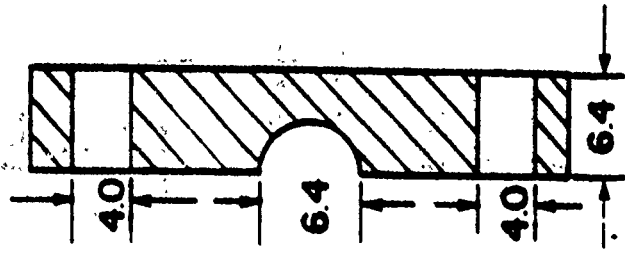
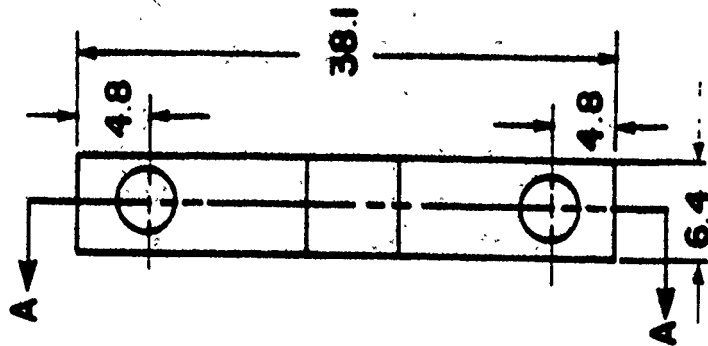
NOTE: ALL DIMENSIONS IN MM.



SECTION A-A

**TITLE: SUPPORT STRIP 3  
PART NO.: 5  
MATERIAL: S.S. 304  
QUANTITY: 1**

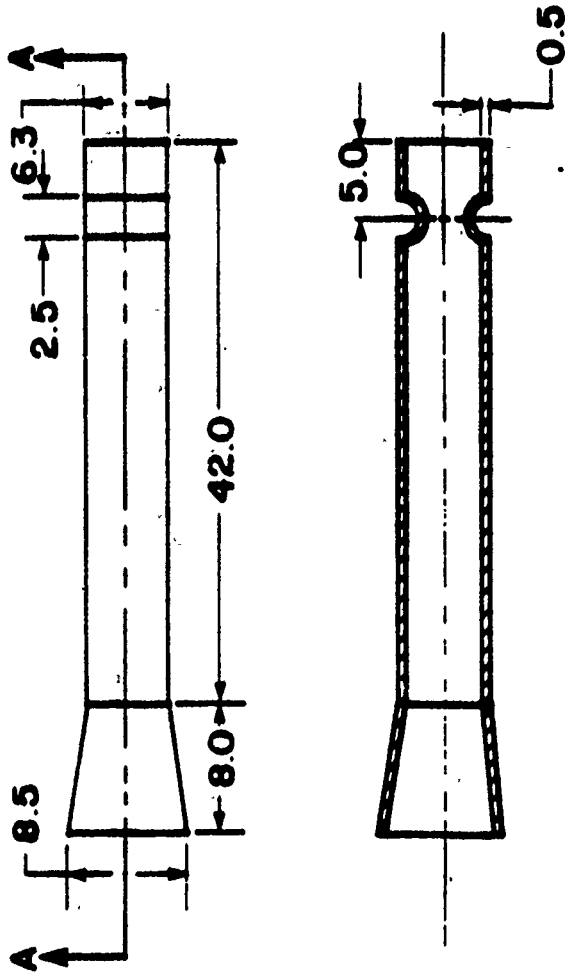
**NOTE: ALL DIMENSIONS IN MM.**



**SECTION A-A**

**TITLE: CESIUM CAPSULE CONTAINER**  
**PART NO.: 6**  
**MATERIAL: TANTALUM**  
**QUANTITY: AS REQUIRED**

**NOTE: ALL DIMENSIONS IN MM.**



TITLE: BASE FOR CESIUM COOLING COIL  
PART NO.: 7  
MATERIAL: S.S. 304  
QUANTITY: AS REQUIRED

NOTE: ALL DIMENSIONS IN MM.

